Facile Fabrication of Functional Membranes through Oxidant-Triggered Plant-Inspired Surface Modification

by

Yulan Chen

A thesis submitted in partial fulfillment of the requirements for the degree of

Master of Science

in

Materials Engineering

Department of Chemical and Materials Engineering
University of Alberta

Abstract

Surface functionalization methods are critically important for materials research community in endowing surfaces with multiple novel and unique properties. Plant-derived polyphenolic compounds exhibit material-independent adhesive affinity and form versatile coatings via synchronous oxidation and self-polymerization in weak alkaline solutions. However, several drawbacks like low homogeneity and time-consuming chemical reactions hinder their practical implementations. A simple and effective surface modification approach based on catechol (CA) by using sodium periodate (SP) as a trigger has been studied in this work to address these concerns. With our strategy, SP-mediated CA films with good uniformity were successfully deposited on various dense and porous substrates in a relatively short time. The polymerization and deposition kinetics of CA under chemical oxidation were identified by UV–vis spectroscopy, atomic force microscopy (AFM), and ellipsometry. The systematic investigation of membrane chemical, wetting, and permeation properties under different coating times demonstrated that the optimal coating time was 2 h.

In water purification, the optimally modified PVDF membranes, showing superhydrophilicity and underwater superoleophobicity, possess outstanding pure water permeability, high adsorption capacity for copper ions, and excellent rejection to oil.

In part II, our modification method was employed to fabricate a hydrophilic-hydrophobic Janus membrane that can be applied in the generation of hollow polymeric capsules. The asymmetric structure of Janus membrane was verified through characterization techniques including X-ray spectroscopy (XPS), attenuated total reflection-Fourier transform infrared spectroscopy (ATR-FTIR), and contact angle measurements. To provide proof-of-concept of Janus membrane emulsification, a homemade apparatus was used to make double emulsions (i.e., gas-in-oil-in-

water emulsions). The experimental parameters (e.g., gas flow rate, pH of continuous phase, and surfactant concentration) controlling the drop size and size distribution were studied comprehensively. The generated double emulsions underwent polymerization upon exposure to UV light, thus producing UV-cured hollow polymeric microspheres.

In addition to reporting a simple and versatile strategy for surface modification and its applications in membrane technology, this dissertation paves a way to illuminate the process of plant phenolic deposition and also provides a feasible method to produce massive double emulsions through membrane emulsification.

Preface

Chapter 4 of this thesis was accepted in *Journal of Membrane Science* as Chen, Y.; Liu, Q., "Oxidant-induced plant phenol surface chemistry for multifunctional coatings: Mechanism and potential applications", *Journal of Membrane Science*, 2019, 570-571, 176-183. I was responsible for the concept formation, experiments, data analysis, and the composition for all the manuscript. Liu, Q. was the supervisory author on this paper, contributing to manuscript edits.

Chapter 5 of this thesis will be submitted for publication in the *Journal of Membrane Science* as Chen, Y., Lu, Z.; Liu, Q., "Janus Membrane Emulsification for Facile Preparation of Hollow Microspheres". I was responsible for all major areas of concept formation, data collection and analysis as well as the manuscript composition. Lu, Z. provided valuable advice on the methodology, drew part of the Table of Content, and contributed to manuscript edits. Liu, Q. was the supervisory author and was involved throughout the project from determining the topic to editing the manuscript.

Chapter 4 was presented at 256th ACS National Meeting in Boston, United States of America.

Acknowledgements

First and foremost, I would like to sincerely thank my supervisor, Professor Qingxia (Chad) Liu, for offering me the opportunity to do research in his lab at University of Alberta and guiding me through the M.Sc. journey. His continuous support and insightful advice have benefited me tremendously. The overall training during the last two and a half years will definitely lay a solid foundation for my professional and personal development in the future.

I would like to express my deep gratitude to the help and friendship with the members in Prof. Liu's research group. Special thanks are directed to Chongdan Luo, who inspires me a lot in the beginning of my research period. Sincere thanks to Carl Corbett and Laurie Kachmaryk for always being resourceful and supportive.

I am also grateful to Jie Ru, Nathan Gearin, Ni Yang, Shihong Xu, and Shiraz Merali, for their trainings and technical supports in performing the contact angle, EDS mappings, TOC, XPS, and AAS measurements.

Both the Canadian Centre for Clean Carbon and Mineral Processing Technologies (CMPT) and the Natural Sciences and Engineering Research Council of Canada (NSERC) are kindly acknowledged for financially supporting this research.

Last but not least, my earnest appreciation goes to my beloved parents for providing me with unconditional love and encouragement throughout my life. They have instilled in me all the values and qualities to help me get to where I am now.

Table of Contents

List of Tables

List of Figures

List of Symbols

E_k	The kinetic energy of the ejected electron, J
hv	The incident photon energy, J
E_b	The binding energy of the ejected electron, J
ϕ	The material work function, J
θ	The solid–liquid contact angle, degree
γ_{sg}	The surface tension of the solid, mN m^{-1}
γ_{sl}	The interfacial tension between liquid and solid, mN m^{-1}
γ_{lg}	The surface tension of the liquid, mN m^{-1}
q_e	The adsorption capacity, mg g^{-1}
C_0	The initial Cu^{2+} ion concentrations, ppm
C_e	The remaining Cu^{2+} ion concentrations, ppm
V (in 4.2.5)	The volume of the solution, L
m	The membrane mass, g
V (in 4.2.6)	The volume of permeate, L
A	The effective membrane area, m^2
C_f	The concentration of oil in the filtrates, ppm
C_o	The initial concentration of oil in the oil/water mixtures or oil-in-water emulsions, ppm
S	The oil spreading coefficient, mN m^{-1}
$\gamma_{A/W}$	The air–water surface tension, mN m^{-1}
$\gamma_{A/O}$	The air–oil surface tension, mN m^{-1}

$\gamma_{O/W}$	The oil–water interfacial tension, mN m^{-1}

List of Abbreviations

PE	Polyethylene
PES	Polyethersulfone
PP	Polypropylene
PS	Polysulfone
PTFE	Polytetrafluroethylene
PVDF	Polyvinylidene fluoride
MF	Microfiltration
UF	Ultrafiltration
NF	Nanofiltration
RO	Reverse osmosis
MD	Membrane distillation
DA	Dopamine
PDA	Polydopamine
UV	Ultraviolet
CA	Catechol
Au_2O_3	Gold oxide
Al_2O_3	Aluminium oxide
SiO_2	Silicon dioxide
TiO_2	Titanium dioxide
HRP	Horseradish peroxidase
ROS	Reactive oxygen species
AP	Ammonium persulfate

PC	Potassium chlorate
SP	Sodium periodate
$CuSO_4$	Copper sulfate
H_2O_2	Hydrogen peroxide
SDS	Sodium dodecyl sulfate
W/O/W	Water-in-oil-in-water
O/W/O	Oil-in-water-in-oil
SPG	Shirasu porous glass
UV-Vis	Ultraviolet-Visible
AFM	Atomic force microscopy
HIM	Helium ion microscope
EDS	Energy dispersive spectroscopy
XPS	X-Ray photoelectron spectroscopy
ATR-FTIR	Attenuated total reflectance-Fourier transform infrared spectroscopy
KCl	Potassium chloride
HCl	Hydrochloric acid
AAS	Atomic adsorption spectrophotometer
CCD	Charge-coupled device
TOC	Total organic carbon
TC	Total carbon
IC	Inorganic carbon
SEM	Scanning electron microscope

PEI	Polyethyleneimine
PPMMs	Polypropylene microfiltration membranes
POSS-$NH_3^+Cl^-$	Octaammonium polyhedral oligomeric silsesquioxane
Tris-HCl	Tris (hydroxymethyl) aminomethane hydrochloride
DI	Deionized
WCA	Water contact angle
G/O/W	Gas-in-oil-in-water
HDDA	1, 6-Hexanediol diacrylate
OCA	Oil contact angle

Chapter 1 Introduction

1.1 Polymer Membranes and Their Applications

Membrane technology has drawn tremendous attention over the past few decades for their wide-ranging applications, such as separations, emulsification, pharmaceutical industry and energy production and storage.[1] Easy to scale-up, simple equipment, low-power operation, are among the main advantages of membrane processes, rendering them the best available technologies in various fields.[2]

Even though interest in ceramic, metal and liquid membranes has increased in recent years, the vast majority of membranes existing in current market are polymer based. This is because polymer materials can provide membranes with a wide variety of structures and desirable properties.[3] A number of commercially available membranes are made of polymeric substances, such as polyethylene (PE), polyethersulfone (PES), polypropylene (PP), polysulfone (PS), polytetrafluroethylene (PTFE), and polyvinylidene fluoride (PVDF) (Figure 1.1). On the basis of the pore sizes, there are four major pressure-driven separation membrane classes, microfiltration (MF), ultrafiltration (UF), nanofiltration (NF) and reverse osmosis (RO).

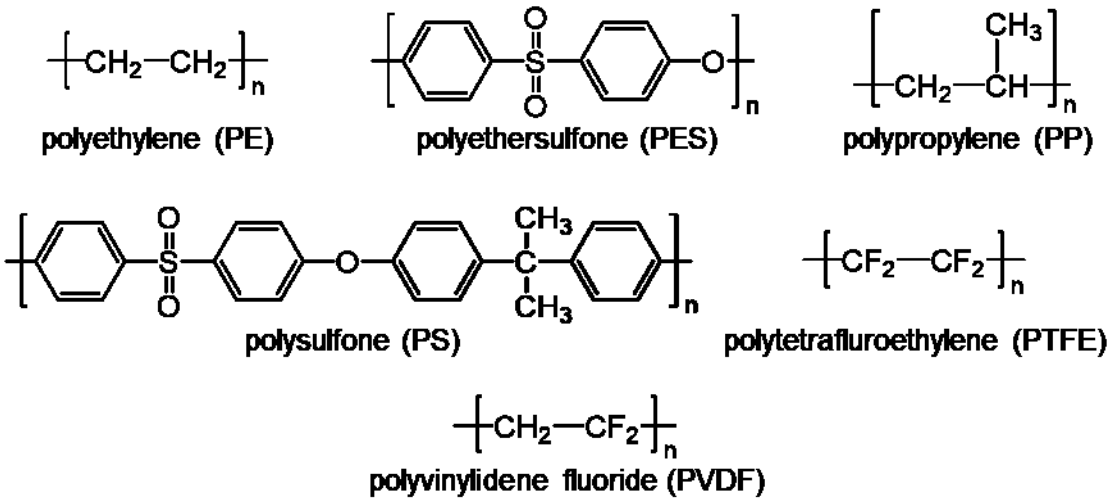

Figure 1.1 Chemical structures of common polymeric membranes.

Water purification is one of the fields in which polymeric membranes are most frequently used. Examples include high-salinity water desalination by membrane distillation (MD),[4] produced water treatment by MF and UF standalone processes,[5] metal recovery by RO,[6] etc. Specifically, membrane technology is considered the most efficient and time-saving technique for remediation of oil-polluted water that is produced in massive amounts from multiple industrial processes and residential facilities.[7] The oil pollutants can cause mutagenic and carcinogenic effects as well as restrain sunlight penetration from water to reduce oxygen dissolution, thus posing a disastrous threat to the ecosystem.[8] Much effort in recent years has been made to solve this challenge using polymeric membranes. However, due to the inherently hydrophobic characteristic of most polymer materials, polymeric membranes are confronted with problems like low water flux and quick decline of water permeation caused by oil droplets clogging the pore.[9] Besides, these membrane surfaces are usually non-selective, allowing both water and oil to pass, which makes them hard to effectively treat either immiscible or emulsified oil-water mixtures.[10] Because oil/water separation largely depends on the selective removal of oil or water, superwetting membranes, namely, superhydrophobic-superoleophilic or superhydrophilic-under-water-superoleophobic, has been deemed promising in oily wastewater remediation.[11, 12] For example, the superhydrophobic-superoleophilic membranes allow oil drops to permeate through the pores, while rejecting water drops, which leads to the removal of water from oil/water mixtures.

Another major application for polymer membranes is emulsification. Production of emulsions plays a significant role in food processing, pharmaceuticals and material science.[13] They are conventionally prepared by high-speed mixing, homogenizers, microfluidizers, and ultrasonic devices. Compared with traditional methods, membrane emulsification offers unique advantages in lower energy demands and better control of the emulsions being formed.[14] In emulsions

prepared by membrane emulsification, the to-be-dispersed phase under an applied pressure is emulsified into the continuous phase by permeation through the uniform membrane pores. The main factors determining membrane emulsification include membrane pore size, surface porosity and wetting property. Thus, the appropriate choice of each parameter enables the continuous mass-production of monodisperse droplets to meet industrial demand.

Other advanced applications of polymeric membranes include protein separations, battery separators, drug delivery and so forth. Technological improvements in polymer membranes are highly needed for the future success of polymer membranes in these advanced applications.

1.2 Membrane Surface Modification

As we mentioned above, surface properties (wettability, chemical composition, morphology, charge) have a significant impact on membrane performance. While the surface properties of pristine polymer materials are often not suitable for specific applications, surface modification allows the construction of surface-enhanced membranes with a variety of functionalities, for instance, hydrophobicity/hydrophilicity,[15] catalytic property,[16] chemical sensing,[17] anti-microbial property,[18] anti-fouling property,[19] charge property,[20] biocompatibility,[21] stimuli-responsibility,[22] and so forth. Also, the attachment of undesired molecules to the membrane surfaces can cause membrane failure during long-term operation. Therefore, surface modification is needed to inhibit this attachment. Coating,[23, 24] grafting,[25, 26] blending with other additives,[27, 28] and plasma treatment[29, 30] are now mainstream methods to functionalize the membrane surfaces. Despite a substantial number of surface modification strategies have been explored, the basic principle has been to focus on immobilizing reactive functional molecules on any membrane surfaces to either prevent undesired interactions or to introduce additional interactions.[31] Among the aforementioned methods, surface coating stands

out as one of the most versatile modification techniques. Coating is often accomplished by binding functional molecules onto membranes in aqueous solution through crosslinking, physical adsorption, or sulfonation, which is convenient and easy to be implemented on a large scale.[32] However, engineering inert polymer surfaces consisting of C–H or C–F bonds is difficult because of their low surface energy and chemical reactivity. Thus, most polymeric membrane coating cases contain two steps, which involves the introduction of adhesive groups on the membrane surfaces and post-functionalization. Under ideal conditions, the coating can modify both the membrane surface and pore walls throughout the membrane cross-section.

1.3 Bioinspired Catecholic Chemistry for Surface Modification

Bioinspired catecholic chemistry has become a hot research focus in surface engineering since the work on mussel-inspired coating was published.[33] Catechol-containing molecules can self-assemble on different materials (for example, metals, mica, oxides, ceramics, synthetic polymers) by immersing objects into a catecholic solution under air. It is widely accepted that the ortho-dihydroxyphenyl group, denoted as a “catechol” group, is responsible for the excellent adhesive ability of these molecules (Figure 1.2). Bioinspired catecholic deposition strategy has brought revolutionary promotion to modification of materials’ surfaces with its simple technical procedure, unprecedented capabilities of material-independent adhesion including the low-surface-energy organics, and post-functionalization accessibility for diverse uses. Moreover, the control of catecholic deposition has been achieved via tuning pH, solution concentration, atmosphere and reaction time. Dopamine (DA), the most representative example among catechol-bearing compounds, has been extensively employed to fabricate multifunctional coatings, especially for the surface engineering of polymeric membranes.[33, 34] During the DA-based coating process, a thin adherent polydopamine (PDA) film is anchored on the surface of a substrate immersed in the

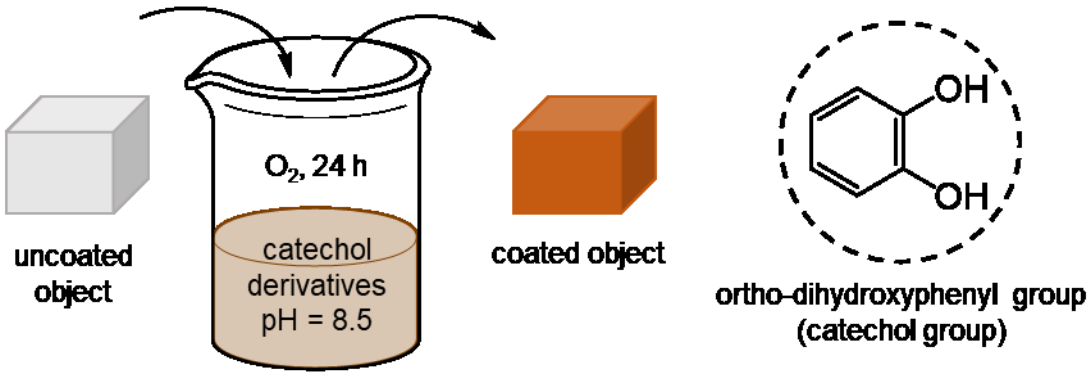

Figure 1.2 A schematic illustration of catecholic surface chemistry by immersing an object in an alkaline solution and chemical formula of the catecholic unit.

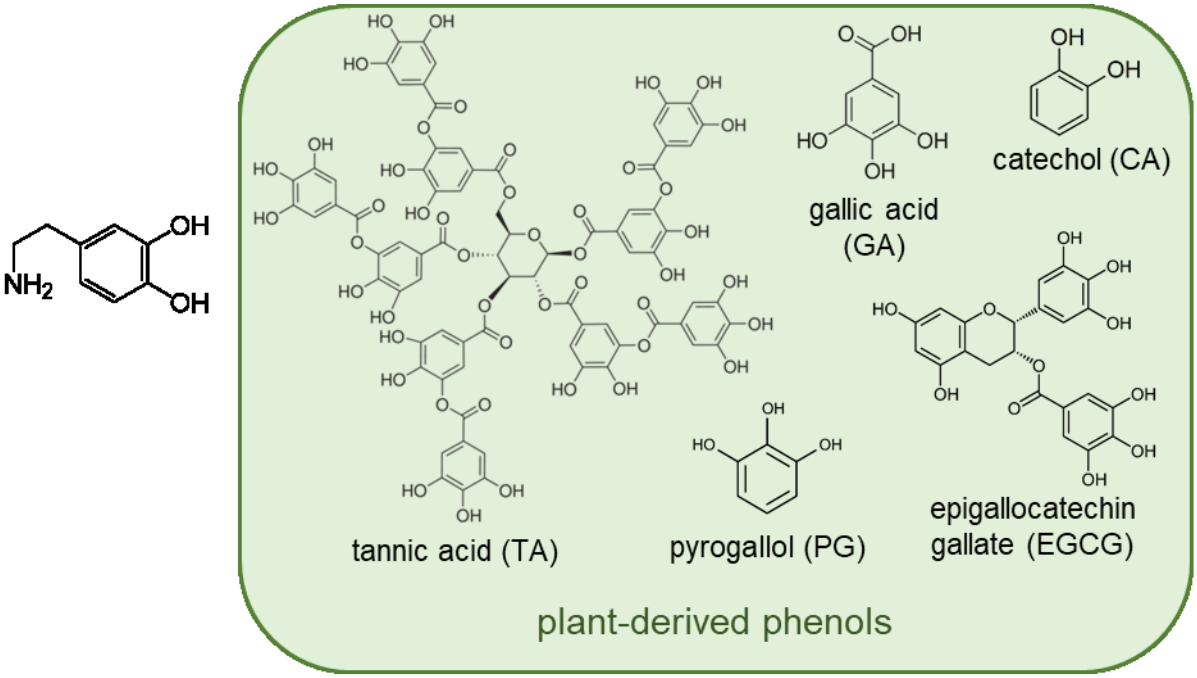

Figure 1.3 Dopamine and other catecholic molecules derived from plant.

DA solution.[35] Although the use of DA in membrane science covers nearly all applications ranging from separation to emulsification,[36-38] several shortcomings exist which limits their industrial applications. For example, DA deposition is a lengthy (normally up to 24 hours) and low-efficient process, thus causing cost overruns and secondary pollution. On the other hand, the dark color of PDA-coated surfaces may become its limitation for some applications. One of the latest developments in this area is using nitrogen-free polyphenols with a structure similar to

dopamine as coating precursors (Figure 1.3). These natural compounds are ubiquitous in nature, and most importantly, share many common advantages with DA, namely simplicity, versatile adhesion capability and multifunctionality.[39] In addition, polyphenols (catechol is 39.8 CAD per 100 gram when purchasing from Sigma-Aldrich) are much cheaper than dopamine (439.0 CAD per 100 gram), making them a perfect candidate for industrial-scale processes. Despite many appealing features of such materials, several limitations hinder their widespread utilization in modifying polymer membranes. These drawbacks comprise low-efficiency deposition rate, multiple steps needed to accommodate all the requirements, and poor coating stability under extreme pH conditions. In these cases, future efforts are needed to address one or more of these challenges for broadening the applicable scope of functional phenolic substances.

1.4 Objectives

Membrane processes are an emerging and attractive future trend in wastewater treatment and emulsification. Tailoring the surface properties of existing membranes is the main direction in developing functionalized and high-performance membranes for a wide array of purposes. In spite of the promise offered by plant-inspired phenolic coatings, only a limited number of applications are served by such coatings because of their aforementioned shortcomings. Therefore, a facial and high-efficient surface modification technology using phenolic compounds is highly desirable. The main objectives of this dissertation are described below:

1. To propose a facile strategy for fast, inexpensive deposition of the plant phenol coatings and demonstrate the versatility of this approach.
2. To study the mechanism of oxidant-induced plant phenol polymerization and deposition.
3. To investigate the influence of plant phenol modification on the surface properties of PVDF membranes.

4. To fabricate optimized membranes for different practices, including copper ion adsorption, oil/water separation, and generation of double emulsions.

1.5 References

[1] A.G.F. Norman N Li, W. S. Winston Ho, Takeshi Matsuura, Advanced membrane technology and applications, John Wiley & Sons, 2011.

[2] M.G. Buonomenna, Membrane processes for a sustainable industrial growth, Rsc Adv, 3 (2013) 5694-5740.

[3] M. Ulbricht, Advanced functional polymer membranes, Polymer, 47 (2006) 2217-2262.

[4] G. Amy, N. Ghaffour, Z.Y. Li, L. Francis, R.V. Linares, T. Missimer, S. Lattemann, Membrane-based seawater desalination: Present and future prospects, Desalination, 401 (2017) 16-21.

[5] M. Peter-Varbanets, F. Hammes, M. Vital, W. Pronk, Stabilization of flux during dead-end ultra-low pressure ultrafiltration, Water Res, 44 (2010) 3607-3616.

[6] N.L. Le, S.P. Nunes, Materials and membrane technologies for water and energy sustainability, Sustain Mater Techno, 7 (2016) 1-28.

[7] Y.Z. Zhu, D. Wang, L. Jiang, J. Jin, Recent progress in developing advanced membranes for emulsified oil/water separation, Npg Asia Mater, 6 (2014).

[8] Z.L. Chu, Y.J. Feng, S. Seeger, Oil/Water Separation with Selective Superantiwetting/Superwetting Surface Materials, Angew Chem Int Edit, 54 (2015) 2328-2338.

[9] W.B. Zhang, Y.Z. Zhu, X. Liu, D. Wang, J.Y. Li, L. Jiang, J. Jin, Salt-Induced Fabrication of Superhydrophilic and Underwater Superoleophobic PAA-g-PVDF Membranes for Effective Separation of Oil-in-Water Emulsions, Angew Chem Int Edit, 53 (2014) 856-860.

[10] Y.Z. Zhu, F. Zhang, D. Wang, X.F. Pei, W.B. Zhang, J. Jin, A novel zwitterionic polyelectrolyte grafted PVDF membrane for thoroughly separating oil from water with ultrahigh efficiency, J Mater Chem A, 1 (2013) 5758-5765.

[11] Z.X. Xue, S.T. Wang, L. Lin, L. Chen, M.J. Liu, L. Feng, L. Jiang, A Novel Superhydrophilic and Underwater Superoleophobic Hydrogel-Coated Mesh for Oil/Water Separation, Adv Mater, 23 (2011) 4270-4273.

[12] X. Yao, Y.L. Song, L. Jiang, Applications of Bio-Inspired Special Wettable Surfaces, Adv Mater, 23 (2011) 719-734.

[13] S.M. Joscelyne, G. Tragardh, Membrane emulsification - a literature review, Journal of Membrane Science, 169 (2000) 107-117.

[14] C. Charcosset, Preparation of emulsions and particles by membrane emulsification for the food processing industry, J Food Eng, 92 (2009) 241-249.

[15] J.P. Ju, T.M. Wang, Q.H. Wang, A facile approach in fabricating superhydrophobic and superoleophilic poly (vinylidene fluoride) membranes for efficient water-oil separation, J Appl Polym Sci, 132 (2015).

[16] K. Sikhwivhilu, R.M. Moutloali, Functionalized PVDF membrane-immobilized Fe/Ni bimetallic nanoparticles for catalytic degradation of methyl orange dye: a comparative study, Mater Today-Proc, 2 (2015) 4070-4080.

[17] K.P. Prathish, V. Vishnuvardhan, T.P. Rao, Rational Design of In Situ Monolithic Imprinted Polymer Membranes for the Potentiometric Sensing of Diethyl Chlorophosphate - a Chemical Warfare Agent Simulant, Electroanal, 21 (2009) 1048-1056.

[18] J.H. Fu, J. Ji, W.Y. Yuan, J.C. Shen, Construction of anti-adhesive and antibacterial multilayer films via layer-by-layer assembly of heparin and chitosan, Biomaterials, 26 (2005) 6684-6692.

[19] C.X. Liu, D.R. Zhang, Y. He, X.S. Zhao, R.B. Bai, Modification of membrane surface for anti-biofouling performance: Effect of anti-adhesion and anti-bacteria approaches, J Membrane Sci, 346 (2010) 121-130.

[20] Y. Xu, Z.H. Li, K.M. Su, T.T. Fan, L. Cao, Mussel-inspired modification of PPS membrane to separate and remove the dyes from the wastewater, Chem Eng J, 341 (2018) 371-382.

[21] R.A. Barb, C. Hrelescu, L. Dong, J. Heitz, J. Siegel, P. Slepicka, V. Vosmanska, V. Svorcik, B. Magnus, R. Marksteiner, M. Schernthaner, K. Groschner, Laser-induced periodic surface structures on polymers for formation of gold nanowires and activation of human cells, Appl Phys a-Mater, 117 (2014) 295-300.

[22] K. Pan, R.M. Ren, H.Z. Li, B. Cao, Preparation of dual stimuli-responsive PET track-etched membrane by grafting copolymer using ATRP, Polym Advan Technol, 24 (2013) 22-27.

[23] H. Shi, Y. He, Y. Pan, H.H. Di, G.Y. Zeng, L. Zhang, C.L. Zhang, A modified mussel-inspired method to fabricate TiO2 decorated superhydrophilic PVDF membrane for oil/water separation, J Membrane Sci, 506 (2016) 60-70.

[24] T. Yuan, J.Q. Meng, T.Y. Hao, Z.H. Wang, Y.F. Zhang, A Scalable Method toward Superhydrophilic and Underwater Superoleophobic PVDF Membranes for Effective Oil/Water Emulsion Separation, Acs Appl Mater Inter, 7 (2015) 14896-14904.

[25] O. Burtovyy, V. Klep, T. Turel, Y. Gowayed, I. Luzinov, POLY 65-Modification of PET membrane surface with nanothin polymer layers via "grafting to" approach, Abstr Pap Am Chem S, 235 (2008).

[26] J.H. Choi, S.J. Gwon, J.Y. Shon, C.H. Jung, Y.E. Ihm, Y.M. Lim, Y.C. Nho, Preparation of polystyrene-grafted poly(vinylidene fluoride) membranes for lithium secondary batteries, J Ind Eng Chem, 14 (2008) 116-119.

[27] W.Z. Lang, Z.L. Xu, H. Yang, W. Tong, Preparation and characterization of PVDF-PFSA blend hollow fiber UF membrane, J Membrane Sci, 288 (2007) 123-131.

[28] F. Liu, Y.Y. Xu, B.K. Zhu, F. Zhang, L.P. Zhu, Preparation of hydrophilic and fouling resistant poly(vinylidene fluoride) hollow fiber membranes, J Membrane Sci, 345 (2009) 331-339.

[29] M.L. Steen, A.C. Jordan, E.R. Fisher, Hydrophilic modification of polymeric membranes by low temperature H2O plasma treatment, J Membrane Sci, 204 (2002) 341-357.

[30] H.Y. Yu, Y. Xie, M.X. Hu, J.L. Wang, S.Y. Wang, Z.K. Xu, Surface modification of polypropylene microporous membrane to improve its antifouling property in MBR: CO2 plasma treatment, J Membrane Sci, 254 (2005) 219-227.

[31] A.G. Fane, R. Wang, M.X. Hu, Synthetic Membranes for Water Purification: Status and Future, Angew Chem Int Edit, 54 (2015) 3368-3386.

[32] L. Ni, J.Q. Meng, X.G. Li, Y.F. Zhang, Surface coating on the polyamide TFC RO membrane for chlorine resistance and antifouling performance improvement, J Membrane Sci, 451 (2014) 205-215.

[33] H. Lee, S.M. Dellatore, W.M. Miller, P.B. Messersmith, Mussel-inspired surface chemistry for multifunctional coatings, Science, 318 (2007) 426-430.

[34] Y.L. Liu, K.L. Ai, L.H. Lu, Polydopamine and Its Derivative Materials: Synthesis and Promising Applications in Energy, Environmental, and Biomedical Fields, Chem Rev, 114 (2014) 5057-5115.

[35] M.E. Yu, J.Y. Hwang, T.J. Deming, Role of L-3,4-dihydroxyphenylalanine in mussel adhesive proteins, J Am Chem Soc, 121 (1999) 5825-5826.

[36] Y. Lv, H.C. Yang, H.Q. Liang, L.S. Wan, Z.K. Xu, Nanofiltration membranes via co-deposition of polydopamine/polyethylenimine followed by cross-linking, J Membrane Sci, 476 (2015) 50-58.

[37] Y. Lv, Y. Du, W.Z. Qiu, Z.K. Xu, Nanocomposite Membranes via the Codeposition of Polydopamine/Polyethylenimine with Silica Nanoparticles for Enhanced Mechanical Strength and High Water Permeability, Acs Appl Mater Inter, 9 (2017) 2966-2972.

[38] M.B. Wu, H.C. Yang, J.J. Wang, G.P. Wu, Z.K. Xu, Janus Membranes with Opposing Surface Wettability Enabling Oil-to-Water and Water-to-Oil Emulsification, Acs Appl Mater Inter, 9 (2017) 5062-5066.

[39] T.S. Sileika, D.G. Barrett, R. Zhang, K.H.A. Lau, P.B. Messersmith, Colorless Multifunctional Coatings Inspired by Polyphenols Found in Tea, Chocolate, and Wine, Angew Chem Int Edit, 52 (2013) 10766-10770.

Chapter 2 Literature Review

2.1 Plant-Inspired Surface Chemistry

The adhesives found in nature offer insights into developing new surface chemical methods. Phenolic compounds, widely distributed in plant tissues, display diverse biological functions ranging from pigmentation to defense of ultraviolet (UV) radiation.[1] Recently natural polyphenols are of particular interest to materials scientists due to their intriguing physicochemical properties. Polyphenols contain an enormous abundance and density of catechol (CA) functional groups that are easily subject to oxidation upon exposure to air, resulting in browning of natural products.[2] Most importantly, they exhibit strong solid–liquid interfacial properties that allow them to attach to all kinds of solid surfaces, which is believed to be the result of high content of CA groups. A clear understanding of the secret of polyphenol coatings is not only necessary for the applications of plant-inspired surface chemistry in membrane science, but is also essential for potential applications in other fields. Therefore, there has been a remarkable increase in the number of published studies on their structures, mechanism of formation, and functions over the past few years.

2.1.1 Mechanism of Polyphenol Coatings

Generally, the overall process of obtaining polyphenol coatings consists of two steps: (1) the formation of phenol-based crosslinked polymers in the solution; (2) the assembly of these polymers on the surface of the immersed object.

Formation of CA-Based Crosslinked Polymers

CA is capable of diverse chemistry, enabling it to react with various molecules through different crosslinking pathways. The following part will be structured according to the possible crosslinking mechanisms that have been most extensively researched so far. Catechols have been known for

years to be susceptible to auto-polymerization in aerated basic conditions. Although not yet fully understood, the mechanism of the oxidative self-polymerization is believed to start from the oxidation of the CA group, followed by further oxidation and polymerization. In the first auto-oxidation step, phenolic compounds, or more typically, CA group, is spontaneously oxidized to *o*-quinone at alkaline pH in the presence of dissolved oxygen in solution. The subsequent couplings between *o*-quinones and catechols can generate oligomers that can further recombine to polymers (Figure 2.1a).[3] The exact structures of these crosslinked polymers have not been perfectly identified yet. However, some hypotheses can be found in publications (Figure 2.1b). Dubey et al. reported that poly(catechol) structure was linked together with ether bonds.[4] Aktas et al. proposed that catechol units were based on C–C linkages rather than bonding with the ether oxygen.[5] The phenol oxidative polymerization is influenced by several factors, such as the phenol concentration, solution pH, the presence of oxidants, etc. Oxygen plays a key role as oxidant during this polymerization process. It has also been proved by experiments that phenol polymerization can only occur in a weak alkaline condition, because the high pH can induce deprotonation of the catecholic dihydroxyl group protons.

In addition to self-polymerization, phenolic compounds can also undergo reactions with compounds bearing amine or thiol groups via the Michael addition or Schiff base reaction, leading to the conjugation or cross-linking of polyphenols (Figure 2.1c). This is because *o*-quinone groups are highly reactive electrophilic intermediates, capable of reacting with nucleophiles.[6] Previous investigations have revealed that in the presence of transition metals, CA can serve as a good ligand for cations, for instance, iron or copper ions, giving rise to catechol–metal complexes through strong coordination bonds (Figure 2.1d).[7] In contrast to the aforementioned crosslinked

polymers (Figure 2.1a-c), the coordination of metal ions with phenols can provide stable, yet reversible, crosslinking points between polymers.

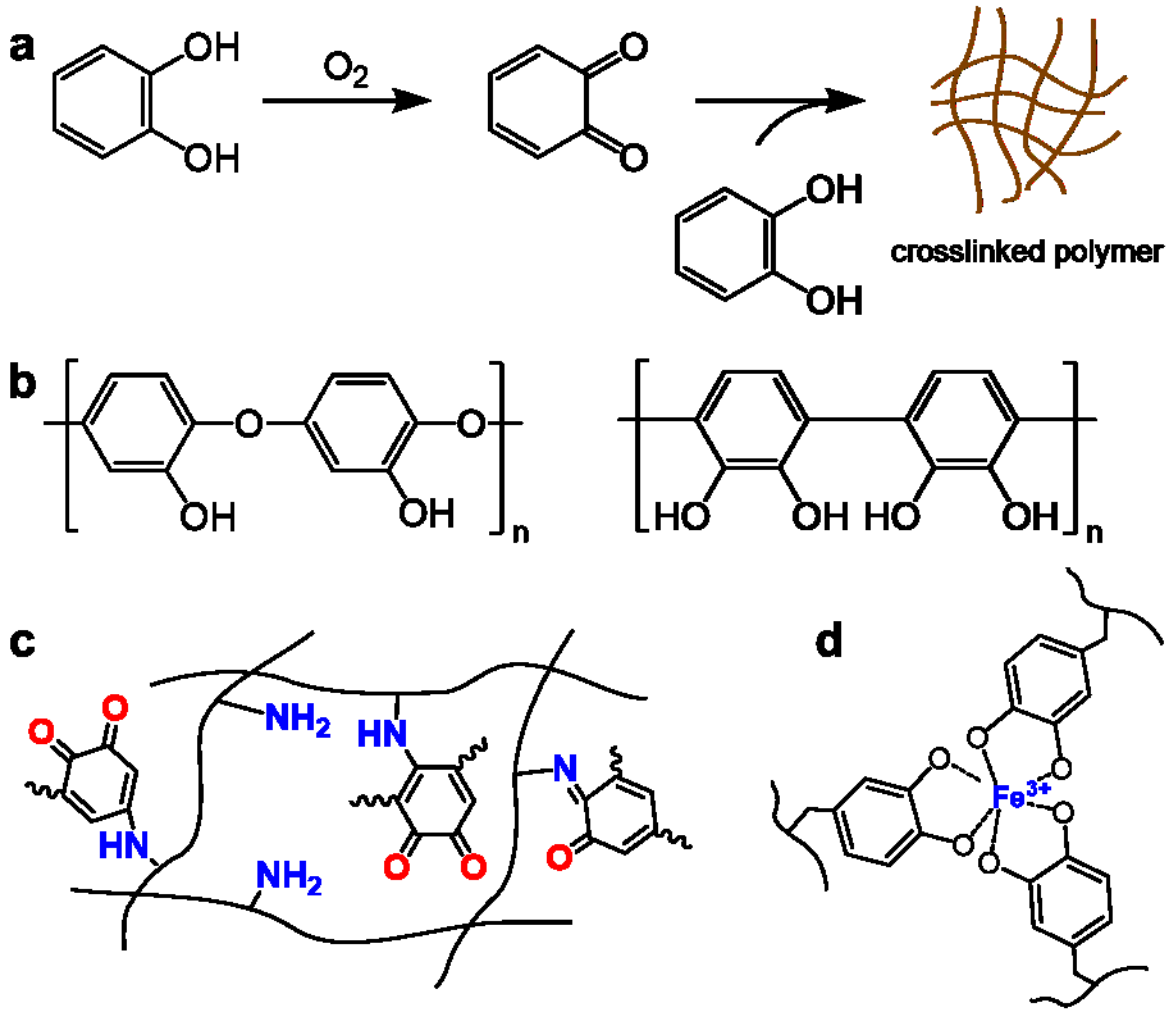

Figure 2.1 (a) A brief scheme of the oxidative crosslinking of catechol. (b) Structures for CA-based oxidative crosslinked polymers proposed by Dubey (left)[4] and Aktas (right)[5]. Proposed structure for the formation of CA-based (c) polyphenol/polyamine aggregates[6] and (d) CA–Fe^{3+} complexes[7].

Polyphenol Deposition on Surfaces

Polyphenols show excellent adhesive properties which can be adhered to virtually any type of bulk material surfaces immersed in the solution. Different interactions, such as covalent and non-

covalent interactions, are believed to be involved in the polyphenol deposition process. For covalent interactions, quinone formed from the oxidation process can form interfacial covalent bonds with various nucleophilic functional groups present on target substrates, such as $–NH_2$, –SH, imidazole. For non-covalent interactions, the benzene ring of CA is able to form π–π stacking

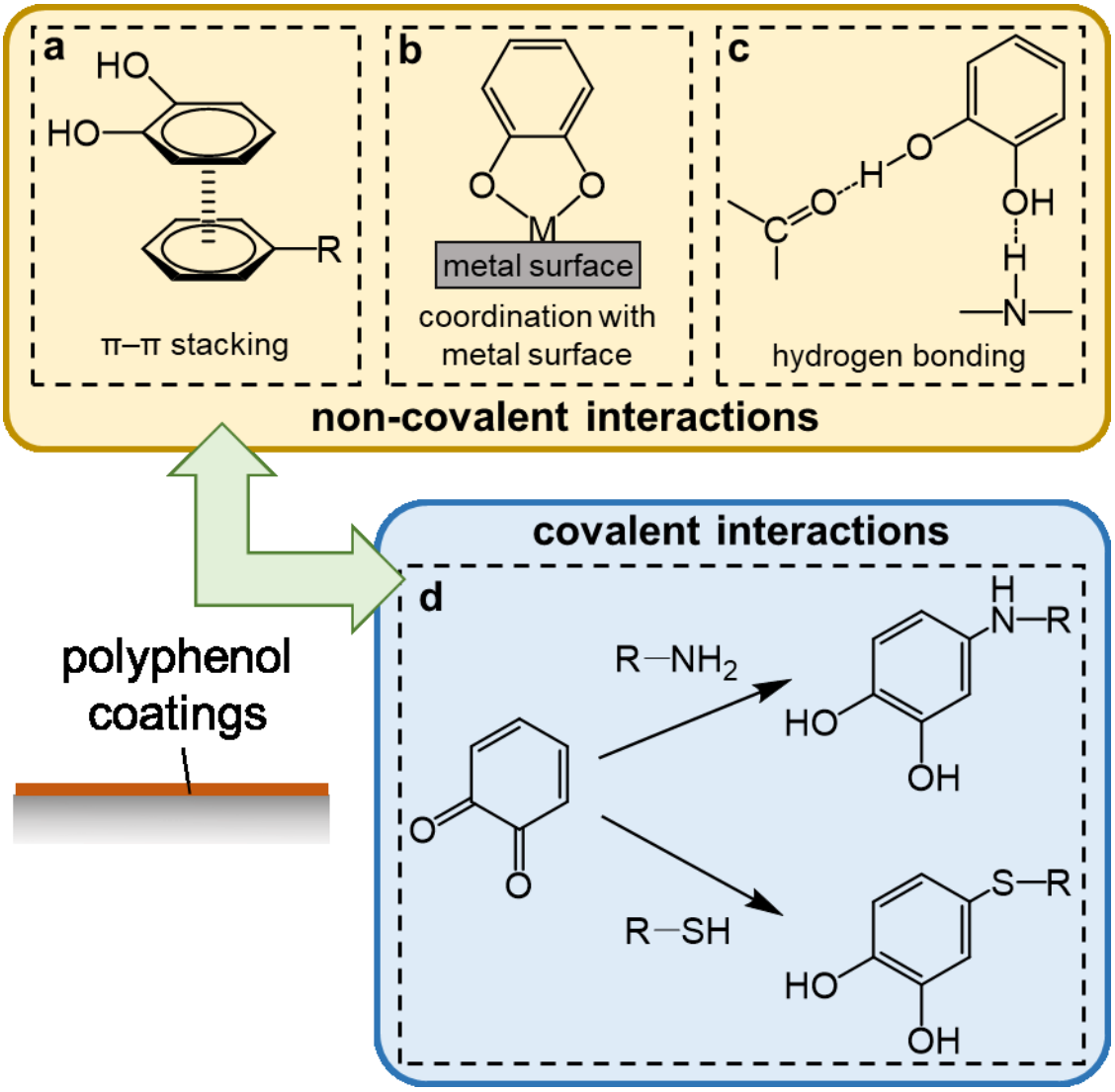

Figure 2.2 Possible interactions of polyphenol coatings with substrates. CA forms (a) π–π stacking with other aromatic rings, (b) coordination bonds with metal surfaces, and (c) hydrogen bonds through its hydroxyl group. (d) Quinone reacts with amines and thiols through Michael addition or Schiff base reaction.

with other aromatic rings, which enables the adsorption of CA-containing molecules to aromatic-rich surfaces (e.g., polystyrene).[8] The ability of CA to bind to metal surfaces has also been reported.[9] During this process, CA forms strong, reversible interfacial bonds with metals (i.e., stainless steel) or metal oxides (i.e., Au_2O_3, Al_2O_3, SiO_2, TiO_2). CA also forms extensive hydrogen bonds through its hydroxyl groups, allowing CA to attach to hydrogen bonding sites.[10, 11]

The CA-decorated surfaces have reactivity toward thiols, amines, and metal ions, enabling subsequent layer-by-layer self-assembly through covalent grafting of polymers via *in-situ* polymerization or deposition of metal films via reduction of metal ions.

2.1.2 Recent Advances in Controllable Deposition of Polyphenol Coatings

Tedious and low-efficient deposition is the major limitation for the practical implementation of catechol-inspired surface modification. One of the most significant developments in the field is achieving fast deposition of polyphenol on substrates with controllability. The dominating step during phenol polymerization is the oxidation of catechol to produce o-quinone. Thus, the primary approach to accelerating phenol polymerization is to enhance the oxidation rate.

Enzymatic Oxidation

During in vivo biosynthesis, small phenolics such as monolignols and flavonoids can be oxidized, in the presence of enzymes, yielding their corresponding semiquinones and quinones. These compounds are highly reactive and can further interact with molecules including phenols, amino acids, and proteins, giving rise to various polymeric phenolic components responsible for the browning reaction.[12] Dosoretz et al. demonstrated that catechol can undergo polymerization under oxidation of horseradish peroxidase (HRP) in aqueous medium and water-soluble polymeric components were obtained.[13] Jeon et al. conducted laccase-catalyzed polymerization of plant phenols on different substrates, such as aluminum, glass, and polymers.[14]

UV Irradiation

UV light is able to generate reactive oxygen species (ROS) speeding up the oxidation.[15] Taking this into account, UV light is a good alternative for reactions requiring an oxidation process, thereby providing the reaction with enhanced controllability. Levkin's group found that UV irradiation could realize rapid and uniform deposition of polyphenolic coatings with spatial and temporal control.[16]

Chemical Oxidation

Catechol groups are also readily oxidized upon addition of chemical oxidants. Studies have suggested that oxidants are capable of inducing dopamine polymerization.[17, 18] The most commonly used oxidants are ammonium persulfate (AP), potassium chlorate (PC), and sodium periodate (SP). Ponzio et al. provided the comparison of different effects presented by three oxidants, and pointed out that polydopamine coatings with adequate thickness and high homogeneity were obtained using 20 mM SP at pH 5.[18] Recently, Zhang et al. have proposed a $CuSO_4/H_2O_2$-triggered strategy for rapid coating of PDA.[19] It was demonstrated that the deposition rate was tremendously enhanced because of the ROS generated by $CuSO_4/H_2O_2$. Nevertheless, the use of metal-containing oxidants unavoidably leads to surface contamination of the PDA film caused by metal ions.

Oxidant-Free Polymerization

Usually, the chemical reagent triggered reaction was not capable of effectively controlling the onset and termination of the polymerization. Hence, attempts have been made to realize fast and controllable formation of PDA coatings without adding oxidizing agents. Microwave irradiation was reported to show enhanced PDA coating kinetics, yielding rapid formation of polydopamine.[20] During the microwave-assisted process, the predominant factor was free

radicals generated from dopamine by radiation, instead of the increased temperature. Microplasma electrochemistry was also used in developing enhanced and controlled PDA coatings since the microplasma cathode could induce and drastically enhance the polymerization behavior of dopamine.[21]

2.2 Membrane in Water Purification

Polymer-based membranes such as PVDF have become a viable alternative method for oily wastewater cleanup. Owing to the different oil/water interfacial tension, utilizing materials having superwetting features (namely, superhydrophobic-superoleophilic or superhydrophilic-underwater superoleophobic) to achieve the demulsification of various types of emulsions has attracted substantial attention.[22] The wetting behaviors of membranes are decided by the combination of surface free energy and surface roughness.[23] Thus, a membrane can be endowed with special wettability and shows selectivity for oil or water through the adjustment of the structure and chemical composition of the material.

2.2.1 Superhydrophobic/Superoleophilic Membranes

Superhydrophobic membranes can selectively remove oil from oil/water mixtures, ascribed to their distinct low surface energy characteristics. For example, Recently, Jang's group made PVDF membranes with superhydrophobicity and superoleophilicity through an ammonia-induced phase-inversion process.[24] The addition of ammonia into a PVDF solution caused localized microphase to separate and PVDF clusters to precipitate, ending up with a membrane constitutive of spherical particles. In another example, Zhou et al. fabricated a nonwoven superhydrophobic membrane via electrospinning of PVDF from its N,N-dimethylformamide/acetone solutions.[25] Moreover, the hydrophobicity of PVDF membranes is tunable by adjusting the PVDF content in the solutions during the electrospinning process.

2.2.2 Superhydrophilic/Underwater Superoleophobic Membranes

The oil-fouling problem in superhydrophobic polymeric membranes can be extremely serious, which leads to frequent cleaning procedures, unavoidable operation cost, and shortened lifespan of membranes. Over the past several years, much attention has been particularly focused on the excellent self-cleaning and anti-fouling properties of fish scales.[26] Studies revealed that a water cushion can be trapped in the rough area of fish scales owing to its hydrophilic materials composed of calcium phosphate, protein, and a thin layer of mucus. The trapped water prevents direct contact between oils and materials, causing an oleophobic surface. If the surface roughness is increased, the surface may become superoleophobic.[27] Inspired from the oil repellency behavior of fish scales, underwater superoleophobic membranes are developed through the synergetic effect of hydrophilic chemical compositions and micro/nanohierarchical structures. Zhang and co-workers developed a superhydrophilic/underwater superoleophobic poly-(acrylic acid)-grafted PVDF membrane, which consisted of hydrophilic coatings and rough micelle aggregates on the porous substrate.[28] It can successfully separate either surfactant-free mixtures or surfactant-stabilized emulsions under very low transmembrane pressure. During the continuous filtration process, the underwater superoleophobicity and low oil-adhesive property prevented the membrane from fouling by oils, giving rise to the ease of recycling. Recently, taking advantage of the simplicity of mussel-inspired chemistry, Zhang's group reported a novel one-step dip-coating methodology that a silane coupling agent was incorporated to co-polymerize with dopamine to directly bind TiO_2 nanoparticles on PVDF membrane surfaces.[29] The as-prepared organic-inorganic hybrid membranes were endowed with selective separation of various types of emulsions and durable oil resistance. These representative publications on the fabrication of superhydrophilic polymeric membranes offer possibilities for their applications in oil/water separation.

2.3 Membrane Emulsification

Over the past few decades, there has been an increasing interest in using membrane emulsification to produce emulsions.[30] This emerging approach gives some potential advantages over the traditional methods, including simplicity of the process, need for less surfactant, energy requirement reduction and narrow size distributions.

2.3.1 Influence of Process Parameters

The membrane emulsification process employs a low pressure to press the dispersed phase to penetrate through a porous membrane into the continuous phase (Figure 2.3).[31] There are several important factors influencing emulsifying performance.

The most crucial parameter determining the droplet size is the geometrical structure of the membrane, namely, the membrane pore size. Membranes having very narrow pore-size distributions are necessary for the preparation of monodispersed emulsions. The membrane porosity, indicative of the distance between two neighboring pores, also plays a key role during the emulsification membrane process.[32] Because when two adjacent drops are sufficiently close to each other, they are prone to minimize the interfacial tension, eventually leading to coalescence.

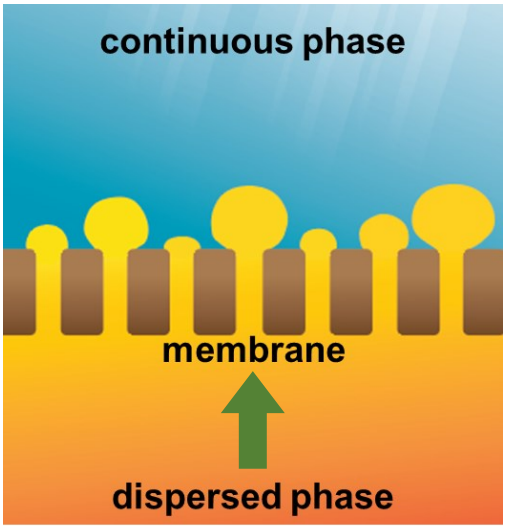

Figure 2.3 Schematic diagram of the membrane emulsification process.

Abrahamse and co-workers determined the maximum porosity for a membrane of 5 μm diameter to be 1.5% in order to avoid coalescing with droplets at adjacent pores.[33] However, a lower dispersed phase release rate is obtained for membranes with lower porosity.

It has been generally observed that the membrane pores should be continuous phase-wettable, that is to say, a hydrophilic membrane wetted with the water phase is suitable for making oil-in-water emulsions and a hydrophobic membrane wetted with the oil phase for water-in-oil emulsions.[34] Observations showed that oil-in-water emulsions generated by hydrophobic membranes have larger drop sizes and are more polydispersed in comparison with hydrophilic membranes.[31, 35] Similar behavior was found when the adsorption of anionic surfactant sodium dodecyl sulfate (SDS) on a positively charged membrane surface radically altered the wettability of the membrane surface.[35]

In addition to membrane parameters, the characteristic properties of the flowing continuous phase droplets (i.e., the velocity) also have significant effects on droplets growing on the surface of the membrane. Typically, the droplet size decreases as the flux increases, but the effect of the flux on decreasing droplet size is governed mainly by the size of membrane pore, which is more efficient for membranes with smaller pore sizes.[36]

2.3.2 Preparation of Double Emulsions

Double emulsions are important in the fabrication of low calorie food products, drugs encapsulating active ingredients, cosmetics, and other high value-added goods. Double emulsions are defined as droplets having smaller droplets contained within them. Water-in-oil-in-water (W/O/W) emulsions and oil-in-water-in-oil (O/W/O) emulsions are examples of double emulsions. Considerable research attention has been paid to the development of new approaches to generating double emulsions over the last several decades. Membrane emulsification is attractive because of

its energy-saving operation, higher degree control of drop size and distribution of drops, simple equipment, and commercial viability compared with the traditional high-pressure homogenization and mechanical stirring.[37]

The commonly used procedures in membrane emulsification can be divided into two groups: cross-flow membrane emulsification and pre-mix membrane emulsification. During cross-flow, the to-be-dispersed phase is pumped through the membrane under gas pressure and forms droplets at the pore mouth. These droplets grow and then are detached by the continuous phase circulating tangentially to the membrane surface.[38] In the latter technique, a coarse pre-mix emulsion is produced, subsequently being compressed through the membrane pores in order to obtain finer drops. Although the resultant droplets have a slightly wider size distribution than those made by cross-flow membrane emulsification, they are still more uniform than commonly obtained by conventional processes.[39] A better control of the resulting emulsion drops can be produced using microfluidic techniques, but at very low production rates.[40]

Mine et al. firstly demonstrated the use of Shirasu porous glass (SPG) membranes to generate W/O/W emulsions in a membrane emulsification system.[41] They prepared simple W/O emulsions first by a microfluidizer, which were permeated through SPG membranes in the following emulsification step. It was found that the membrane has to be prewetted with the continuous phase and should have a mean pore size larger than or equal to twice the diameter of the inner droplets in the simple emulsion. Otherwise, the membrane pores will hinder the penetration of these emulsion drops and it will be impossible to make double emulsions. Since then, a number of studies have been carried out on the usage of similar procedures to fabricate double emulsions with different chemical compositions for a variety of applications.[30] For example, Su's group successfully prepared insulin-loaded microcapsules that can be used as drug

carriers in controlled-release delivery systems via membrane emulsification.[42] A water-in-oil primary emulsion firstly made by a homogenizer passed through an SPG membrane into an external aqueous phase under the pressure of nitrogen gas, eventually forming narrow-dispersed W/O/W emulsion drops. Upon solvent evaporation from the double emulsions, solid polymer microcapsules were obtained. In another example, Berendsen and co-workers reported the fabrication of procyanidin-loaded W/O/W drops through a similar two-step procedure, where a water-in-oil emulsion produced by a rotor-stator homogenizer was dispersed to the outside aqueous phase by repeated premix membrane emulsification.[43] These double emulsions were subsequently fed into a spray dryer and the rapid water evaporation resulted in microcapsule formation. Overall, membrane emulsification has been proved to be a powerful and reliable technique used for the generation of double emulsions.[44-46]

2.4 References

[1] S. Quideau, D. Deffieux, C. Douat-Casassus, L. Pouysegu, Plant Polyphenols: Chemical Properties, Biological Activities, and Synthesis, Angew Chem Int Edit, 50 (2011) 586-621.

[2] H. Wagreich, J.M. Nelson, On the oxidation product of catechol when oxidized by means of tyrosinase, J Biol Chem, 115 (1936) 459-465.

[3] J. Yang, M.A.C. Stuart, M. Kamperman, Jack of all trades: versatile catechol crosslinking mechanisms, Chem Soc Rev, 43 (2014) 8271-8298.

[4] S. Dubey, D. Singh, R.A. Misra, Enzymatic synthesis and various properties of poly(catechol), Enzyme Microb Tech, 23 (1998) 432-437.

[5] N. Aktas, N. Sahiner, O. Kantoglu, B. Salih, A. Tanyolac, Biosynthesis and characterization of laccase catalyzed poly(catechol), J Polym Environ, 11 (2003) 123-128.

[6] A.A. Kutyrev, Nucleophilic Reactions of Quinones, Tetrahedron, 47 (1991) 8043-8065.

[7] N. Bandara, H.B. Zeng, J.P. Wu, Marine mussel adhesion: biochemistry, mechanisms, and biomimetics, J Adhes Sci Technol, 27 (2013) 2139-2162.

[8] A.M. Baty, P.K. Leavitt, C.A. Siedlecki, B.J. Tyler, P.A. Suci, R.E. Marchant, G.G. Geesey, Adsorption of adhesive proteins from the marine mussel, Mytilus edulis, on polymer films in the hydrated state using angle dependent X-ray photoelectron spectroscopy and atomic force microscopy, Langmuir, 13 (1997) 5702-5710.

[9] R. Kummert, W. Stumm, The Surface Complexation of Organic-Acids on Hydrous Gamma-Al2o3, J Colloid Interf Sci, 75 (1980) 373-385.

[10] M.P. Deacon, S.S. Davis, J.H. Waite, S.E. Harding, Structure and mucoadhesion of mussel glue protein in dilute solution, Biochemistry-Us, 37 (1998) 14108-14112.

[11] K. Huang, B.P. Lee, D.R. Ingram, P.B. Messersmith, Synthesis and characterization of self-assembling block copolymers containing bioadhesive end groups, Biomacromolecules, 3 (2002) 397-406.

[12] L. Pourcel, J.M. Routaboul, V. Cheynier, L. Lepiniec, I. Debeaujon, Flavonoid oxidation in plants: from biochemical properties to physiological functions, Trends Plant Sci, 12 (2007) 29-36.

[13] G. Ward, R.E. Parales, C.G. Dosoretz, Biocatalytic synthesis of polycatechols from toxic aromatic compounds, Environ Sci Technol, 38 (2004) 4753-4757.

[14] J.R. Jeon, J.H. Kim, Y.S. Chang, Enzymatic polymerization of plant-derived phenols for material-independent and multifunctional coating, J Mater Chem B, 1 (2013) 6501-6509.

[15] H. Bayir, Reactive oxygen species, Crit Care Med, 33 (2005) S498-S501.

[16] F. Behboodi-Sadabad, H.J. Zhang, V. Trouillet, A. Welle, N. Plumere, P.A. Levkin, UV-Triggered Polymerization, Deposition, and Patterning of Plant Phenolic Compounds, Adv Funct Mater, 27 (2017).

[17] Q. Wei, F.L. Zhang, J. Li, B.J. Li, C.S. Zhao, Oxidant-induced dopamine polymerization for multifunctional coatings, Polym Chem-Uk, 1 (2010) 1430-1433.

[18] F. Ponzio, J. Barthes, J. Bour, M. Michel, P. Bertani, J. Hemmerle, M. d'Ischia, V. Ball, Oxidant Control of Polydopamine Surface Chemistry in Acids: A Mechanism-Based Entry to Superhydrophilic-Superoleophobic Coatings, Chem Mater, 28 (2016) 4697-4705.

[19] C. Zhang, Y. Ou, W.X. Lei, L.S. Wan, J. Ji, Z.K. Xu, CuSO4/H2O2-Induced Rapid Deposition of Polydopamine Coatings with High Uniformity and Enhanced Stability, Angew Chem Int Edit, 55 (2016) 3054-3057.

[20] M. Lee, S.H. Lee, I.K. Oh, H. Lee, Microwave-Accelerated Rapid, Chemical Oxidant-Free, Material-Independent Surface Chemistry of Poly(dopamine), Small, 13 (2017).

[21] Z. Wang, C. Xu, Y.X. Lu, G.Y. Wei, G. Ye, T.X. Sun, J. Chen, Microplasma-assisted rapid, chemical oxidant-free and controllable polymerization of dopamine for surface modification, Polym Chem-Uk, 8 (2017) 4388-4392.

[22] Z.X. Xue, Y.Z. Cao, N. Liu, L. Feng, L. Jiang, Special wettable materials for oil/water separation, J Mater Chem A, 2 (2014) 2445-2460.

[23] X.J. Feng, L. Jiang, Design and creation of superwetting/antiwetting surfaces, Adv Mater, 18 (2006) 3063-3078.

[24] W.B. Zhang, Z. Shi, F. Zhang, X. Liu, J. Jin, L. Jiang, Superhydrophobic and Superoleophilic PVDF Membranes for Effective Separation of Water-in-Oil Emulsions with High Flux, Adv Mater, 25 (2013) 2071-2076.

[25] Z.P. Zhou, X.F. Wu, Electrospinning superhydrophobic-superoleophilic fibrous PVDF membranes for high-efficiency water-oil separation, Mater Lett, 160 (2015) 423-427.

[26] M.J. Liu, S.T. Wang, Z.X. Wei, Y.L. Song, L. Jiang, Bioinspired Design of a Superoleophobic and Low Adhesive Water/Solid Interface, Adv Mater, 21 (2009) 665-+.

[27] T. Jiang, Z.G. Guo, W.M. Liu, Biomimetic superoleophobic surfaces: focusing on their fabrication and applications, J Mater Chem A, 3 (2015) 1811-1827.

[28] W.B. Zhang, Y.Z. Zhu, X. Liu, D. Wang, J.Y. Li, L. Jiang, J. Jin, Salt-Induced Fabrication of Superhydrophilic and Underwater Superoleophobic PAA-g-PVDF Membranes for Effective Separation of Oil-in-Water Emulsions, Angew Chem Int Edit, 53 (2014) 856-860.

[29] H. Shi, Y. He, Y. Pan, H.H. Di, G.Y. Zeng, L. Zhang, C.L. Zhang, A modified mussel-inspired method to fabricate TiO2 decorated superhydrophilic PVDF membrane for oil/water separation, J Membrane Sci, 506 (2016) 60-70.

[30] E. Piacentini, E. Drioli, L. Giorno, Membrane emulsification technology: Twenty-five years of inventions and research through patent survey, J Membrane Sci, 468 (2014) 410-422.

[31] S.M. Joscelyne, G. Tragardh, Membrane emulsification - a literature review, Journal of Membrane Science, 169 (2000) 107-117.

[32] R.A. Williams, S.J. Peng, D.A. Wheeler, N.C. Morley, D. Taylor, M. Whalley, D.W. Houldsworth, Controlled production of emulsions using a crossflow membrane part II: Industrial scale manufacture, Chem Eng Res Des, 76 (1998) 902-910.

[33] A.J. Abrahamse, A. van der Padt, R.M. Boom, W.B.C. de Heij, Process fundamentals of membrane emulsification: Simulation with CFD, Aiche J, 47 (2001) 1285-1291.

[34] C. Charcosset, I. Limayem, H. Fessi, The membrane emulsification process - a review, J Chem Technol Biot, 79 (2004) 209-218.

[35] T. Nakashima, M. Shimizu, M. Kukizaki, Membrane Emulsification by Microporous Glass, Inorganic Membranes : Icim2-91, (1991) 513-516.

[36] V. Schroder, H. Schubert, Production of emulsions using microporous, ceramic membranes, Colloid Surface A, 152 (1999) 103-109.

[37] W. Liu, X.L. Yang, W.S.W. Ho, Preparation of Uniform-Sized Multiple Emulsions and Micro/Nano Particulates for Drug Delivery by Membrane Emulsification, J Pharm Sci-Us, 100 (2011) 75-93.

[38] A.J. Gijsbertsen-Abrahamse, A. van der Padt, R.M. Boom, Status of cross-flow membrane emulsification and outlook for industrial application, J Membrane Sci, 230 (2004) 149-159.

[39] K. Suzuki, I. Fujiki, Y. Hagura, Preparation of Corn Oil/Water and Water/Corn Oil Emulsions Using PTFE Membranes, Food Sci. Technol. Int. Tokyo, 4 (1998) 164-167.

[40] G.T. Vladisavljevic, M. Shimizu, T. Nakashima, Production of multiple emulsions for drug delivery systems by repeated SPG membrane homogenization: Influence of mean pore size, interfacial tension and continuous phase viscosity, J Membrane Sci, 284 (2006) 373-383.

[41] Y. Mine, M. Shimizu, T. Nakashima, Preparation and stabilization of simple and multiple emulsions using a microporous glass membrane, Colloid Surface B, 6 (1996) 261-268.

[42] R. Liu, S.S. Huang, Y.H. Wan, G.H. Ma, Z.G. Su, Preparation of insulin-loaded PLA/PLGA microcapsules by a novel membrane emulsification method and its release in vitro, Colloid Surface B, 51 (2006) 30-38.

[43] R. Berendsen, C. Guell, M. Ferrando, Spray dried double emulsions containing procyanidin-rich extracts produced by premix membrane emulsification: Effect of interfacial composition, Food Chem, 178 (2015) 251-258.

[44] R. Liu, G.H. Ma, F.T. Meng, Z.G. Su, Preparation of uniform-sized PLA microcapsules by combining Shirasu Porous Glass membrane emulsification technique and multiple emulsion-solvent evaporation method, J Control Release, 103 (2005) 31-43.

[45] G.H. Ma, H. Sone, S. Omi, Preparation of uniform-sized polystyrene-polyacrylamide composite microspheres from a W/O/W emulsion by membrane emulsification technique and subsequent suspension polymerization, Macromolecules, 37 (2004) 2954-2964.

[46] J. Lee, D.R. Hwang, S.E. Shim, Y.M. Rhym, Controlling Morphology of Polymer Microspheres by Shirasu Porous Glass (SPG) Membrane Emulsification and Subsequent Polymerization: from Solid to Hollow, Macromol Res, 18 (2010) 1142-1147.

Chapter 3 Experimental Techniques

3.1 Ultraviolet-Visible (UV-Vis) Spectroscopy

The use of UV-Vis spectroscopy to analyze a material's structure, concentration and identity is quite prevalent, which measures the light absorbance, transmittance or reflection of a sample after the UV-Vis light passes through the sample.[1] An absorbance spectrum shows the selective absorption of a compound in the UV-Vis region, which is due to excitation of electrons within the molecule. If a molecule is exposed to particular wavelengths of light matching its energy gap, this light with the precise amount of energy will be absorbed and used to bump one of the electrons to a higher energy orbital. Organic compounds having double- and triple-bonded carbons (such as carbonyl groups, carboxyl groups, or nitro groups) are the best absorbers of UV radiation in the 200 – 800 nm range because these groups possess electrons with relatively low excitation energies.

UV-Vis spectrophotometer consists of five components – source of radiation, a monochromator isolating specific wavelength, a sample holder (cuvette), a detector and a signal processor. The light source usually uses a deuterium lamp for UV measurements and switches to a tungsten filament lamp for visible measurements. Sample holders must be made of a material exhibiting adequate transmission in the wavelength range of interest.

In this research, the absorption spectra of catechol solutions in the range of 250 to 650 nm were taken from a Shimadzu UV-3600 spectrophotometer.

3.2 Atomic Force Microscopy (AFM)

AFM has a capability of high-resolution imaging, which utilizes a cantilever with a very sharp tip to scan over regions of interests, thereby producing three-dimensional images of surfaces at sub nanometer scales. As the probe approaches the surface, the force between atoms on the surface and the probe causes the cantilever to deflect towards or away from the surface. The surface profile

is imaged by measuring the deflection of the cantilever, providing sensitive topographical information.

In this thesis, the morphology of the CA-treated silicon wafers was studied with an AFM (Asylum Research, MFP-3D, Santa Barbara, USA) operated in tapping mode in air to avoid surface damage. The samples were fixed on a magnetic support using double-sided tape. The data were achieved by a Bruker Dimension Icon AFM, with the help of Liyuan Feng.

3.3 Ellipsometry

Ellipsometry is able to measure a change in polarization of light as light reflects or transmits from layered materials without destroying the materials. By taking advantage of the polarizability of light, it allows for accurate analysis of thin film properties like the refractive index and the thickness.[2] In typical ellipsometry, light from a light source passes through a linear polarizer that modifies any incident polarization state to the linear state. Upon interaction with a sample, the phase of the reflected light becomes elliptically polarized. The angle and polarization dependent response is recorded by a detector and fitted to a theoretical model. Subsequently, the film thickness and refractive index of an unknown film can be deduced. It is worth noting that the supporting substrate beneath the investigated layer must have very well-defined and uniform surface structures, for example, silicon wafers, glass sheets, and metallic discs, otherwise appreciable scattering effects will occur which leads to distorted results.[3]

In this study, ellipsometry measurements were performed on a spectroscopic ellipsometer (Sopra, GESP-5) in the National Institute for Nanotechnology (NINT), with the help of Ni Yang. The incident angle is 75°.

3.4 Helium Ion Microscope (HIM)

HIM utilizes helium ions instead of electrons to scan and image surfaces. Except for the imaging source, it resembles a scanning electron microscope in its general architecture. Since helium ions have very high source brightness and shorter wavelength compared to electrons, it can be brought to a focus with an extremely small probe size, yielding resolution performance three times that of a scanning electron microscope.[4] Most importantly, HIM can be used to image insulating samples. During imaging, insulating samples quickly get positively charged when the helium ions accumulate on the surface, which severely prevents electron emission from the insulator surface and causes a drastic reduction in contrast quality of images.[5] This issue can be addressed by using an electron flood gun mounted in the HIM chamber that can deliver electrons compensating the positive charge on the sample surface. The flood gun parameters should be carefully adjusted in order to effectively neutralize the surface charge and achieve high-contrast imaging of uncoated, electrically insulating samples.

Throughout this work, HIM images of uncoated samples ranging from polymeric membranes to polymeric microcapsules were captured on an Orion HIM (Carl Zeiss, USA) at the University of Alberta's micro and nanofabrication facility (nanoFAB).

3.5 Energy Dispersive Spectroscopy (EDS)

EDS detects the characteristic X-ray spectrum emitted by a specimen during bombardment with a high-energy beam of electrons to realize the qualitative and quantitative analysis of chemical constituents. This process consists of the identification of emission lines appeared in the spectrum and measurements of intensities of spectral lines of each element to determine the concentrations of the elements present.

EDS mappings in this thesis were done by Nathan Gerein in the Department of Earth and Atmospheric Sciences at University of Alberta. The EDS elemental maps were taken at 10 keV on

a Bruker energy dispersive X-ray spectrometer. Prior to measurements, a thin carbon layer was deposited on the samples using a Nanotek SEMprep 2 sputter coater.

3.6 X-Ray Photoelectron Spectroscopy (XPS)

XPS is a useful surface chemical analysis tool operating on the theory of the photoelectric effect that electrons of an atom can absorb a photon and then be ejected as photoelectrons.[6] By irradiating X-ray beams, electron emission from the specimen surface was initiated and the kinetic energy of the emitted photoelectrons was recorded. Therefore, according to Einstein's famous equation (3.1), the binding energy of the electrons can be calculated[7]:

$$E_k = hv - (E_b + \phi) \tag{3.1}$$

where E_k (J) is the kinetic energy of the ejected electron, hv (J) is the incident photon energy, E_b (J) is the binding energy of the ejected electron, and ϕ (J) is the material work function. In a typical XPS test, since hv and ϕ are known values, the measurement of E_k returns the E_b of the photo-ejected electron.

All XPS measurements presented in this research were conducted by Dr. Shihong Xu on an X-ray photoelectron spectrometer (AXIS 165, Kratos Analytical Ltd.) at nanoFAB, University of Alberta. Survey-scans with 0-1100 eV binding energy range were run using an Al Kα X-ray source. Data analysis was accomplished using the Casa XPS software (Casa Software Ltd., UK), and atomic concentrations were quantified by integration of the relevant photoelectron peaks.

3.7 Attenuated Total Reflectance-Fourier Transform Infrared Spectroscopy (ATR-FTIR)

FTIR can identify molecule structures and their chemical bonds with molecules' characteristic absorption of infrared radiation. The major advantage of FTIR imaging in ATR mode is that it avoids the complex samples preparations. For each ATR-FTIR test, the infrared beam enters the ATR crystal and a total internal reflection of the beam occurs at the interface between the crystal

and the studied sample. This reflection process results in the formation of an evanescent wave that extends beyond the crystal–sample interface with a penetration depth of 0.5–5 μm into the sample.[8] In regions of the infrared spectrum at which energy absorption by the sample occurs, the intensity of the reflected evanescent wave is reduced (attenuated). After undergoing multiple reflections in the crystal, the attenuated beam is eventually recorded by a detector when it exits the crystal. The spectrometer then creates an infrared spectrum.

Various membrane samples in this study were characterized using an Agilent Cary 600 Series ATR-FTIR spectrophotometer. Each spectrum was collected from 1500 to 4500 cm^{-1}, with 32 scans at a resolution of 4 cm^{-1}.

3.8 Contact Angle Measurements

The contact angle of different fluids, indicative of the surface wettability, is a parameter strongly affected by chemical and morphological characteristics. On smooth surfaces, the water contact angle (WCA) can be determined by Young's equation (Figure 3.1)[9]:

$$\gamma_{sg} = \gamma_{sl} + \gamma_{lg} \cdot \cos\theta \tag{3.2}$$

where θ (°) is the solid–liquid contact angle, γ_{sg} (mN m^{-1}) is the surface tension of the solid, γ_{sl} (mN m^{-1}) is the interfacial tension between liquid and solid, and γ_{lg} (mN m^{-1}) is surface tension of the liquid. Typically, the hydrophobic surface exhibits a static WCA larger than 90°, while the hydrophilic surface shows a static WCA smaller than 90°.

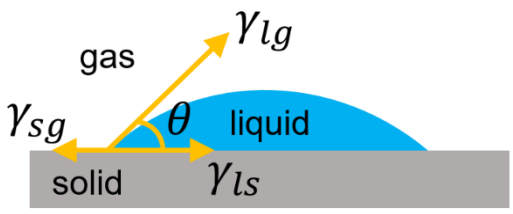

Figure 3.1 Schematic illustration showing a liquid drop on a smooth solid substrate.

In this dissertation, contact angles measurements were performed using the sessile drop technique with an Attension theta optical tensiometer (T200, Biolin Scientific). Droplets of deionized water or oil were placed on the sample surface with a syringe, and the droplet images were taken by the digital camera. Contact angles were then calculated using the Biolin software by fitting the Young-Laplace equation around the outline of the droplet.

3.9 Surface Zeta Potential Measurements

When a membrane is in contact with an aqueous fluid, charges are developed on the membrane surface, leading to the formation of an electrical double layer.[10] Characterizing the surface charge of a membrane is crucial because membrane charge strongly affects its adsorption property. The zeta potential, originating from electrical charges at a solid-liquid interface where an electrical double layer forms, provides insights into the charge characteristics of surfaces. Streaming potential measurements are widely utilized to determine the zeta potential.

When an electrolyte solution flows through a capillary channel under a hydrostatic pressure difference, this fluid carries the counter ions to downstream, resulting in a streaming current, thereby generating a potential difference known as streaming potential. Subsequently, the zeta potential is determined following the approximation of the Helmholtz-Smoluchowski equation.[11]

In this thesis, the zeta potential was measured using a SurPASS electrokinetic analyzer (Anton Paar, GmbH) equipped with an adjustable disk gap cell (14 mm diameter). Measurements were performed by pumping 1 mM KCl electrolyte solution through the channel under 100 mbar. Prior to measurements, the electrolyte solution was tuned to pH 5.5 via drop wise addition of 0.1 M HCl.

3.10 Atomic Adsorption Spectrophotometer (AAS)

AAS is a widely applied technique for the quantitative determination of element concentration. This technique employs the specific wavelengths of light absorbed by free atoms in the gaseous state. For each test, the solution sample supplied to a thermal atomizer is atomized. The concentration of the atom is determined by the amount of radiation absorption with calibration to the standard absorption spectrometry of a known concentration of the element.

In this research, the remaining copper ion concentration was measured by Shiraz Merali with an atomic adsorption spectrophotometer (AAS, Varian 220FS).

3.11 Optical Microscope

Optical microscopes, using visible light and lenses to create magnified visual or photographic images of small objects, are the oldest and broadest type of microscopes. An optical microscope usually contains objective lens for collecting light from the specimen, and another eyepiece to bring the image to focus for the eye. A charge-coupled device (CCD) camera equipped with the optical microscope can record the images in the digital format and then transfer these digital images to the computer storage devices, enabling real-time monitoring of these digital images on the computer.[12]

In this dissertation, optical microscope images of the surfactant-stabilized hexane-in-water emulsion before and after filtration were taken on the optical microscope (Carl-Zeiss, Axioskop 40). For polymeric capsule characterization, optical microscope and fluorescence images were captured using a Carl Zeiss Axiovert 200M inverted microscope mounted with a CCD camera (Photron fastcam mini AX200).

3.12 Total Organic Carbon (TOC) Analysis

TOC analysis can be used for determining the total amount of organic carbon in an aqueous system. Most TOC analyzers are based on the TC-IC (total carbon-inorganic carbon) technique,

where the TOC concentration is calculated as a result of subtraction of the IC concentration from the obtained TC concentration. Typically, the sample undergoes combustion at a temperature of 680°C on a platinum catalyzer in the combustion furnace, decomposing to carbon dioxide that is detected by a non-dispersive infrared detector to determine total carbon of the sample.[13] Furthermore, the oxidized specimen is subjected to acidification, to convert only the IC in the specimen to carbon dioxide. Eventually, the IC value is determined by the same detector and TOC is the difference between TC and IC.

The TOC in this work was determined using a Shimadzu TOC-L analyzer in NINT with the assistance of Ni Yang.

3.13 Scanning Electron Microscope (SEM)

SEM scans the sample's surface with an electron beam. A beam of high-energy accelerated electrons strikes atoms in the sample and produces various signals, such as backscattered electrons, secondary electrons, auger electrons, and characteristic X-rays, generating images for evaluation of morphological and elemental changes.

The most common detection mode of SEM imaging is the secondary electron mode because these electrons can be easily collected. Secondary electrons are atomic electrons from the loosely bound outermost shell, gaining enough kinetic energy from the incoming electrons to eventually escape from the specimen.[14] When studying a conducting object, its conductivity permits electrons to be transported away from the incident beam location. However, excess electrons can build up rapidly in a specimen made of non-conducting material. The charge buildup deflects the incoming electrons from their path, resulting in image distortion. In order to obviate this problem, a thin layer of conducting material, typically gold or carbon with thicknesses 5-10 nm, can be sputtered onto the surface.

In this thesis, the surface morphology of membranes was observed by SEM (FEI Quanta 250). Before performing SEM imaging on membrane specimens, the membranes were sputtered with a ~ 10 nm thick gold layer using a Denton Vacuum Desk II sputter.

3.14 References

[1] M. Hunger, J. Weitkamp, In situ IR, NMR, EPR, and UV/Vis spectroscopy: Tools for new insight into the mechanisms of heterogeneous catalysis, Angew Chem Int Edit, 40 (2001) 2954-2971.

[2] W. Ogieglo, H. Wormeester, K.J. Eichhorn, M. Wessling, N.E. Benes, In situ ellipsometry studies on swelling of thin polymer films: A review, Prog Polym Sci, 42 (2015) 42-78.

[3] W. Ogieglo, H. Wormeester, M. Wessling, N.E. Benes, Spectroscopic Ellipsometry Analysis of a Thin Film Composite Membrane Consisting of Polysulfone on a Porous alpha-Alumina Support, Acs Appl Mater Inter, 4 (2012) 935-943.

[4] M.T. Postek, A.E. Vladar, Helium Ion Microscopy and Its Application to Nanotechnology and Nanometrology, Scanning, 30 (2008) 457-462.

[5] S.A. Boden, A. Asadollahbaik, H.N. Rutt, D.M. Bagnall, Helium ion microscopy of Lepidoptera scales, Scanning, 34 (2012) 107-120.

[6] C.S. Fadley, X-ray photoelectron spectroscopy: Progress and perspectives, J Electron Spectrosc, 178 (2010) 2-32.

[7] B. Feuerbacher, B. Fitton, R.F. Willis, Photoemission and the electronic properties of surfaces, Wiley, London ; New York, 1978.

[8] M.M. Blum, H. John, Historical perspective and modern applications of Attenuated Total Reflectance - Fourier Transform Infrared Spectroscopy (ATR-FTIR), Drug Test Anal, 4 (2012) 298-302.

[9] J. Genzer, K. Efimenko, Recent developments in superhydrophobic surfaces and their relevance to marine fouling: a review, Biofouling, 22 (2006) 339-360.

[10] S. Ferraris, M. Cazzola, V. Peretti, B. Stella, S. Spriano, Zeta Potential Measurements on Solid Surfaces for in Vitro Biomaterials Testing: Surface Charge, Reactivity Upon Contact With Fluids and Protein Absorption, Front Bioeng Biotech, 6 (2018).

[11] S. Nishimura, K. Yao, M. Kodama, Y. Imai, K. Ogino, K. Mishima, Electrokinetc study of synthetic smectites by flat plate streaming potential technique, Langmuir, 18 (2002) 188-193.

[12] X.D. Chen, B. Zheng, H. Liu, Optical and digital microscopic imaging techniques and applications in pathology, Anal Cell Pathol, 34 (2011) 5-18.

[13] E.T. Urbansky, Total organic carbon analyzers as tools for measuring carbonaceous matter in natural waters, J Environ Monitor, 3 (2001) 102-112.

[14] L. Marton, L.I. Schiff, Determination of object thickness in electron microscopy, J Appl Phys, 12 (1941) 759-765.

Chapter 4 Oxidant-Induced Plant Phenol Surface Chemistry for Multifunctional Coatings: Mechanism and Potential Applications[1]

4.1 Introduction

Mussel-inspired chemistry offers a universal and versatile route for engineering the surface functionalities in diverse fields, e.g., biomedical science, energy storage, and environmental issues.[1-7] Dopamine (DA), the most renowned representative, has been widely applied for fabricating multifunctional coatings on natural or synthetic substrates via simple immersion into a slightly alkaline dopamine solution in the presence of oxygen.[8] Despite all the merits of polydopamine (PDA) coatings, i.e., broad applicability and post-functionalization accessibility, the practical applications of PDA coatings are impeded by their toxicity, undesirable dark color coatings, large aggregates and limited precursors which leads to expensive costs.[9-11]

Recently, phenolic compounds isolated from various plants have attracted extensive attention due to the structural resemblance to dopamine.[12, 13] These plant-derived phenols have been demonstrated by the ability to modify the surface chemistry of almost any type of surfaces in a manner similar to that of dopamine. Plant polyphenol-inspired coatings retain many of the benefits of PDA coatings, yet induce less discoloration and morphological changes to the substrate and have a remarkable abundance of coating precursors less costly than dopamine.[14] Moreover, of particular interest is the much smaller aggregates formed from plant polyphenols, which leads to a coating layer with high uniformity.[15] Nevertheless, their time-consuming deposition processes (up to 24 hours or even several days) and multiple post-functionalization steps hinder more widespread use. Recent studies have incorporated the deposition and functionalization of

[1] A version of this chapter was published on *Journal of Membrane Science* as Chen, Y.; Liu, Q., Oxidant-induced plant phenol surface chemistry for multifunctional coatings: Mechanism and potential applications, *Journal of Membrane Science*, 2019, 570-571, 176-183.

polyphenol coatings in a single simultaneous step via co-depositing phenols with polymers or organics containing amine groups.[16-18] For example, Qiu et al. described the co-deposition of catechol (CA) and polyethyleneimine (PEI) conferred the polypropylene microfiltration membranes (PPMMs) noticeable surface charges capable of treating dye water.[19] Xu et al. fabricated a CA/nanoparticles decorated-polyimide membrane via co-deposition of CA and octaammonium polyhedral oligomeric silsesquioxane (POSS-$NH_3^+Cl^-$) to accomplish organic solvent nanofiltration.[20] While the aforementioned methods typically mimic the molecular structure of dopamine through binary coating systems, the intrinsic deficiencies of phenol deposition still remain unaddressed. Therefore, it is highly desirable to develop facile and low-cost strategies for the rapid construction of pure polyphenol coatings. On the other hand, other investigated one-step approaches of pure plant phenol coatings including enzyme catalysis and UV irradiation improved the deposition rate of polyphenol coatings to some extent, but the performances were mediocre with limited hydrophilicity.[21, 22] Central to polyphenol polymerization is an alkaline pH-induced oxidation. Why could not induce polyphenol polymerization by an oxidant? Although it has been mentioned to oxidize dopamine by oxidants in some literature,[23-28] addition of oxidants to the polyphenol coating systems has never been reported. We previously[26] reported that SP can efficiently construct a superhydrophilic PDA coating on PVDF membranes. However, the visible aggregates of PDA coatings are unavoidable, and the potential application of SP-induced coatings in metal ion adsorption has remained unexplored. Moreover, polyphenols alone succeeding in the formation of superhydrophilic coatings will undoubtedly broaden the scope of plant phenols.

Herein, we report a straightforward and general approach to greatly improve the polyphenol-coating kinetics for construction of an ultrathin skin layer by using SP as a trigger. The simplest

and most economically advantageous compound in plant-derived phenols, CA, was selected to investigate the reaction mechanisms and the deposition behaviors upon the addition of SP. SP was chosen on account of not only its application in PDA synthesis but also the elimination of metal contamination in the coating. We found that the deposition rate of CA coatings induced by SP was dozens of times faster than the traditional methods. Moreover, our SP-accelerated CA coatings were successfully assembled on several substrates, including polar and non-polar materials. Notably, the optimally constructed PVDF membranes that are rapidly deposited by CA for 2 hours exhibit ultrahigh water permeability, excellent heavy metal adsorption ability, and successful separation of several oil-in-water emulsions. To the best of our knowledge, this is the first comprehensive study reporting SP-mediated plant-inspired surface chemistry and its potential use in water purification.

4.2 Experimental Section

4.2.1 Materials

Polypropylene (PP) and polytetrafluoroethylene (PTFE) membranes with diameter of 47 mm and average pore size of 0.22 μm were purchased from Yibo Co. (Haining, China). PVDF membranes (mean pore size 0.45 μm, diameter 47 mm) were obtained from the Millipore Co. CA, sodium dodecyl sulfate (SDS), hexane, ethanol, and silicon wafers were purchased from Sigma-Aldrich. Anhydrous cupric sulfate ($CuSO_4$), anhydrous sodium acetate, cover glasses, glacial acid, kerosene, petroleum ether, potassium chloride (KCl), SP, and tris (hydroxymethyl) aminomethane hydrochloride (Tris-HCl) were purchased from Fisher Scientific. All chemicals were used without further purification.

4.2.2 Preparation of CA Solutions

CA (2 mg mL^{-1}) and SP (4 mg mL^{-1}) were dissolved in a beaker containing 30 mL of acetate

buffer (50 mM, pH = 5.0). The container was covered with aluminum foil, shaken at 135 rpm at room temperature for different times (0.5, 1, 2, 4 h). In addition, CA (2 mg mL^{-1}) was dissolved in Tris-HCl buffer solution (pH = 8.5, 50 mM) for 24 h. The following operations are the same as the above-mentioned procedures.

4.2.3 SP-Assisted Deposition of CA on Various Substrates

The substrate was first prewetted thoroughly with ethanol and then submerged in the freshly prepared deposition solution. The container was covered with aluminum foil, shaken at 135 rpm at room temperature for different times (0.5, 1, 2, 4 h). Subsequently, the modified substrate was rigorously rinsed with Milli-Q water and then dried at 40 °C overnight before use. PVDF membranes were selected to study the surface properties of CA coatings and present potential applications. The as-prepared PVDF membranes were denoted as CA-SP-0.5, CA-SP-1, CA-SP-2, and CA-SP-4 according to their oxidizer and reaction times. For comparison, the pristine PVDF membrane was immersed in Tris-HCl buffer (50 mM, pH = 8.5) in an open vessel for 24 h which was designated as CA-O-24.

4.2.4 Characterizations

UV-vis absorption of the solutions was measured with an ultraviolet spectrophotometer (UV 3600, Shimadzu, Japan) from 650 nm to 250 nm. The surface roughness of as-coated silicon wafers was evaluated by an atomic force microscopy (AFM, Asylum Research, MFP-3D, Santa Barbara, USA) using the tapping mode in air. The thickness was detected by a spectroscopic ellipsometer (Sopra, GESP-5) at an incident angle of 75°. A light spot size of 360 × 360 μm^2 was scanned for each sample. Helium ion microscope (HIM) images were captured on an Orion HIM (Carl-Zeiss, USA). The element distribution maps of samples were obtained via energy dispersive spectroscopy (EDS, Carl-Zeiss Sigma). Elemental compositions of the membrane surfaces were analyzed by an

X-ray photoelectron spectrometer (XPS, Kratos, AXIS 165). The surface chemical structure of membranes was characterized by an attenuated total reflectance-Fourier transform infrared spectroscopy (ATR-FTIR, Agilent, Cary 600 Series). The water contact angles in air and oil contact angles underwater were measured through a theta optical tensiometer (Attension, Biolin Scientific T200). The surface zeta potential of membranes was measured by an electrokinetic analyzer (SurPASS Anton Paar, GmbH). 1 mM KCl solution was used as the electrolyte solution. The copper ions concentration in the solution was measured using an atomic adsorption spectrophotometer (AAS, Varian 220FS). Optical microscopy images of the feed and filtrate solution were taken on the Axioskop 40 (Carl-Zeiss). The concentration of oils remaining in the filtrate was determined using a total organic carbon analyzer (Shimadzu, TOC-L).

4.2.5 Copper Ions Adsorption

Copper ion solution with a starting concentration of 10 ppm was prepared by dissolving a certain amount of $CuSO_4$ in Milli-Q water. The membrane sample was loaded in 50 mL copper ion solution, which was shaken at 100 rpm under ambient conditions. Solution specimens were taken at certain intervals (6 h, 12 h, and 24 h) for Cu^{2+} ion concentration measurements. The adsorption capacity was defined as the below formula (4.1):

$$q_e \text{ (mg g}^{-1}) = \frac{(C_0 - C_e) \cdot V}{m} \tag{4.1}$$

where C_0 (ppm) and C_e (ppm) are the initial and remaining Cu^{2+} ion concentrations, V (L) is the volume of the solution, and m (g) is the membrane mass, respectively.

The long-term performance of the representative membrane was evaluated through 4 sequential adsorption and desorption cycles. The membrane was first bathed in copper ion solution for 24 h using the foregoing procedure, followed by immersion in HCl solution at pH =3 for 30 min and a water wash. Repeating cycles were conducted with the same membrane.

4.2.6 Oil/Water Separation

The surfactant-free oil/water mixtures were prepared by sonicating oil and water in a ratio of 1:99 (v/v) for 30 min to obtain homogenous and white emulsions. The surfactant-stabilized oil-in-water emulsions were prepared by dissolving 0.04 mg mL^{-1} of sodium dodecyl sulfate (SDS) in oil/water mixtures via a similar process. All these mixtures and emulsions are stable at least for 12 h without de-emulsification. The droplet sizes of the emulsions were in the range of several to tens of micrometers, as determined by optical microscopy observation.

The separation experiments were carried out in a vacuum filtration setup (Millipore) with the optimum PVDF membrane being fixed between two glass vessels. For each separation experiment, the fabricated membrane was prewetted with water and 100 ml of the prepared mixture or emulsion was poured into the filtration cup and filtered under a relatively low transmembrane pressure of 0.075 MPa. The filtrate water was collected. The permeation flux (4.2) and the separation efficiency (4.3) were calculated using the following equations:

$$\text{flux}\left(\text{L m}^{-2}\ \text{h}^{-1}\right) = \frac{V}{A \cdot t} \tag{4.2}$$

$$\text{separation efficiency (\%)} = \left(1 - \frac{C_f}{C_o}\right) \times 100 \tag{4.3}$$

where V (L) is the volume of permeate, A (m^2) is the effective membrane area (11.34 cm^2), t (h) is the time of permeate collection, C_f (ppm) is the concentration of oil in the filtrates, and C_o (ppm) is the initial concentration of oil in the oil/water mixtures or oil-in-water emulsions.

4.2.7 Oil Fouling Test

The reusability of the membrane was evaluated by repeated filtration experiments. For each cycle, 100 mL of the SDS-stabilized hexane-in-water emulsion was poured into the funnel and filtered until 20% of the emulsion was left in the funnel. Then, the funnel was emptied before

another 100 mL of the original hexane-in-water emulsion was added to repeat the filtration separation. This procedure was repeated for 10 times. Between two cycles, the membrane was washed with DI water to remove the oils fouled on the membrane.[29] The variations of the permeation flux and separation efficiency during this process were measured.

4.3 Results and Discussion

4.3.1 Oxidant-Induced Polymerization and Deposition of CA

Previous studies suggested that the plant phenolic compounds deposition mechanism involves oxidation of the catechol group to quinone.[30] Therefore, the reactivity of CA under different experimental conditions was determined by UV-vis absorption of quinone (Figure 4.1a). In addition to the intrinsic characteristic adsorption peak of CA at 260 nm, the UV-Vis spectra showed significant absorbances at around 390 nm, attributed to the formation of quinone group, which proved that both SP and oxygen oxidation of CA lead to quinone formation.[31] For the spectra of solutions with SP, the peak intensity was getting stronger with increasing reaction time; however, it increased very slowly after 2 h, indicating that a maximum conversion of catechols to quinones was achieved. Figure 4.1b illustrates the color difference between the CA solutions under various conditions, and the CA solution oxidized by O_2 for 24 h exhibited a faint yellow color. When SP was added, the colorless solution turned brown immediately and displayed a gradient color depth as a function of time. The increase of absorbance intensity at 390 nm and darkening of the solutions under chemical oxidation suggested that SP tremendously accelerated the oxidation and polymerization of CA.

To demonstrate the competence for constructing phenolic coatings using SP as a trigger, CA coatings were deposited on silicon wafers. The surface roughness of the nascent silicon wafer was 0.795 nm (Figure 4.1c) and this value increased to 0.814 nm (Figure 4.1d) for coatings deposited

by air oxidation for 24 h and 4.503 nm (Figure 4.1e) for coatings deposited by chemical oxidation for 2 h, respectively. These results strongly supported the hypothesis that SP can substantially enhance the CA-coating kinetics. The evolution of the SP-mediated CA films was further studied by an ellipsometer. As presented in Figure 4.1f, the thickness of the CA films increased quickly within the first hour and then increased linearly with the deposition time at a slower rate, which was in accordance with results shown by deposition degree. It should be noted that although the oxidation of catechols to quinones was largely complete in 2 hours, to a higher degree of deposition a longer immersion time was allowed. To confirm the versatility of our strategy, these CA coatings were deposited on other material substrates, including glass sheets and polymeric membranes.

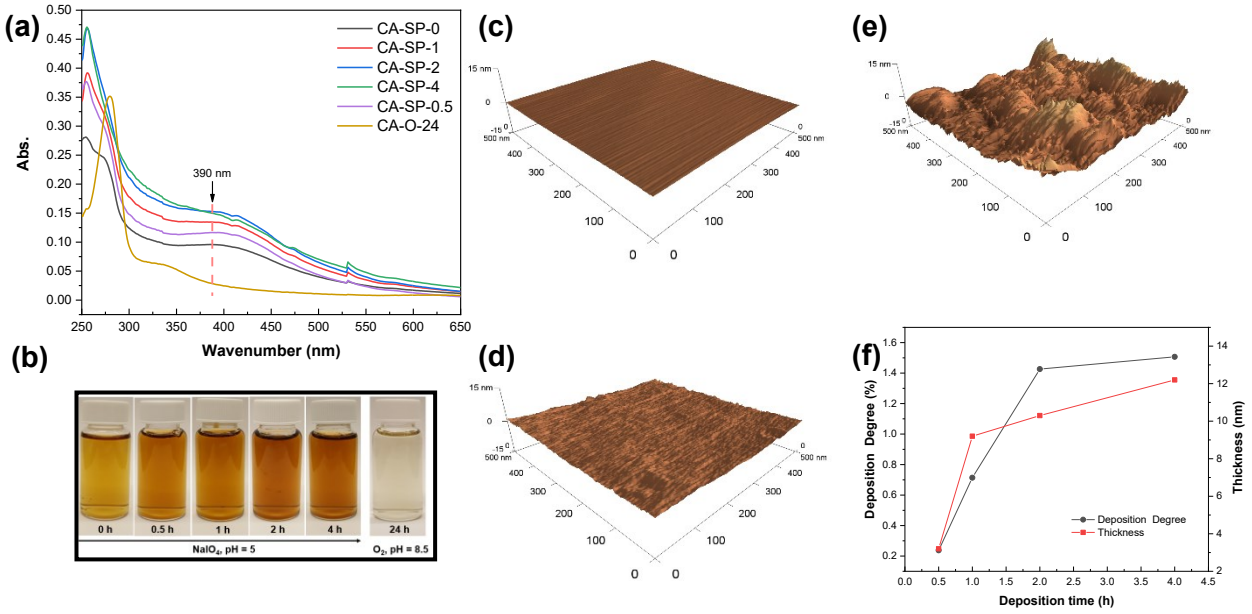

Figure 4.1 (a) UV-vis spectra of 100-fold diluted CA solutions; (b) Color of 20-fold diluted solutions with different reaction time and condition. AFM images of the (c) nascent, CA-coated silicon wafers triggered by (d) air for 24 h, and (e) sodium periodate for 2 h. (f) Time-dependence of thickness for the CA coatings deposited on silicon wafers, as determined by ellipsometry.

Successful formation of a CA layer onto the surface was clearly seen from the development of a yellow or brown color on these substrates (Figure 4. S1).

4.3.2 Surface Properties of the CA-Coated PVDF Membranes

CA coatings have been regarded as a versatile platform for hydrophilic modification of a variety of materials, especially for hydrophobic porous membranes. In this study, PVDF microfiltration membranes were employed to perform surface functionalization by the SP-controlled deposition of CA. The surface morphologies of the nascent and the optimally modified PVDF membranes are presented in Figure 4.2. The surface of the nascent PVDF membrane was really smooth. There was no obvious difference between the surface morphology of the CA/SP-decorated membrane and that of the nascent one. This result indicated that an ultrathin, uniform and particle-less skin layer was fabricated on the PVDF membrane. Overall, these coatings had almost no impact on the pore structure of the pristine substrate, thus avoiding decreases of surface area and pore size, a very common phenomenon in the cases of polydopamine coatings.

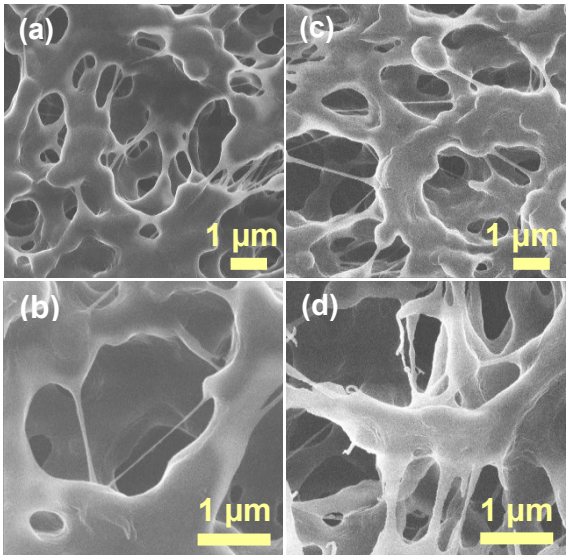

Figure 4.2 Surface morphologies of the nascent (a, b), and CA-SP-2 (c, d) PVDF membrane. The scale bars are 1µm at different magnifications.

The EDS elemental mapping images of C, O, and F are exhibited in Figure 4. S2. The dispersion

of the O element was very homogenous as the same as C and F element, which confirmed that a superhydrophilic coating was deposited uniformly on the top surface and cross-section of the membrane. Furthermore, the surface chemistry of the pristine and as-constructed PVDF membranes was analyzed by ATR-FTIR and XPS. The FTIR spectra (inset in Figure 4. S3) display one broad absorption band between 3600 and 3150 cm^{-1} in all modified PVDF membranes, attributed to the phenolic hydroxyl groups O−H stretching vibrations, while the broadness of the absorption bands is an indicator for intramolecular hydrogen bonds.[15] In the spectra of CA/SP-decorated membranes (Figure 4. S3), the absorption peak at 1717 cm^{-1} is assigned to the stretching vibration of C=O of the carboxylic acid groups, and the absorption peak at 1608 cm^{-1} is attributed to the resonance vibration of C=C groups. In comparison, there is no discernable peak at these positions in the spectrum of CA-O-24.[15, 26] Meanwhile, for CA/SP-decorated membranes, the intensity of these peaks became stronger with an increase in coating time from 0.5 h to 2 h and marginally increased after 2 h. The existence of these two peaks offers strong proof that the addition of SP enormously speeds up the oxidation and deposition rate of CA, hence remarkably enhancing the hydrophilicity of PVDF membranes.

Figure 4.3a-c presents the high-resolution C1s XPS spectra of the nascent and as-modified PVDF membranes. As shown in Figure 4.3a, the C1s peak of the nascent PVDF membrane could be split into two main satellite peaks corresponding to C-F at 288.3 eV and C-C at 283.6 eV.[32] For the C1s spectra (Figure 4.3b-c and Figure 4. S4) of PVDF membranes after different modifications, two new peaks appeared, including C=C at 281.8 eV and O−C=O at 284.2 eV, respectively. In addition, the higher intensity ratio O−C=O/C−C of CA-SP-2 coating than that of CA-O-24 indicated that the SP-triggered oxidation leads to a thicker CA film. Survey scan XPS spectra (Figure 4. S5) of PVDF membranes demonstrate that F1s peaks weakened and the O1s

peaks were identified after decoration with CA or CA/SP. Compared with the bare and CA-decorated PVDF membranes, the stronger peak intensity and the higher atomic concentrations of element O (Table 4.1) on the CA-SP-2 (17.38%) and CA-SP-4 (17.24%) surfaces suggested higher contents of hydrophilic groups were generated, indicative of better hydrophilicity of the CA/SP-modified PVDF membranes. It is worth noting that SP was not detected in the resulting coatings, confirming that the deposited films were composed of only polyphenols. The overall results verified the successful formation of pure CA coatings, resulting in the introduction of a large number of carboxylic groups onto the membrane surface. Figure 4.3d outlines the possible mechanism for SP-triggered CA coatings, where CA was first oxidized to o-quinine and then further oxidation led to side-chain cleavage, yielding to carboxyl functions. Meanwhile, the obtained oligomers crosslinked with each other to deposit on the PVDF surface. This phenomenon could be explained by the fact that SP produced radicals that are more active than molecular oxygen, such as superoxide radicals ($O_2^{\cdot-}$) and hydroxyl radicals (·OH).[33] More importantly, CA coatings can act as a "primer" layer for further functionalization, on which a variety of secondary layers can be induced via Michael addition or Schiff base reaction to meet specific application

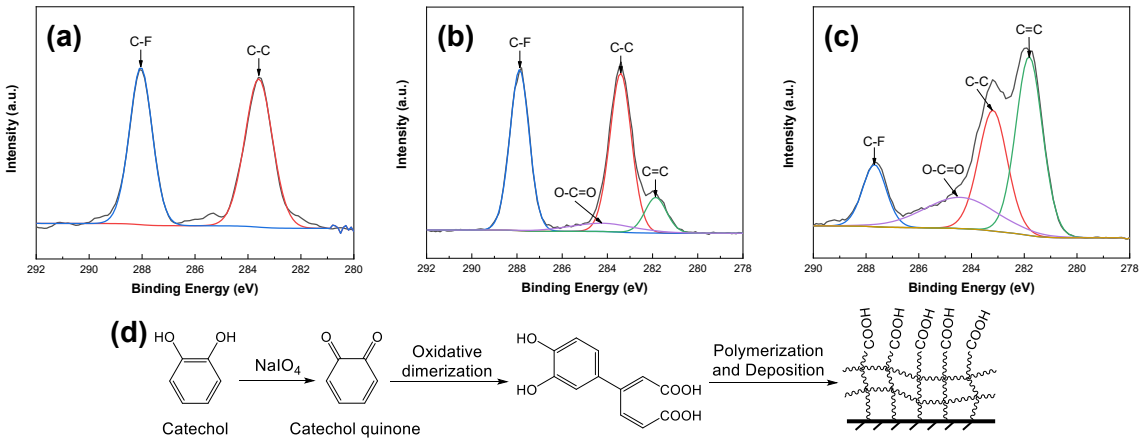

Figure 4.3 C1s XPS spectra of the (a) nascent, (b) CA-O-24 and (c) CA-SP-2 PVDF membranes. (d) Schematic illustration of the possible polymerization mechanism of CA.

demands.

Table 4.1 Elemental compositions of the nascent and modified membranes

Membrane	Composition (%)			Atomic ratio
	C	F	O	O/C
Nascent PVDF	59.76	40.24		
CA-O-24	62.63	33.79	3.59	0.06
CA-SP-0.5	70.97	15.71	13.32	0.19
CA-SP-1	73.55	11.36	15.08	0.21
CA-SP-2	73.62	9.00	17.38	0.24
CA-SP-4	73.11	9.65	17.24	0.24

Special wettable surfaces can be obtained by the synergistic effect of micro-/nano-hierarchical structures and chemical affinity.[34] The wettability of different membranes was investigated by time-dependent water contact angle (WCA) as shown in Figure 4.4a. The nascent PVDF membrane exhibited high hydrophobicity with the steady water contact angle of 114° in 30 s due to the low surface energy. After 24-hour modification using dissolved oxygen, the WCA of the CA-O-24 membrane decreased to around 89°. In contrast, the water drop permeated through the membrane and reached a final WCA of 0° when the membrane surfaces were deposited with CA under chemical oxidation for more than 0.5 h. And the optimally decorated surface, CA-SP-2, showed excellent superhydrophilicity with the water contact angle instantaneously dropping to zero in 6 s. It is worth mentioning that our oxidant-triggered method showed the shortest modification time in comparison with recent advances (Table 4. S1). Figure 4.4b presents photographic images of the wettability of the membranes. Both the nascent and CA-O-24 PVDF membranes were resistant to water droplet permeation, while the water droplet immediately spread on and soaked through the CA-SP-2 membrane. The underwater oil contact angle of the CA-SP-2

membrane was measured (Figure 4.4c). As observed, the CA/SP-coated PVDF membrane displayed a high underwater oil contact angle of 156° for chloroform, showing excellent underwater superoleophobicity. The oil adhesion of the CA/SP-decorated PVDF membrane was characterized by dynamic underwater oil adhesion measurement, as demonstrated in Figure 4.4d. An oil droplet was forced to contact sufficiently with the membrane surface and then lifted up. During this process, the oil droplet could be completely detached from the membrane surface and no observable oil was left, thus indicating the low affinity of the membrane surface to oil. This superoleophobicity and low oil-adhesion behavior could be attributed to the "Cassie-Baxter" state at the water/oil/solid interface, where water was trapped in the micro/nanostructured CA/SP-

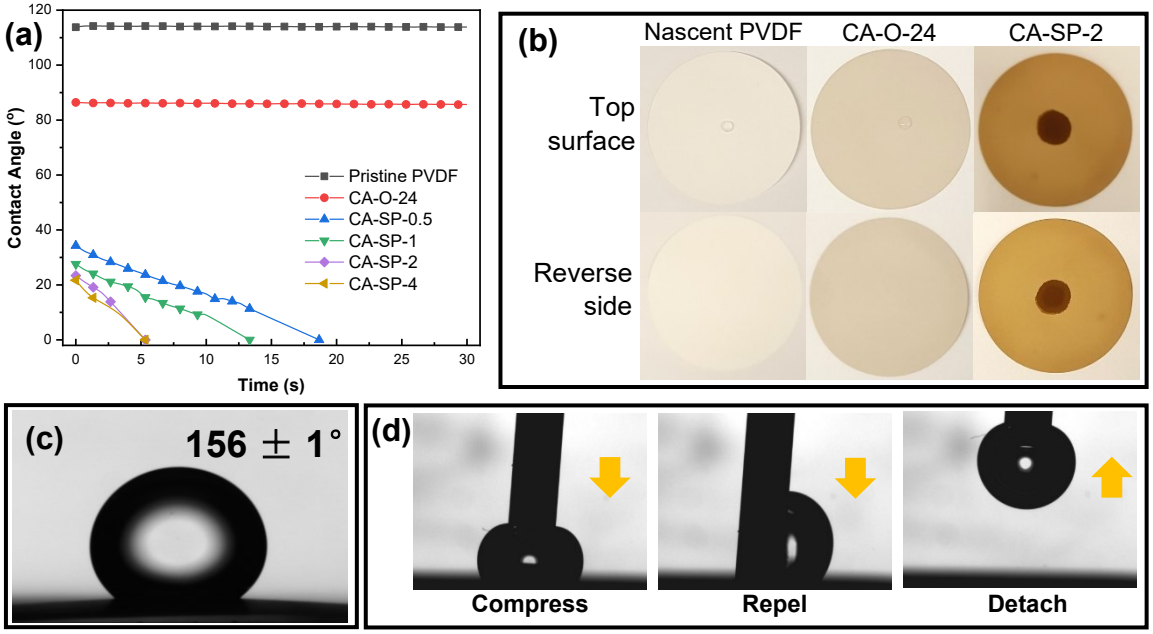

Figure 4.4 (a) Water contact angle of the nascent and as-modified PVDF membranes. (b) Digital photographs of a water drop on the membrane surface of the nascent, CA-O-24, and CA-SP-2 PVDF membranes (above) and the reverse side of the membranes (below). (The water droplet is about 5 μL.) (c) Underwater oil contact angle and (d) dynamic underwater oil-adhesion of the CA-SP-2 PVDF membrane.

coated membrane due to its high surface energy composition of numerous O−H groups, forming a repulsive hydration layer that can avoid direct contact between the solid phase and the oil phase.[35] To investigate the influence of solely SP on the PVDF membranes, another control experiment without adding CA was conducted. After 2 h of SP treatment, neither the color change nor the enhanced hydrophilicity of the membrane was observed (Figure 4. S6), providing an indication that SP only served as a trigger in the phenol deposition.

4.3.3 Potential Applications of the CA-Coated PVDF Membranes

The dynamic hydrophilicity of the membranes was examined by pure water flux measurements (Figure 4.5a). Due to the poor hydrophilicity of the pristine and CA-O-24 PVDF membranes, the membranes were pre-wetted by ethanol before the flux measurements. The water fluxes of pre-wetted PVDF membranes were initially high, while there was a reduction in water flux of the CA-SP-0.5 membrane, attributed to the lower density of hydrophilic groups in this membrane than those of the pre-wetted membranes. When the oxidant-induced deposition time exceeded 1 hour, the water flux dramatically improved to over 21000 L m^{-2} h^{-1}, at least twofold higher than other state-of-the-art materials.[26, 36-40] The higher water flux of the CA-SP-4 membrane than that of the CA-SP-2 membrane can probably be attributed to the higher deposition degree of hydrophilic moieties. The pure water fluxes of these CA/SP-modified PVDF membranes were exceptional compared to the pre-wetted membranes, which can be reasonably explained by the substantial enhancement of the hydrophilicity with negligible change on the effective average pore size.

The stability of the CA/SP coatings is of vital importance for long-term practical service. In this paper, the superhydrophilic robustness of the CA coatings deposited by chemical oxidation in the presence of salty (seawater) and erosive media (pH = 2 and pH = 12) was investigated, respectively. All the membranes were immersed into seawater and harsh pH solutions for 6 h,

followed by drying and then contact angle measurements. As observed in Figure 4.5b, the CA-SP-2 membrane showed exceptional tolerance against acidic and high-salinity environments, maintaining its original superhydrophilic feature with a WCA of 0°. However, the WCA of the as-prepared membrane increased slightly after being rinsed by a strongly basic solution for 6 h. This was because a little CA/SP coatings disintegrate at high pH conditions, which was consistent with the change in color from colorless to yellow in the alkaline solution (inset of Figure 4.5b). The deprotonation of the carboxylic acid and phenol moieties at alkaline pH may contribute to the dissolution of CA coatings.[41] In addition, the superhydrophilicity of the membrane can be easily restored by a simple immersion into the coating solution. The mechanic stability of the CA-SP-2 membrane was also evaluated by a five-minute sonication. No obvious color changes could be seen in the sonicating solution (inset of Figure 4.5b) and the WCA of the sonicated CA-SP-2 membrane remained constant with a value of zero (Figure 4.5b), suggesting outstanding mechanical stability of the CA/SP coatings. The strong resistance of CA-SP-2 against harsh environments is beneficial for applications in oil-seawater separation under typical marine

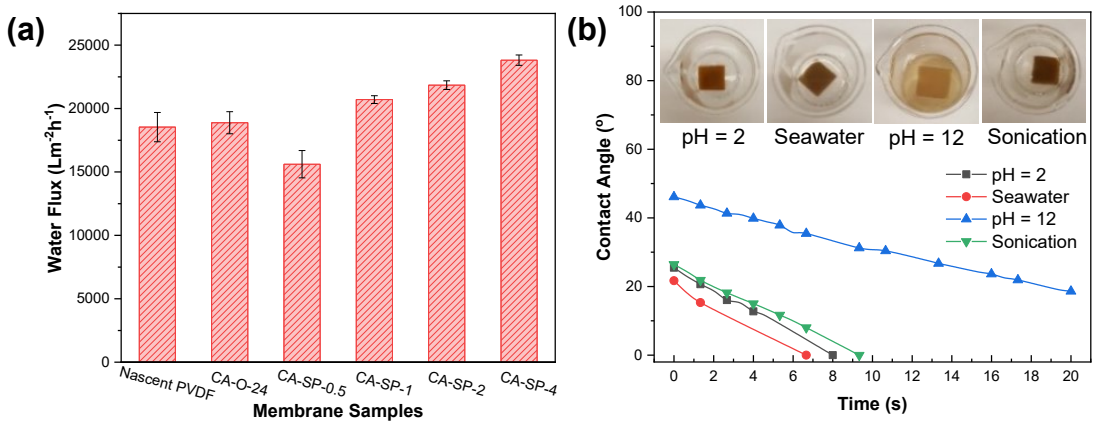

Figure 4.5 (a) Pure water flux of the nascent and as-modified PVDF membranes. (b) Water contact angle of CA-SP-2 PVDF membranes after various treatments. All membranes were cut into 2 × 2 cm^2, immersed into 5 mL of corresponding solutions.

environments.

Copper ion removal experiment was conducted to examine the adsorption ability of CA coatings towards heavy metal ions. As shown in Figure 4.6a, the heavy metal adsorption capacity of both the nascent and as-coated membranes increased with adsorption time, while better affinity to Cu (II) was observed for the CA-SP-2 PVDF membranes in each group, confirming the superior Cu^{2+} collecting performance of the CA coatings. Specifically, the CA-SP-2 PVDF membrane sample incubated in the Cu^{2+} solution for 24 h exhibited q_e of about 36.2 mg g^{-1}, comparable to other newly developed absorbents (e.g. PVDF/PDA blended membranes,[42] PDA/PEPA coated sponges,[43] etc.). Four sequential adsorption/desorption cycles were conducted to investigate the reusability of the CA-SP-2 PVDF membrane. Figure 4.6b illustrates that its adsorption efficiency decreased at an acceptable rate of about 6% after each treatment, suggesting a possible application in industry.

The adsorption mechanism can be predominantly ascribed to the strong cation attraction between copper ions and hydroxyl functional groups in CA coatings. Catechol-Cu^{2+} ion coordination, meanwhile, may also play a role. The improvement of copper ion adsorption was further explained by the zeta potential (Figure 4.6c). At pH = 5.5, the pH value of 10 ppm $CuSO_4$ solution, the nascent PVDF membrane was negatively charged, while a shift towards more negative direction was observed on the CA-SP-2 membrane.

The obtained membrane (CA-SP-2) exhibited excellent selective wettability for oil and water, indicative of its superior oil rejection property. To examine the oil/water separation performance of the CA-SP-2 membrane, a series of oil/water mixtures and surfactant-stabilized oil-in-water emulsions with micrometer-sized droplets were prepared to permeate through the membranes, respectively. The separation process was conducted in a vacuum suction filter driven by a 0.075

MPa transmembrane pressure. When a mixture/emulsion was poured onto the optimum membrane (CA-SP-2), water quickly passed through the membrane while oil droplets were retained above. The optical microscopy images of the feed solution and its collected filtrate were firstly used to evaluate the separation effectiveness, where SDS-stabilized hexane-in-water emulsion was taken as an example. It can be seen from the Figure 4. S7 that the original milky white feed emulsion (left) became totally transparent (right) after performing the separation. In the optical microscopy images, numerous droplets with the size ranging from several to tens of micrometers in the feed emulsion were not detectable in the filtrate at all, suggesting the successful separation of oil droplets from water. The precise oil concentration of the filtered phase was determined by TOC. Figure 4.6d summarizes the separation efficiency of the CA-SP-2 PVDF membrane for all the examined mixtures and emulsions, including 99.93% for hexane/water, 99.96% for kerosene/water, 99.95% for petroleum ether/water, 99.96% for toluene/water, 99.77% for hexane-in-water, 99.92% for kerosene-in-water, 99.05% for petroleum ether-in-water, and 99.80% for toluene-in-water.

The separation flux of the optimally prepared membrane was calculated by measuring the time needed to separate a certain volume of the feed solution. As shown in Figure 4.6e, the CA-SP-2 membrane exhibited extremely high permeability for all four oil/water mixtures, including 10354.44 L m^{-2} h^{-1} for the hexane/water mixture, 9006.12 L m^{-2} h^{-1} for the kerosene/ water mixture, 9609.85 L m^{-2} h^{-1} for the petroleum ether/water mixture and 9992.59 L m^{-2} h^{-1} for the toluene/water mixture, respectively. For oil-in-water emulsions, the corresponding permeation fluxes decreased a little bit but were still comparable, such as 9536.98 L m^{-2} h^{-1} for hexane-in-water emulsion, 6660.67 L m^{-2} h^{-1} for kerosene-in-water emulsion, 8248.91 L m^{-2} h^{-1} for petroleum ether-in-water emulsion, and 8573.98 L m^{-2} h^{-1} for toluene-in-water emulsions. The obtained separation fluxes

were superior to those of previously reported membranes with similar rejection properties.[26, 44] In contrast, an extremely low flux of 105.08 L m^{-2} h^{-1} was observed for the pristine PVDF membrane (Figure 4. S8). This might be attributable to the immediate oil fouling on the membrane surface.

Oil antifouling ability is a key criterion for membrane filters in the treatment of oil-containing wastewater. Given the ultralow oil adhesion to the CA-SP-2 PVDF membrane, we expect that it has outstanding antifouling properties. Here, the antifouling performance and reusability of the CA-SP-2 membrane were investigated by measuring the variations in permeation flux and

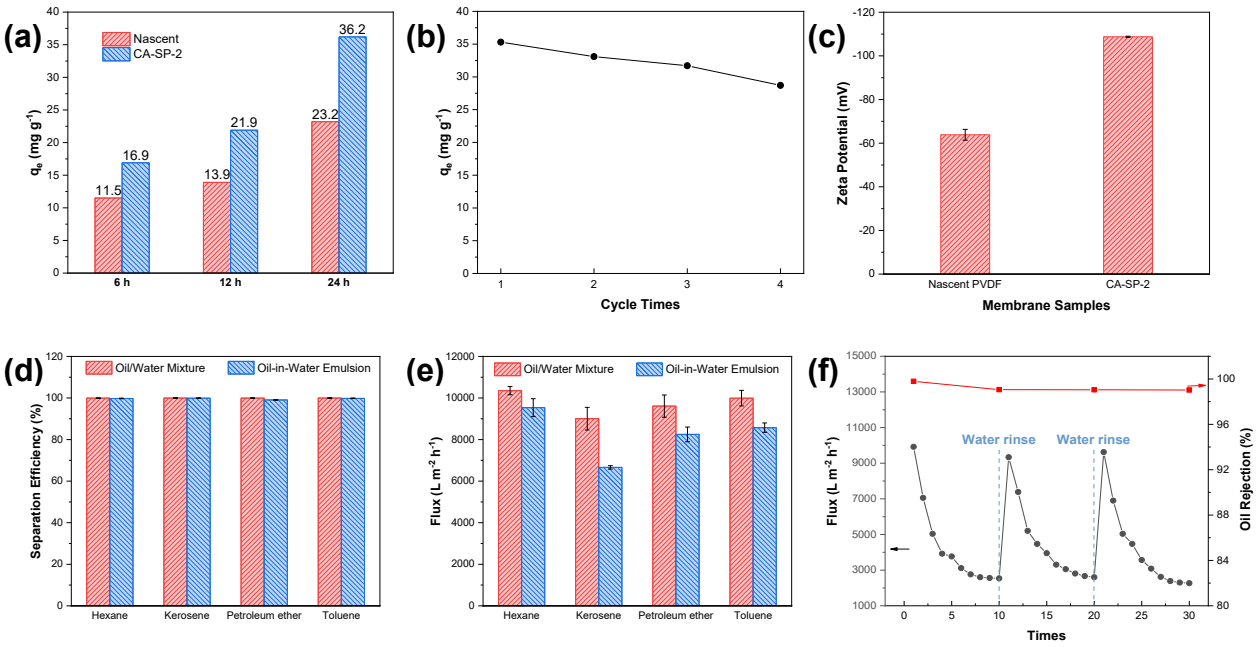

Figure 4.6 (a) Cu^{2+} adsorption capacity of nascent and CA-SP-2 PVDF membranes with different experimental time. (b) Reusability of Cu^{2+} adsorption of the CA-SP-2 membrane. (c) Zeta potential of nascent and CA-SP-2 PVDF membranes at pH = 5.5. (d) Separation efficiency and (e) filtrate flux of various oil/water mixtures and oil-in-water emulsions. (f) Cycling separation performances of the CA-SP-2 PVDF membrane using surfactant-stabilized hexane-in-water emulsion as an example.

separation efficiency in a 3-cycle SDS-stabilized hexane-in-water emulsion separation operation. As illustrated in Figure 4.6f, a sharp permeation flux decrease was observed at the beginning of each cycle, owing to the high flux-induced oil accumulation on the membrane surface.[45] Then the decline rate reached stable and the flux decreased gradually with increasing filtration times, resulting from the formation of oil cake on the membrane surface.[26] However, the flux could be recovered completely to the starting level after water flushing. The oil rejection ratios after each cycle were all above 99 %, indicating that the separation efficiency drops insignificantly after multi-separation processes. Considering all observations together, SP-assisted plant-inspired coating technology has great potential application in metal reclamation as well as water purification with respectable durability for long time usage.

4.4 Conclusions

In summary, a universal single-step method was developed for the fast deposition of high-performance CA coatings. Under the trigger of SP, the CA was steadily anchored on various substrates and formed a uniform “pure” coating without any metal salt contamination. Remarkably, the CA/SP-decorated PVDF membranes are imparted with ultrahigh water permeability, excellent adsorption ability towards Cu^{2+} and outstanding rejection of oil. In comparison to PDA coatings, plant phenolic coatings are quite attractable for their abundant natural resources and nontoxicity. This oxidant-assisted CA deposition method, applicable for other natural phenolic deposition systems, shows significant superiorities over conventional phenol coating methods (using dissolved oxygen, enzymes and UV irradiation) in their high-efficient deposition process and unparalleled wetting performance, which may point a direction for the fabrication of functional polyphenol coatings.

4.5 References

[1] H. Lee, S.M. Dellatore, W.M. Miller, P.B. Messersmith, Mussel-inspired surface chemistry for multifunctional coatings, Science, 318 (2007) 426-430.

[2] S.H. Ku, J. Ryu, S.K. Hong, H. Lee, C.B. Park, General functionalization route for cell adhesion on non-wetting surfaces, Biomaterials, 31 (2010) 2535-2541.

[3] V.K. Thakur, M.-F. Lin, E.J. Tan, P.S. Lee, Green aqueous modification of fluoropolymers for energy storage applications, Journal of Materials Chemistry, 22 (2012) 5951.

[4] Z.-X. Wang, C.-H. Lau, N.-Q. Zhang, Y.-P. Bai, L. Shao, Mussel-inspired tailoring of membrane wettability for harsh water treatment, J. Mater. Chem. A, 3 (2015) 2650-2657.

[5] N.G.P. Chew, S. Zhao, C. Malde, R. Wang, Superoleophobic surface modification for robust membrane distillation performance, J. Membr. Sci., 541 (2017) 162-173.

[6] G. Wang, X. Huang, P. Jiang, Bio-Inspired Fluoro-polydopamine Meets Barium Titanate Nanowires: A Perfect Combination to Enhance Energy Storage Capability of Polymer Nanocomposites, ACS Appl. Mater. Interfaces, 9 (2017) 7547-7555.

[7] M. Liao, P. Wan, J. Wen, M. Gong, X. Wu, Y. Wang, R. Shi, L. Zhang, Wearable, Healable, and Adhesive Epidermal Sensors Assembled from Mussel-Inspired Conductive Hybrid Hydrogel Framework, Adv. Funct. Mater., 27 (2017) 1703852.

[8] Y. Liu, K. Ai, L. Lu, Polydopamine and its derivative materials: synthesis and promising applications in energy, environmental, and biomedical fields, Chem Rev, 114 (2014) 5057-5115.

[9] Y. Bozzi, E. Borrelli, The role of dopamine signaling in epileptogenesis, Front Cell Neurosci, 7 (2013) 157.

[10] D.G. Barrett, T.S. Sileika, P.B. Messersmith, Molecular diversity in phenolic and polyphenolic precursors of tannin-inspired nanocoatings, Chem. Commun. (Cambridge, U. K.), 50 (2014) 7265-7268.

[11] W.-Z. Qiu, Q.-Z. Zhong, Y. Du, Y. Lv, Z.-K. Xu, Enzyme-triggered coatings of tea catechins/chitosan for nanofiltration membranes with high performance, Green Chem., 18 (2016) 6205-6208.

[12] T.S. Sileika, D.G. Barrett, R. Zhang, K.H. Lau, P.B. Messersmith, Colorless multifunctional coatings inspired by polyphenols found in tea, chocolate, and wine, Angew. Chem., Int. Ed. Engl., 52 (2013) 10766-10770.

[13] J. Yang, M.A. Cohen Stuart, M. Kamperman, Jack of all trades: versatile catechol crosslinking mechanisms, Chem Soc Rev, 43 (2014) 8271-8298.

[14] Q. Wei, R. Haag, Universal polymer coatings and their representative biomedical applications, Materials Horizons, 2 (2015) 567-577.

[15] S. Geissler, A. Barrantes, P. Tengvall, P.B. Messersmith, H. Tiainen, Deposition Kinetics of Bioinspired Phenolic Coatings on Titanium Surfaces, Langmuir, 32 (2016) 8050-8060.

[16] X. Zhang, P.-F. Ren, H.-C. Yang, L.-S. Wan, Z.-K. Xu, Co-deposition of tannic acid and diethlyenetriamine for surface hydrophilization of hydrophobic polymer membranes, Appl. Surf. Sci., 360 (2016) 291-297.

[17] Z. Wang, S. Ji, F. He, M. Cao, S. Peng, Y. Li, One-step transformation of highly hydrophobic membranes into superhydrophilic and underwater superoleophobic ones for high-efficiency separation of oil-in-water emulsions, J. Mater. Chem. A, 6 (2018) 3391-3396.

[18] H. Wang, J. Wu, C. Cai, J. Guo, H. Fan, C. Zhu, H. Dong, N. Zhao, J. Xu, Mussel inspired modification of polypropylene separators by catechol/polyamine for Li-ion batteries, ACS Appl. Mater. Interfaces, 6 (2014) 5602-5608.

[19] W.-Z. Qiu, H.-C. Yang, L.-S. Wan, Z.-K. Xu, Co-deposition of catechol/polyethyleneimine on porous membranes for efficient decolorization of dye water, J. Mater. Chem. A, 3 (2015) 14438-14444.

[20] Y.C. Xu, Y.P. Tang, L.F. Liu, Z.H. Guo, L. Shao, Nanocomposite organic solvent nanofiltration membranes by a highly-efficient mussel-inspired co-deposition strategy, J. Membr. Sci., 526 (2017) 32-42.

[21] J.-R. Jeon, J.-H. Kim, Y.-S. Chang, Enzymatic polymerization of plant-derived phenols for material-independent and multifunctional coating, J. Mater. Chem. B, 1 (2013).

[22] F. Behboodi-Sadabad, H. Zhang, V. Trouillet, A. Welle, N. Plumeré, P.A. Levkin, UV-Triggered Polymerization, Deposition, and Patterning of Plant Phenolic Compounds, Adv. Funct. Mater., 27 (2017).

[23] Q. Wei, F. Zhang, J. Li, B. Li, C. Zhao, Oxidant-induced dopamine polymerization for multifunctional coatings, Polymer Chemistry, 1 (2010) 1430.

[24] S.H. Hong, S. Hong, M.-H. Ryou, J.W. Choi, S.M. Kang, H. Lee, Sprayable Ultrafast Polydopamine Surface Modifications, Adv. Mater. Interfaces, 3 (2016) 1500857.

[25] C. Zhang, Y. Ou, W.X. Lei, L.S. Wan, J. Ji, Z.K. Xu, CuSO4/H2O2-Induced Rapid Deposition of Polydopamine Coatings with High Uniformity and Enhanced Stability, Angew. Chem., Int. Ed. Engl., 55 (2016) 3054-3057.

[26] C. Luo, Q. Liu, Oxidant-Induced High-Efficient Mussel-Inspired Modification on PVDF Membrane with Superhydrophilicity and Underwater Superoleophobicity Characteristics for Oil/Water Separation, ACS Appl. Mater. Interfaces, 9 (2017) 8297-8307.

[27] F. Ponzio, J. Barthès, J. Bour, M. Michel, P. Bertani, J. Hemmerlé, M. d'Ischia, V. Ball, Oxidant Control of Polydopamine Surface Chemistry in Acids: A Mechanism-Based Entry to Superhydrophilic-Superoleophobic Coatings, Chemistry of Materials, 28 (2016) 4697-4705.

[28] N.G.P. Chew, S. Zhao, C. Malde, R. Wang, Polyvinylidene fluoride membrane modification via oxidant-induced dopamine polymerization for sustainable direct-contact membrane distillation, J. Membr. Sci., 563 (2018) 31-42.

[29] F.-N. Meng, M.-Q. Zhang, K. Ding, T. Zhang, Y.-K. Gong, Cell membrane mimetic PVDF microfiltration membrane with enhanced antifouling and separation performance for oil/water mixtures, J. Mater. Chem. A, 6 (2018) 3231-3241.

[30] S. Hong, Y.S. Na, S. Choi, I.T. Song, W.Y. Kim, H. Lee, Non-Covalent Self-Assembly and Covalent Polymerization Co-Contribute to Polydopamine Formation, Adv. Funct. Mater., 22 (2012) 4711-4717.

[31] G.F.P.a.M.V. Chaubal, Enzyme-catalysed polymer modification: reaction of phenolic compounds with chitosan films, Polymer, 37 4643−4648.

[32] H. Shi, Y. He, Y. Pan, H. Di, G. Zeng, L. Zhang, C. Zhang, A modified mussel-inspired method to fabricate TiO2 decorated superhydrophilic PVDF membrane for oil/water separation, J. Membr. Sci., 506 (2016) 60-70.

[33] S.W.W.a.E.T. Kaiser, The Mechanism of the Periodate Oxidation of Aromatic Systems. III. A Kinetic Study of the Periodate Oxidation of Catechol, Journal of the American Chemical Society, 88 (1966) 5820-5827.

[34] Z. Shami, S.M. Amininasab, P. Shakeri, Structure-Property Relationships of Nanosheeted 3D Hierarchical Roughness MgAl-Layered Double Hydroxide Branched to an Electrospun Porous

Nanomembrane: A Superior Oil-Removing Nanofabric, ACS Appl. Mater. Interfaces, 8 (2016) 28964-28973.

[35] M. Liu, S. Wang, Z. Wei, Y. Song, L. Jiang, Bioinspired Design of a Superoleophobic and Low Adhesive Water/Solid Interface, Adv. Mater., 21 (2009) 665-669.

[36] G.-E. Chen, W.-G. Sun, Y.-F. Kong, Q. Wu, L. Sun, J. Yu, Z.-L. Xu, Hydrophilic Modification of PVDF Microfiltration Membrane with Poly (Ethylene Glycol) Dimethacrylate through Surface Polymerization, Polym.-Plast. Technol. Eng., 57 (2017) 108-117.

[37] Y. Chen, Q. Deng, J. Xiao, H. Nie, L. Wu, W. Zhou, B. Huang, Controlled grafting from poly(vinylidene fluoride) microfiltration membranes via reverse atom transfer radical polymerization and antifouling properties, Polymer, 48 (2007) 7604-7613.

[38] H. Fan, Y. Peng, Application of PVDF membranes in desalination and comparison of the VMD and DCMD processes, Chem. Eng. Sci., 79 (2012) 94-102.

[39] J. Gu, P. Xiao, L. Zhang, W. Lu, G. Zhang, Y. Huang, J. Zhang, T. Chen, Construction of superhydrophilic and under-water superoleophobic carbon-based membranes for water purification, RSC Adv., 6 (2016) 73399-73403.

[40] Z. Zhou, W. Lin, X.-F. Wu, Electrospinning ultrathin continuous cellulose acetate fibers for high-flux water filtration, Colloids Surf., A, 494 (2016) 21-29.

[41] J.P. Bothma, J. de Boor, U. Divakar, P.E. Schwenn, P. Meredith, Device-Quality Electrically Conducting Melanin Thin Films, Adv. Mater., 20 (2008) 3539-3542.

[42] F.-f. Ma, N. Zhang, X. Wei, J.-h. Yang, Y. Wang, Z.-w. Zhou, Blend-electrospun poly(vinylidene fluoride)/polydopamine membranes: self-polymerization of dopamine and the excellent adsorption/separation abilities, J. Mater. Chem. A, 5 (2017) 14430-14443.

[43] Y. Cao, N. Liu, W. Zhang, L. Feng, Y. Wei, One-Step Coating toward Multifunctional Applications: Oil/Water Mixtures and Emulsions Separation and Contaminants Adsorption, ACS Appl. Mater. Interfaces, 8 (2016) 3333-3339.

[44] J. Sun, H. Bi, S. Su, H. Jia, X. Xie, L. Sun, One-step preparation of GO/SiO 2 membrane for highly efficient separation of oil-in-water emulsion, J. Membr. Sci., 553 (2018) 131-138.

[45] Y. Huang, H. Li, L. Wang, Y. Qiao, C. Tang, C. Jung, Y. Yoon, S. Li, M. Yu, Ultrafiltration Membranes with Structure-Optimized Graphene-Oxide Coatings for Antifouling Oil/Water Separation, Adv. Mater. Interfaces, 2 (2015).

4.6 Supporting Information

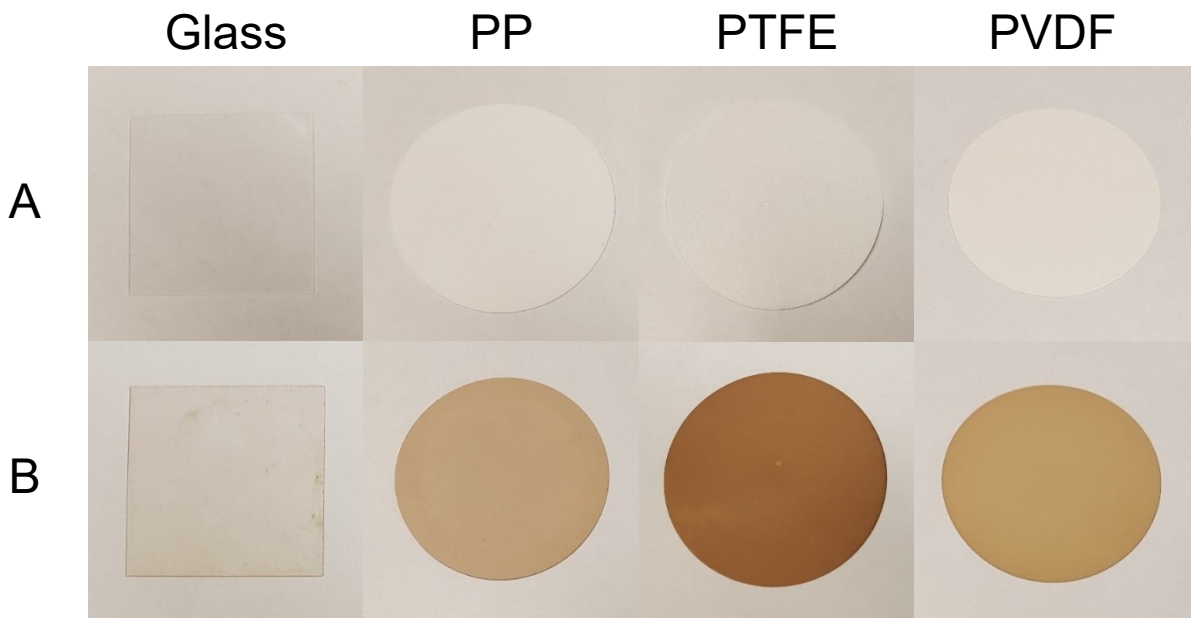

Figure 4. S1 Digital photographs of the (A) nascent substrates, (B) CA/SP-coated substrates after 2 h deposition. PP: polypropylene; PTFE: polytetrafluoroethylene; PVDF: polyvinylidene fluoride.

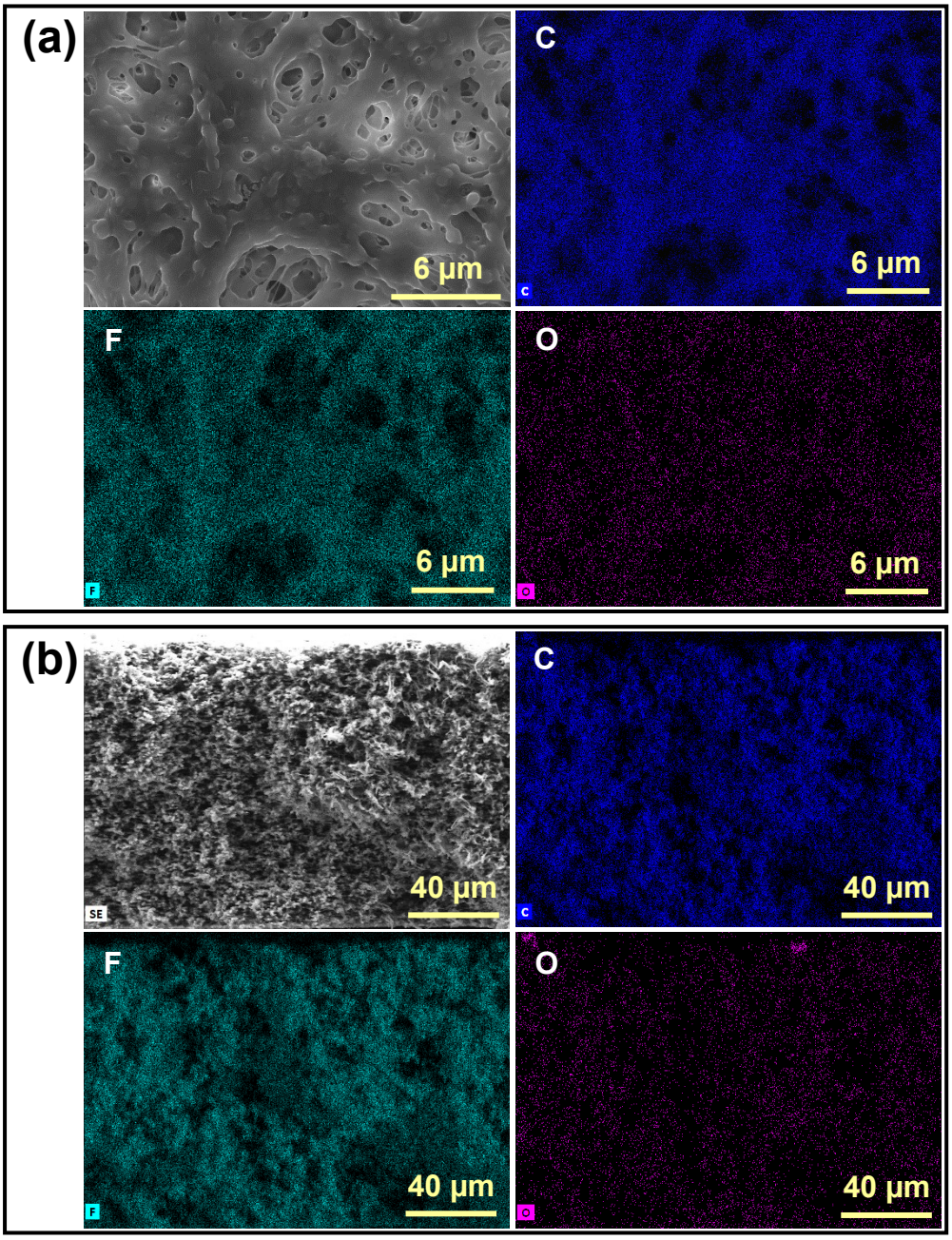

Figure 4. S2 FESEM images and EDS mappings of (a) top surface and (b) cross-section of the CA-SP-2 PVDF membrane.

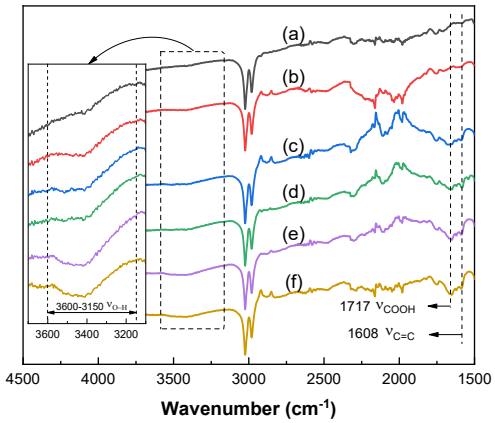

Figure 4. S3 ATR-FTIR spectra of the (a) nascent, (b) CA-O-24, (c) CA-SP-0.5, (d) CA-SP-1, (e) CA-SP-2 and (f) CA-SP-4 PVDF membranes.

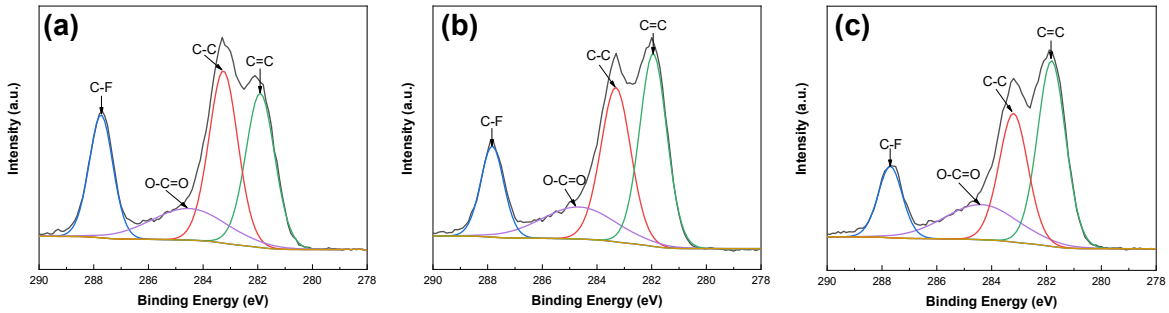

Figure 4. S4 C1s XPS spectra of (a) CA-SP-0.5, (b) CA-SP-1 and (c) CA-SP-4 PVDF membranes.

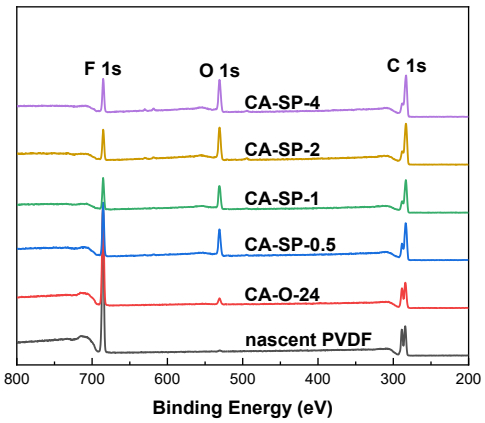

Figure 4. S5 Survey scan XPS spectra of the nascent and as-modified PVDF membranes.

Table 4. S1 Recent advances in polyphenol-based superhydrophilic coatings

Materials	Time (h)	Ref
Tannic Acid + Ovalbumin	15	[1]
CA + PEI	6	[2]
CA + POSS-$NH_3^+Cl^-$	3.5	[3]
CA + SP	2	This work

PEI: polyethyleneimine; POSS-$NH_3^+Cl^-$: octaammonium polyhedral oligomeric silsesquioxane.

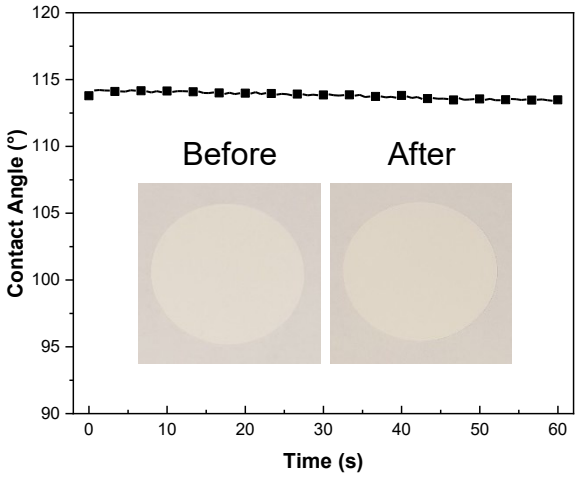

Figure 4. S6 Water contact angle in air of the PVDF membrane after SP treatment. Inset shows the photographs of PVDF membrane before (left) and after (right) SP treatment.

Figure 4. S7 Optical microscope images and digital photos of the SDS-stabilized hexane-in-water emulsion before and after separation.

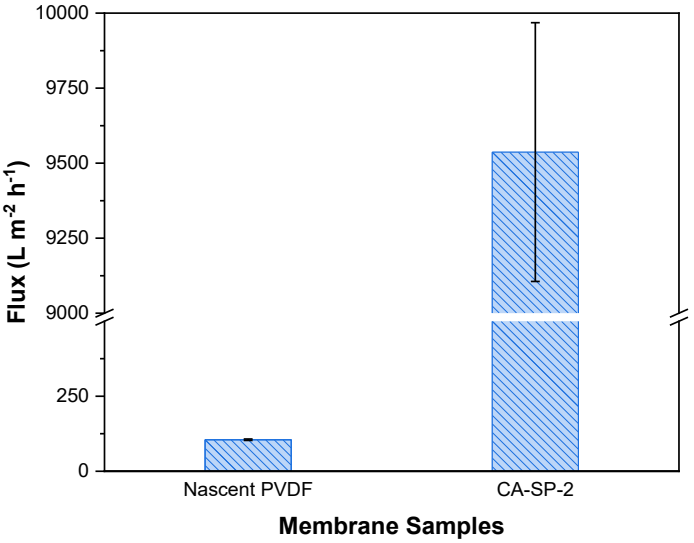

Figure 4. S8 Flux of hexane-in-water emulsion for different membranes.

4.7 References

[1] Z. Wang, S. Ji, J. Zhang, Q. Liu, F. He, S. Peng, Y. Li, Tannic acid encountering ovalbumin: a green and mild strategy for superhydrophilic and underwater superoleophobic modification of various hydrophobic membranes for oil/water separation, J. Mater. Chem. A, 6 (2018) 13959-13967.

[2] W.-Z. Qiu, H.-C. Yang, L.-S. Wan, Z.-K. Xu, Co-deposition of catechol/polyethyleneimine on porous membranes for efficient decolorization of dye water, J. Mater. Chem. A, 3 (2015) 14438-14444.

[3] Y.C. Xu, Y.P. Tang, L.F. Liu, Z.H. Guo, L. Shao, Nanocomposite organic solvent nanofiltration membranes by a highly-efficient mussel-inspired co-deposition strategy, J. Membr. Sci., 526 (2017) 32-42.

Chapter 5 Janus Membrane Emulsification for Facile Preparation of Hollow Microspheres[2]

5.1 Introduction

Double emulsions are emulsions within the emulsions which have been attracting great research interest because they hold tremendous promise in food products, material science, wastewater treatment, mineral processing, and pharmaceuticals.[1-4] A majority of double emulsions are either water-in-oil-in-water (W/O/W) or oil-in-water-in-oil (O/W/O). Specifically, gas-in-oil-in-water (G/O/W) emulsions that are microbubbles stabilized with a thin oil layer can be very useful in various areas. For example, oily bubbles containing oil-soluble collectors in the oil layer can be applied in mineral flotation, ensuring high-efficient recovery and low-cost operations.[5] Nanoparticle-shelled bubbles are capable of acting as ultrasonic contrast agents in biomedical imaging.[6] Most importantly, these emulsions are versatile templates for making different kinds of hollow polymeric microspheres. Under UV illumination, the polymerizations of monomers encapsulated in the oil layer of G/O/W emulsion droplets transfer the reactive oil layer into a solid layer; hence, the hollow polymeric microspheres are produced.

There are a variety of methods that have been studied to produce G/O/W double emulsions, such as ultrasonication, high shear mixing, and mechanical agitation.[7, 8] However, it is still difficult to develop a technique having a high production rate, uniformity of the structure, and cost effectiveness by a facile and simple procedure. The limitations for these traditional approaches are energy-intensive and difficult to control the size distributions of droplets. Many alternative methods have been developed using microfluidic devices to form monodispersed double emulsions on a drop-by-drop basis.[9, 10] This technology can produce one droplet at a time with excellent control over composition, dimension, and structure, but commercial applications on the

[2] A version of this chapter will be submitted for publication on *Journal of Membrane Science*.

microfluidic techniques remain very few due to the limited throughput. Improving production rates by designing parallelized microfluidic chips seems to be feasible, but encountered the problems in channel blockage and leakage that are difficult to be located and resolved.[11]

Among these approaches, membrane emulsification holds a promise as it enables us to produce near-monodisperse emulsion droplets in low energy consumption with a high throughput.[12] In the membrane emulsifying process, the to-be-dispersed phase is extruded from the membrane pores to form drops, which are detached from its surface into the continuous phase once the drag and buoyancy force acting on each drop become balanced.[13] Traditionally, the production of double emulsions by membrane emulsification contains two steps, which means that the single emulsion was first prepared through a non-membrane method (e.g. ultrasonication, high-shear processing) and served as the to-be-dispersed phase to pass a membrane in the latter step. For example, Eisinaite at al. reported the formation of W/O/W emulsions enclosing beetroot juice in the inner aqueous phase using a two-step emulsification process.[14] Recently, the two-step premix membrane emulsification process was used by Na et al. to enable the construction of double-emulsion-templated porous microspheres.[15] There is only one peer-reviewed journal article we can find in which membranes were employed in both emulsification steps to generate double emulsions. A water-in-oil emulsion was first prepared using a hydrophobic membrane and then permeated through a hydrophilic membrane to generate W/O/W emulsions.[16] Besides, we are unaware of any previous studies that have managed to prepare double emulsions in a one-step membrane emulsification process. Among different types of membranes, such as ceramic, metal, polymer, and Shirasu porous glass (SPG) membranes, the polymeric membranes stand out because of their high flexibility, cost-effectiveness, and the possibility of being used as a disposable membrane in industrial production.[17]

Surface wettability plays a crucial role in droplet growth and detachment. As a rule of thumb, the membrane pores should be wetted by the continuous phase in order to make drops of the dispersed phase at a small size. Hence, only membranes wetted by water (hydrophilic) are suitable for making oil drops suspended in a continuous water phase.[13] Nakashima and co-workers have reported that violation of the rule (using membranes with opposite wetting characteristics) would lead to a polydispersed emulsion with larger average droplet size.[18] An explanation of this difference is that the oil droplet is likely to quickly detach from the hydrophilic surface at a small size, while tending to form a spreading film on the hydrophobic surface. However, the direct utilization of a hydrophilic membrane increases the gas intrusion pressure drastically, leading to extra energy cost and membrane failures.[19] Therefore, a membrane with hydrophilic/hydrophobic asymmetry is believed to be favorable for making G/O/W emulsions because the hydrophilic side achieves fast detachment of oily bubbles at small sizes and the hydrophobic side allows gas/oil permeation.

Herein, nearly-monodispersed G/O/W double emulsions were prepared using a porous polymeric membrane in a one-step membrane emulsification process. The inherently hydrophobic PVDF membrane was first modified via single-sided catechol (CA) deposition. Under a pressurized nitrogen supply, the gas stream passed through organic phase containing organic additives (reactive monomers) and then ran through the membrane pores into the aqueous phase to generate double emulsions G/O/W. The effects of pHs of the continuous aqueous phase on generation of double emulsions G/O/W were studied. The mean droplet size as a function of gas permeation flux has also been investigated. Moreover, hollow polymeric microspheres were successfully synthesized after UV irradiation of reactive oil layer of G/O/W double emulsions. Considering the operational efficiency of membrane emulsification, it is entirely feasible to scale

it up for massively manufacturing various microcapsules for a wide range of applications in food products, composite functional materials, and pharmaceuticals.

5.2 Experimental Section

5.2.1 Materials

Polyvinylidene fluoride microporous membranes (PVDF, 70 mm, pore size is ~ 2 μm) were purchased from Yibo Co., Ltd (China). 2-Hydroxy-2-methylpropiophenone, catechol, ethanol, and oleic acid were obtained from Sigma-Aldrich. 1, 6-Hexanediol diacrylate (HDDA), anhydrous sodium acetate, glacial acid, Nile Red and sodium periodate were bought from Fisher Scientific. All reagents were analytical grade and used as received. Water used throughout the experiments was purified in a Milli-Q (Millipore, Billerica, MA, USA) system.

5.2.2 Membrane Modification

The superhydrophilic modification was conducted on PVDF membranes as reported in our previous work.[20] These as-made membranes were labelled as superhydrophilic membranes. For the single-sided deposition,[19] catechol (2 mg mL^{-1}) was dissolved in acetate buffer (50 mM, pH = 5.0) with sodium periodate (4 mg mL^{-1}) by ultrasonication. The nascent PVDF membrane was floated on the above solution after pre-wetted by ethanol and placed between two filter papers for the adsorption of residual ethanol. Then the aluminum foil-covered beaker was put on a shaker with slow shaking (50 rpm) under ambient conditions. After 20 min, the as-made membranes were rinsed by water, followed by drying at 40 °C overnight. The hydrophilic side of the resulting membrane was referred to as Janus-Hydrophilic, and the hydrophobic side as Janus-Hydrophobic.

5.2.3 Membrane Characterization

The surface morphology variation of membrane before and after modification was observed using scanning electron microscopy (SEM, FEI Quanta 250) after coating with gold. X-ray

photoelectron spectroscopy (XPS, Kratos, AXIS 165) was performed to characterize elemental compositions of the membrane surfaces. Characteristic peaks of the membranes were analyzed by attenuated total reflectance-Fourier transform infrared spectroscopy spectra (ATR-FTIR, Agilent, Cary 600 Series). The surface wettability of membrane was evaluated in terms of water contact angle (WCA) and oil contact angle (OCA). The WCA in air and the OCA underwater were detected using a theta optical tensiometer at room temperature (Attension, Biolin Scientific T200).

5.2.4 Membrane Emulsification

A custom built device (Figure 5. S1) was used to conduct membrane emulsification. The apparatus was separated into two parts with the tested membrane in between. The bottom chamber connecting a nitrogen gas inlet and an oil inlet was first filled with 150 mL HDDA containing 10^{-2} M oleic acid, 50 ppm Nile Red, and 10 mol% photo-initiator (2-hydroxy-2-methylopropiophenone). Subsequently, 300 mL of Milli-Q water was added into the upper container. The compressed nitrogen from the bottom of the cell was forced to pass through the membrane at flow rates from 100 to 400 mL min^{-1}.

For the fabrication of hollow polymeric microspheres, the oil droplets encapsulating microbubbles were solidified upon UV light exposure for 30 s with a 120 W UV spot light source (XE 120-Q, Photonic Solution Inc.).

5.2.5 Emulsion and Polymer Capsule Characterization

Optical microscope and fluorescence images were captured with an inverted microscope (Carl Zeiss Axiovert 200M) equipped with a CCD camera (Photron fastcam mini AX200). The average droplet diameter and droplet distribution were counted and analyzed by Image J software. For this determination, a total of 200 microspheres produced at pH 7 and 150 microspheres at pH 9 were counted respectively, during which only the gas bubble surrounded by an obvious oil layer was

counted for size analysis of double emulsion. Surface morphology of the polymerized microbubbles was viewed by a helium ion microscope (HIM, Zeiss Orion).

5.3 Results and Discussion

5.3.1 Fabrication of Janus Membranes

Our Janus membrane was obtained after the asymmetric deposition by floating the nascent PVDF membrane on the CA/SP solution surface for 20 min. The side contacting with the solution was darker after deposition. In this process, a hydrophilic coating was formed on the immersed membrane surface via oxidant-induced CA cross-linking. The top view SEM images of the nascent, each side of the Janus, and the superhydrophilic membranes are shown in Figure 5.1a. We can see that both modifications introduced ignorable pore size changes to PVDF membranes. The asymmetric chemistry of Janus membrane was identified by comparison of the chemical compositions of each membrane surface. From the high-resolution C 1s spectra as shown in Figure 5. S2, compare with pure PVDF, two new peaks at 283.8 eV and 286.9 eV, attributed to C=C and O−C=O respectively, appeared in the spectra of modified membranes. The higher intensity of these peaks in the Janus-Hydrophilic side than that of the Janus-Hydrophobic side provided direct evidence of the asymmetric deposition of CA. The surface elemental compositions are listed in Table 5. S1. As suggested, a higher concentration of O (11.96%) can be observed on the Janus-Hydrophilic surface than the Janus-Hydrophobic surface (8.47%). There was more CA coated on bottom membrane surface than on the top due to the capillary effect during the modification process.[19] Survey scan XPS spectra (Figure 5.1b) of the modified PVDF membranes reveal strong O signals and weakened F signals, suggesting different amounts of functional groups were generated on each side. The asymmetric surface components were further evidenced by ATR-FTIR spectra (Figure 5.1c). The new peaks at 3500 – 3100, 1717 and 1608 cm^{-1} in the spectra of

as-modified membranes were ascribed to the O−H stretching vibrations of phenolic hydroxyl groups, the C=O stretching vibrations of carboxylic acids, and the C=C resonance vibrations of aromatic rings, correspondingly. The Janus-Hydrophilic side exhibited stronger peak intensity than the Janus-Hydrophobic side, which was in good agreement with the XPS analysis. The overall results showed that more functional groups adhered to the Janus-Hydrophilic side compared with the Janus-Hydrophobic side.

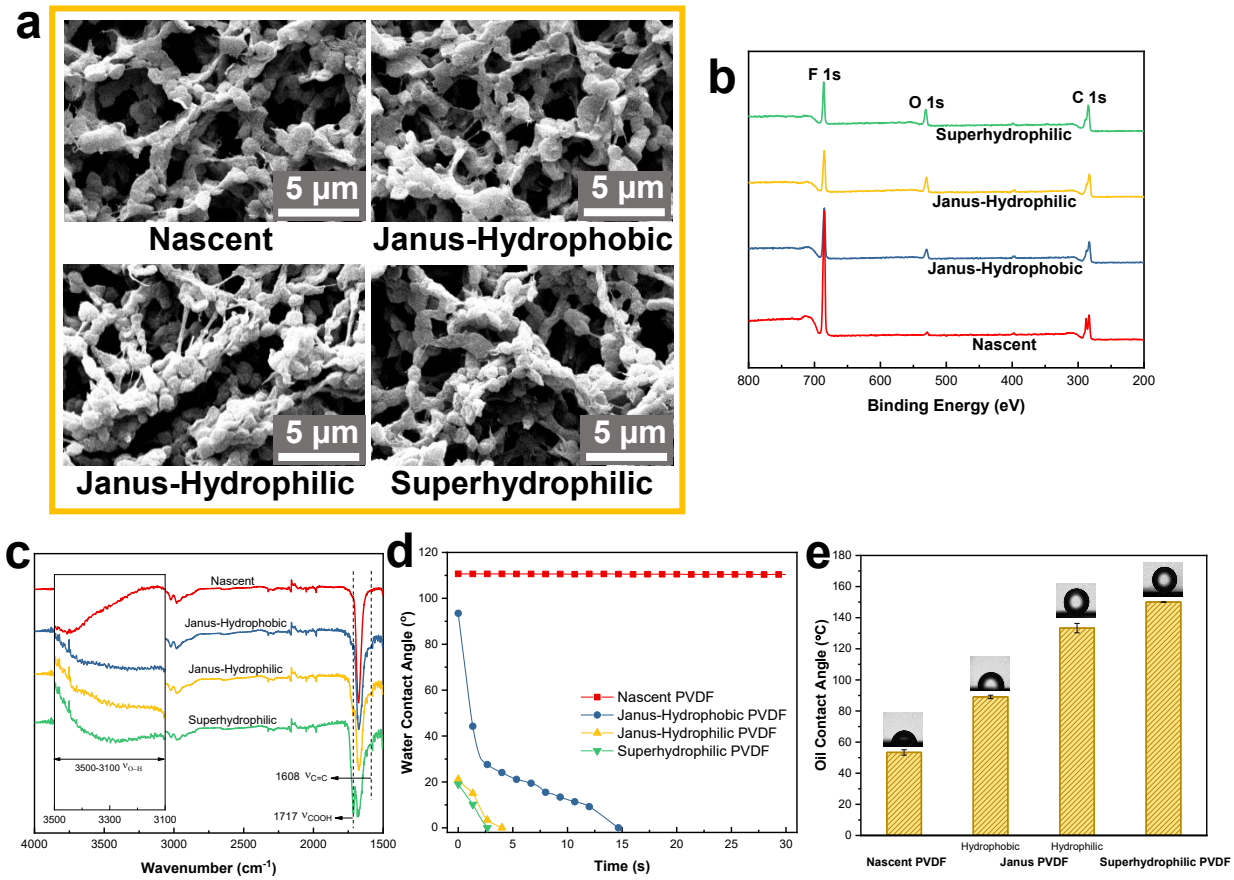

Figure 5.1 (a) SEM top view images of the nascent, Janus-Hydrophobic, Janus-Hydrophilic, and Superhydrophilic PVDF membranes. (b) XPS wide scans and (c) ATR-FTIR spectra for nascent and as-modified PVDF membranes. (d) Water contact angles of the nascent and as-modified PVDF membranes. (e) Oil contact angles under water on nascent, each surface of the Janus, and superhydrophilic PVDF membranes. The oil is 1, 6-hexanediol diacrylate.

The surface wettability is a crucial factor in membrane emulsification performance. Therefore, the WCA on each type of surface was measured (Figure 5.1d). As presented, the initial WCA of the Janus-Hydrophilic membrane was 21.2° and then the water drop penetrated into the membrane pores in 4 s. Compared with the Janus-Hydrophilic side, the Janus-Hydrophobic side showed hydrophobicity with an initial water contact angle of about 93°, while instantly decreased to 68° and gradually permeated through the membrane pores reaching 0° in 15 s. To demonstrate the Janus membrane's anisotropic surface affinity towards water and oil, we further investigated the OCAs in water on the nascent, the superhydrophilic and the Janus membranes (Figure 5.1e). The pristine PVDF surface was moderate lyophilic with an OCA around 53°, arising from its hydrophobicity and air trapped in the membrane pores. After asymmetric modification with CA/SP, the OCA of the modified side increased to ~133°, suggesting oleophobicity. The OCA of the Janus-Hydrophobic side also increased to ~89° because of a little CA coating formed on this surface. These phenomena proved that our Janus membrane exhibited anisotropic surface wettability.

5.3.2 Spreading of the Oil over the Gas Bubble

The formation of the oil-coated bubbles depends on the successful spreading of oil droplets over the gas bubbles, which is governed by the balance between the surface tensions (γ) at the contact line of the air (A), oil (O) and water (W) interfaces.[21] The spreading interactions between different fluids can be described by the spreading coefficient. For the air–oil–water system, the oil spreading coefficient is defined as (5.1):

$$S\ (\mathrm{mN\ m^{-1}}) = \gamma_{A/W} - \gamma_{A/O} - \gamma_{O/W} \tag{5.1}$$

where $\gamma_{A/W}$ (mN m^{-1}), $\gamma_{A/O}$ (mN m^{-1}), and $\gamma_{O/W}$ (mN m^{-1}) are the air–water surface tension, air–oil surface tension and oil–water interfacial tension respectively. In order for the oil to spread entirely across the air bubble, the S has to be positive. In our work, the interfacial tension of

HDDA–water under various conditions was investigated to estimate the corresponding *S*. The interfacial tension measurements (Table 5. S2) revealed positive values for the spreading coefficients, suggesting that the monomer oil is capable of spreading along the air–water interface within the experimented range. It was also found that changing either the water pH or the surfactant concentration has little effects on the HDDA–water interfacial tension.

5.3.3 Generation of G/O/W Emulsions

As an experimental proof of concept, the as-fabricated membranes were used to generate G/O/W emulsions through membrane emulsification. The emulsification process is illustrated in Figure 5.2. It should be mentioned that the feed volume of oil was fixed from the beginning and not extra supply was added to the system until the end of an experiment. The membrane was fixed in a home-built emulsification system with the hydrophilic side faced to the water, and the oil (HDDA) was dyed with Nile Red so as to improve visibility. When the gas valve was open, numerous droplets grew on the membrane surface and rose to the air/water interface to form stable emulsions.

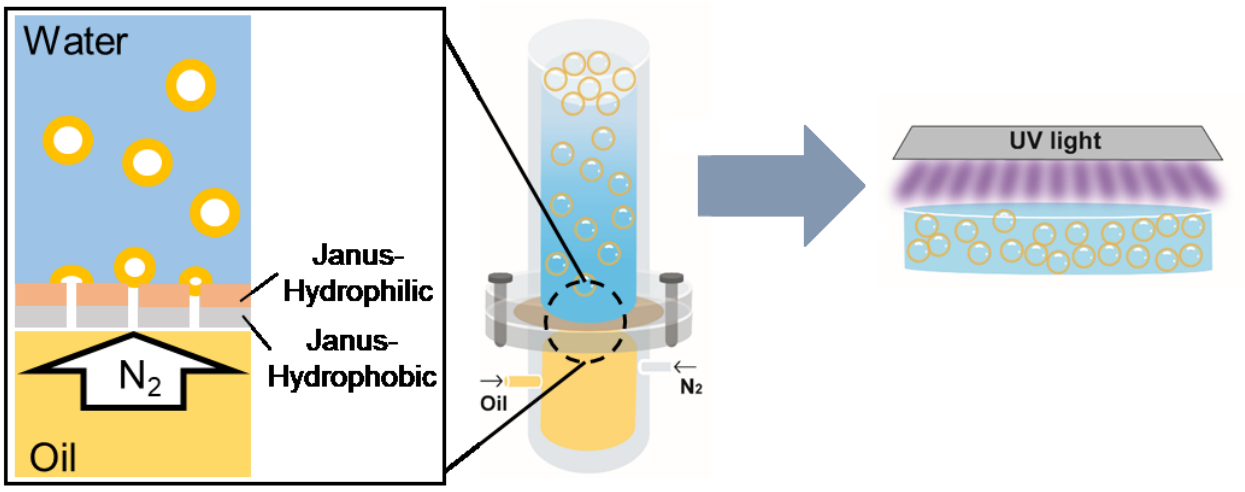

Figure 5.2 Schematic illustration of generating hollow microspheres through Janus membrane in a homemade emulsification device.

To verify the advantages of Janus membranes, the nascent and superhydrophilic membranes were also involved for comparison. A gas flow rate of 300 mL min^{-1} was chosen for these experiments. As suggested in Figure 5.3b and c, both the Janus and superhydrophilic membranes were able to produce G/O/W emulsions. In addition to G/O/W emulsions, gas bubbles were also produced. In contrast, the nascent (Figure 5.3a) membrane failed in double emulsion generation. As we mentioned above, the wettability of the membrane surfaces contributed to these results. When being forced out of the membrane pores, the oil was inclined to form a tiny droplet on a hydrophilic/oleophobic surface, while it preferred to spread on a hydrophobic surface and then form an oil film, thereby the Janus and the superhydrophilic membranes succeeding in emulsion fabrication owing to their similar wetting behaviors. Notably, the smaller quantities of double emulsions in the case of the superhydrophilic membrane may be caused by the less spreading time.

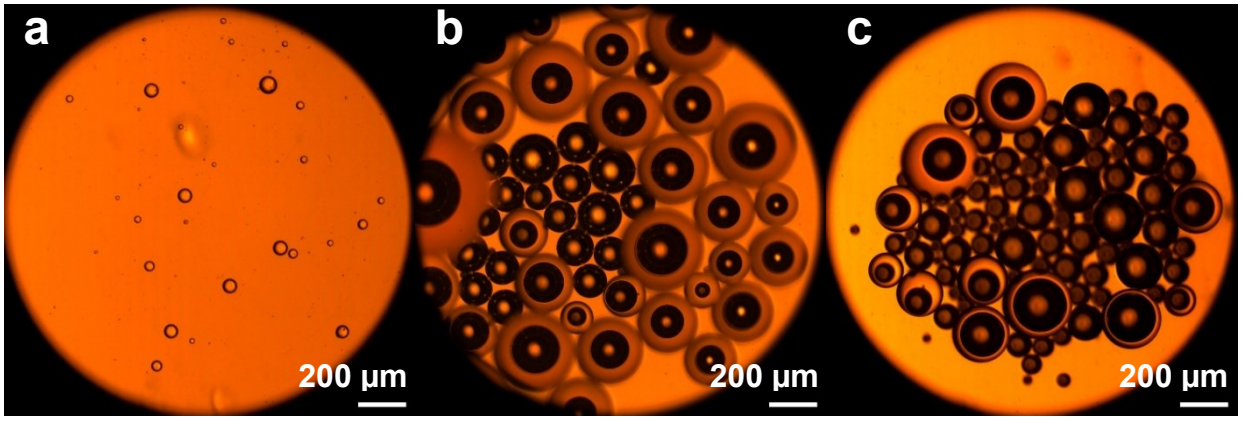

Figure 5.3 Optical micrographs of the G/O/W emulsion prepared by (a) nascent, (b) Janus, and (c) superhydrophilic PVDF membranes.

To achieve the controllable generation of the G/O/W emulsions, it is significant to determine the optimal parameters that provided the best control over drop size and particularly the size distribution. Therefore, the influence of water pH was investigated by generating G/O/W emulsions in water with different pH values (3, 7 and 9) and results were shown in Figure 5.4. In these experiments the gas flow rate was kept constant at 300 mL min^{-1}. In acidic aqueous media

(pH = 3), the fabricated G/O/W emulsions were unstable and eventually no G/O/W droplets or other emulsions was observed under the optical microscope (Figure 5.4b). This is because the carboxylate head groups of oleic acid is protonated at low pH and prefers to stay in the oil phase instead of the oil/water interface.[22] In contrast, the emulsion droplets produced at pH 7 and 9 were more stable, due to the strong deprotonation of oleic acid which leads to an increase in the

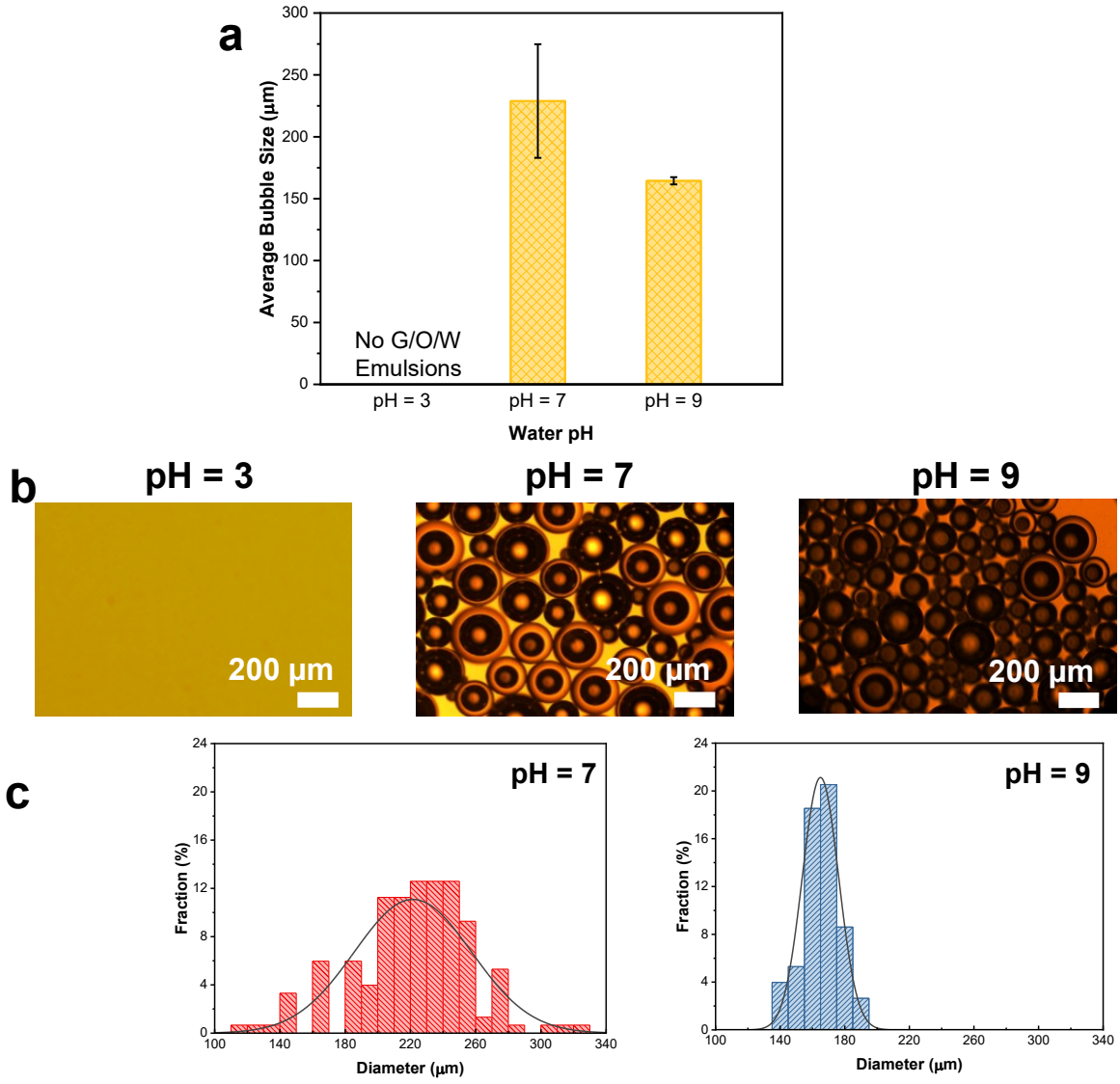

Figure 5.4 (a) Variation in the average size of G/O/W droplets prepared in water with different pH values (3, 7 and 9). (b) Microscope images of G/O/W droplets prepared at pH = 3, 7 and 9. (c) Size distributions of emulsions prepared at pH = 7 and 9.

stability of the double emulsions. It is interesting to note that at high pH value of 9 G/O/W droplets with smaller sizes (~160 μm) and narrower size distributions were produced in comparison with those produced at neutral pH (~228 μm), but an accompanying drastic decrease in the production yield of G/O/W emulsions occurred (Figure 5.4b and c). Although high pH gave better control over the size and size distribution, pH 7 was selected in the following experiments in order to obtain high yields.

The effects of the gas flow rates on the size of the droplets and size distribution were further studied. Figure 5. S3 shows the optical photos of the G/O/W emulsions prepared under different gas fluxes. As can be seen, a decrease in gas flow rates created larger emulsion drops. It was assumed that the time for an emulsion drop to grow and detach from membrane surface was dependent upon the gas flow rates. Therefore, the increase of gas flow rate allowed less time for the drops to grow.[23] Data for the average droplet size as a function of gas flux are summarized in Figure 5.5, including ~268 μm at 100 mL min^{-1}, ~248 μm at 200 mL min^{-1}, ~228 μm at 300 mL min^{-1}, and ~220 μm at 400 mL min^{-1}, respectively. To determine the size of microspheres produced at each gas flow rate, approximately 100 microspheres were counted correspondingly. These

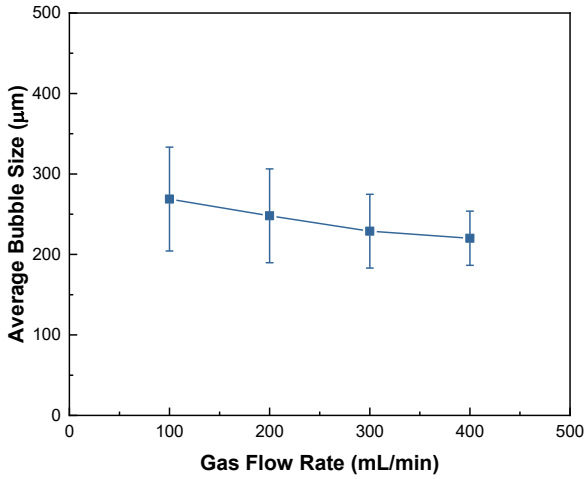

Figure 5.5 The effect of the gas flow rate on droplet size.

results demonstrated that the optimized gas flux at which relatively uniform-sized double emulsions were efficiently produced was 300 mL min^{-1}.

For the production of hollow microspheres, the G/O/W emulsions were exposed to a mercury UV source for 30 s. Upon UV illumination, the monomer polymerized immediately and hard-shelled microcapsules were produced. Figure 5.6a and b reveal the successful formation of microcapsules of good spherical shape and relatively uniform size (192 – 285 μm). In the fluorescence micrograph as illustrated in Figure 5.6b, the existence of a bright green ring encapsulating a cavity in the interior was indicative of a hollow structure instead of a porous structure or a solid particle. The solidification of our double emulsion drops was further confirmed

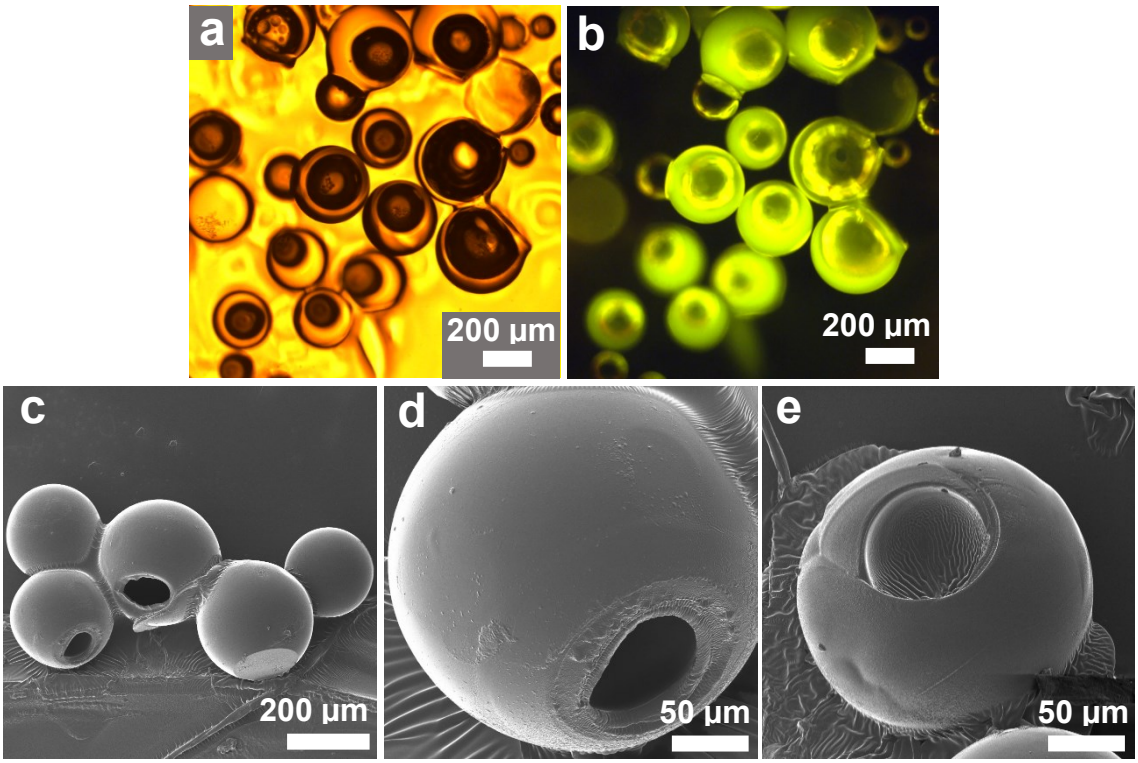

Figure 5.6 (a) The microscope photograph of the hollow microspheres after polymerization. (b) The fluorescent image of hollow microspheres with the shell containing fluorescent dye Nile red. The pH of water is 7. HIM micrographs of the hollow polymeric microcapsule prepared at (c, d) pH =7 and (e) pH = 9, respectively.

by HIM characterization results (Figure 5.6c–e) and convincing hollow–sphere structures can be identified. We can see from the HIM images that the microspheres produced at both pHs are in perfect spherical shape, while we obtained smaller-sized hollow microspheres at pH 9. In Figure 5.6c, we note that the neighboring microspheres are connected, which may be caused by the reason that the concentration of deprotonated oleic acid was too low to stabilize the double emulsion drops and keep them perfectly separated. The high magnification of intentionally broken capsules also reveals the thickness of the shell at pH 7 and 9 was approximately 20 μm, indicating that pH has little or no effect on the shell wall thickness.

5.4 Conclusions

In this study, we facilely prepared a hydrophilic/hydrophobic Janus membrane via single-sided CA/SP deposition. Narrowly distributed G/O/W double emulsions were successfully fabricated by a one-step membrane emulsification process for the first time. Such a method was demonstrated as a successful one-step preparation of double emulsions and a precursor for hollow microspheres. The hollow structured microspheres may find potential applications in catalysis, drug delivery, cosmetics, and modern electronics. We believe that our approach, which only needs one dispersion step as compared to the common complicated micro fabrication with multiple-step emulsification processes, is promising in a high throughput production of double emulsions at a low cost. This work provides a new opportunity in the preparation of double emulsions and the fabrication of hollow microspheres for many applications in enhanced oil and mineral recovery, drug delivery vehicles, and water treatment. More research on the mechanism and control of the formation of double emulsions will be conducted in the future.

5.5 References

[1] J. Liu, T. Mak, Z. Zhou, Z. Xu, Fundamental study of reactive oily-bubble flotation, Miner Eng, 15 (2002) 667-676.

[2] G. Muschiolik, Multiple emulsions for food use, Curr Opin Colloid In, 12 (2007) 213-220.

[3] E. Lorenceau, A.S. Utada, D.R. Link, G. Cristobal, M. Joanicot, D.A. Weitz, Generation of polymerosomes from double-emulsions, Langmuir, 21 (2005) 9183-9186.

[4] S. Okushima, T. Nisisako, T. Torii, T. Higuchi, Controlled production of monodisperse double emulsions by two-step droplet breakup in microfluidic devices, Langmuir, 20 (2004) 9905-9908.

[5] F. Zhou, L.X. Wang, Z.H. Xu, Q.X. Liu, M.J. Deng, R. Chi, Application of reactive oily bubbles to bastnaesite flotation, Miner Eng, 64 (2014) 139-145.

[6] B. Xu, H.J. Dou, K. Tao, K. Sun, J. Ding, W.B. Shi, X.S. Guo, J.Y. Li, D. Zhang, K. Sun, "Two-in-One" Fabrication of Fe3O4/MePEG-PLA Composite Nanocapsules as a Potential Ultrasonic/MRI Dual Contrast Agent, Langmuir, 27 (2011) 12134-12142.

[7] K.P. Pancholi, U. Farook, R. Moaleji, E. Stride, M.J. Edirisinghe, Novel methods for preparing phospholipid coated microbubbles, Eur Biophys J Biophy, 37 (2008) 515-520.

[8] Q. Xu, M. Nakajima, S. Ichikawa, N. Nakamura, P. Roy, H. Okadome, T. Shiina, Effects of surfactant and electrolyte concentrations on bubble formation and stabilization, J Colloid Interf Sci, 332 (2009) 208-214.

[9] M.B. Romanowsky, A.R. Abate, A. Rotem, C. Holtze, D.A. Weitz, High throughput production of single core double emulsions in a parallelized microfluidic device, Lab Chip, 12 (2012) 802-807.

[10] A. Abbaspourrad, W.J. Duncanson, N. Lebedeva, S.H. Kim, A.P. Zhushma, S.S. Datta, P.A. Dayton, S.S. Sheiko, M. Rubinstein, D.A. Weitz, Microfluidic Fabrication of Stable Gas-Filled Microcapsules for Acoustic Contrast Enhancement, Langmuir, 29 (2013) 12352-12357.

[11] M.S. Manga, D.W. York, Production of Concentrated Pickering Emulsions with Narrow Size Distributions Using Stirred Cell Membrane Emulsification, Langmuir, 33 (2017) 9050-9056.

[12] S. van der Graaf, C.G.P.H. Schroen, R.M. Boom, Preparation of double emulsions by membrane emulsification - a review, Journal of Membrane Science, 251 (2005) 7-15.

[13] S.M. Joscelyne, G. Tragardh, Membrane emulsification - a literature review, Journal of Membrane Science, 169 (2000) 107-117.

[14] V. Eisinaite, D. Juraite, K. Schroen, D. Leskauskaite, Preparation of stable food-grade double emulsions with a hybrid premix membrane emulsification system, Food Chem, 206 (2016) 59-66.

[15] X. Na, W. Zhou, T. Li, D. Hong, J. Li, G. Ma, Preparation of double-emulsion-templated microspheres with controllable porous structures by premix membrane emulsification, Particuology, (2019).

[16] T. Nakashima, M. Shimizu, M. Kukizaki, Particle control of emulsion by membrane emulsification and its applications, Adv Drug Deliver Rev, 45 (2000) 47-56.

[17] N. Yamazaki, H. Yuyama, M. Nagai, G.-H. Ma, S. Omi, A Comparison of Membrane Emulsification Obtained Using SPG (Shirasu Porous Glass) and PTFE [Poly(Tetrafluoroethylene)] Membranes, Journal of Dispersion Science and Technology, 23 (2002) 279-292.

[18] T. Nakashima, M. Shimizu, M. Kukizaki, Membrane Emulsification by Microporous Glass, Inorganic Membranes : Icim2-91, (1991) 513-516.

[19] M.B. Wu, H.C. Yang, J.J. Wang, G.P. Wu, Z.K. Xu, Janus Membranes with Opposing Surface Wettability Enabling Oil-to-Water and Water-to-Oil Emulsification, ACS Appl Mater Interfaces, 9 (2017) 5062-5066.

[20] Y. Chen, Q. Liu, Oxidant-induced plant phenol surface chemistry for multifunctional coatings: Mechanism and potential applications, Journal of Membrane Science, 570-571 (2019) 176-183.

[21] N.E. Hotrum, T. van Vliet, M.A.C. Stuart, G.A. van Aken, Monitoring entering and spreading of emulsion droplets at an expanding air/water interface: A novel technique, J Colloid Interf Sci, 247 (2002) 125-131.

[22] J.J. Janke, W.F.D. Bennett, D.P. Tieleman, Oleic Acid Phase Behavior from Molecular Dynamics Simulations, Langmuir, 30 (2014) 10661-10667.

[23] R. Chen, P.F. Dong, J.H. Xu, Y.D. Wang, G.S. Luo, Controllable microfluidic production of gas-in-oil-in-water emulsions for hollow microspheres with thin polymer shells, Lab Chip, 12 (2012) 3858-3860.

5.6 Supporting Information

Figure 5. S1 Digital photograph of the home-built emulsification apparatus.

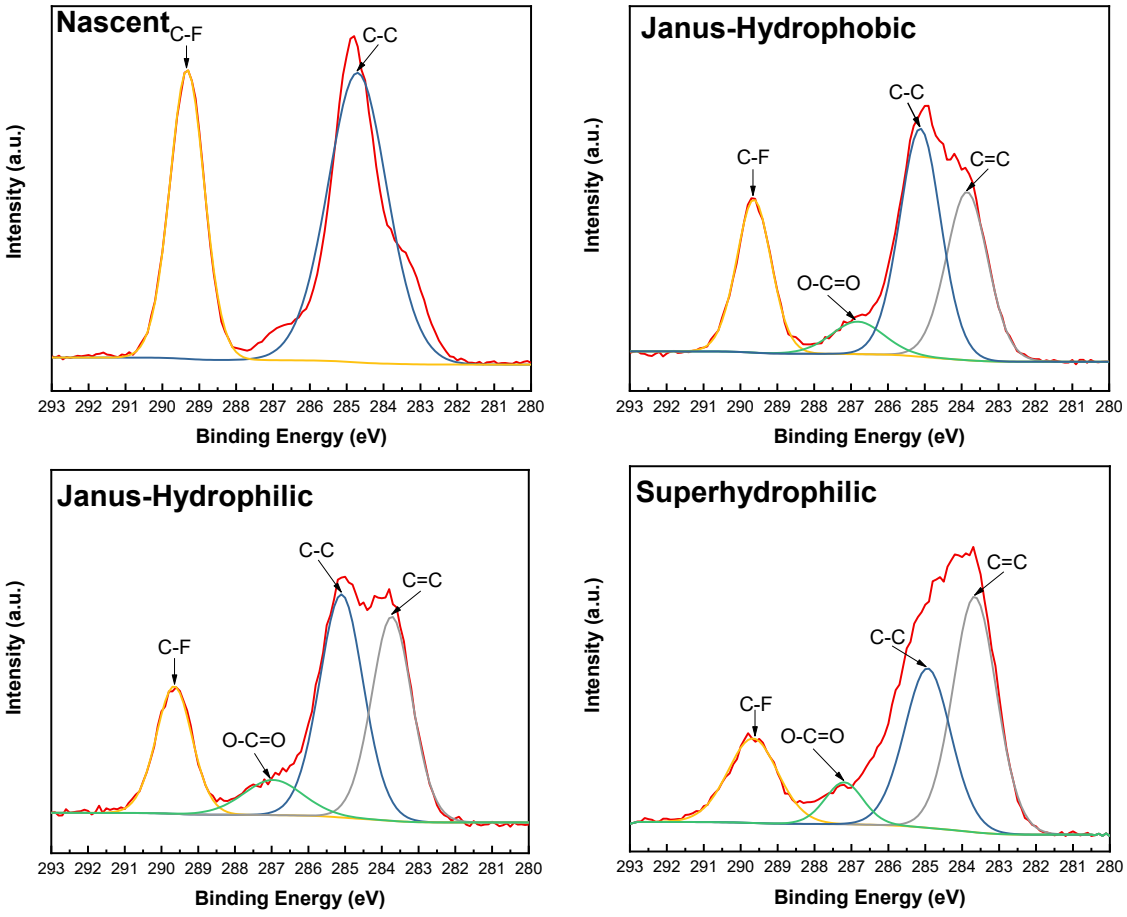

Figure 5. S2 High-resolution XPS spectra of C 1s for the nascent and modified membranes.

Table 5. S1 Elemental composition of each membrane surface as determined by XPS

Membrane	Composition (%)			Atomic ratio
	C	F	O	O/C
Nascent	54.03	45.97		
Janus-Hydrophobic	64.44	27.10	8.47	0.13
Janus-Hydrophilic	68.04	20.00	11.96	0.18
Superhydrophilic	69.27	18.01	12.72	0.18

Table 5. S2 The interfacial tension between monomer oil and water and the calculated spreading coefficient

Condition	Oleic acid concentration (the pH of water is 7)		Water pH (the oleic acid concentration is 10^{-2} M)		
	10^{-1} M	10^{-3} M	3	7	9
$\gamma_{O/W}$ (mN m^{-1})	7.17	9.09	7.23	6.52	8.45
S (mN m^{-1})	31.43	29.52	31.37	32.08	30.15

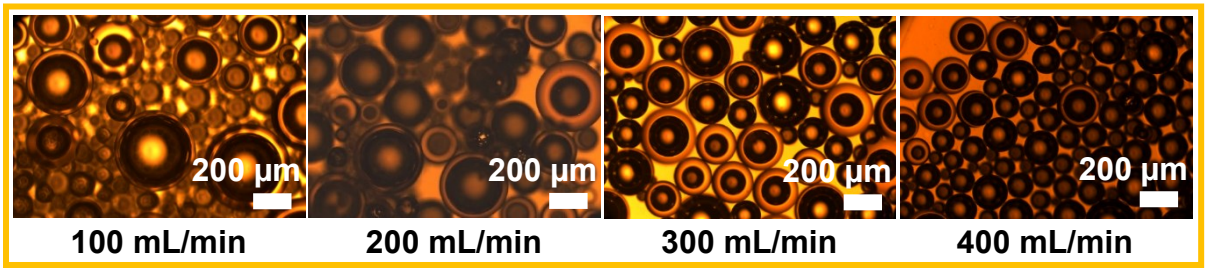

Figure 5. S3 Microscope images of G/O/W droplets fabricated by tuning the gas flow rates from 100 to 400 mL min^{-1}.

Chapter 6 Conclusions and Contributions

6.1 Major Conclusions

This dissertation has provided a novel one-step surface modification strategy and investigated its several potential applications in combination with membranes. This technique is expected to be commercially relevant, requiring a single synthesis step and having no unusual requirements with respect to post-functionalization. By adopting this technique, two types of membranes were developed and experimentally applied in areas including: (1) water purification and (2) emulsification.

We have found that sodium periodate could significantly accelerate CA polymerization and deposition under acidic pH. The possible crosslinking mechanisms of catechol under chemical oxidation has been explored. To test the versatility of CA coatings, immersion coating from aqueous catechol/sodium periodate solutions was performed on a variety of substrates. Oxidant-assisted CA polymerization was applied for modifying both the inner porous structures and the outer surfaces of the PVDF membranes uniformly, and to tune the functionalization degree of the surfaces by varying the immersion time. The pure water flux, permeate flux during the filtration of oil/water emulsion, and oil rejection of these CA-modified membranes were determined and compared to those of pristine membranes. Further characterization of the CA films demonstrated that the CA deposition under the oxidation of sodium periodate is an easy and effective means of surface functionalization. The resulting membrane exhibited robust mechanical stability, evidenced by its tolerance of caustic environments. Meanwhile, the as-made PVDF membranes showed outstanding copper ion adsorption and excellent resistance to oil, while maintaining high oil rejection over the testing time. This study clearly demonstrated the promising potential of preparing high performance superwetting membranes by using oxidant-assisted CA deposition.

In an attempt toward creating asymmetrically wettable surfaces using a catechol-inspired approach, CA/SP-anchored Janus membranes were fabricated via single-sided deposition. The asymmetric structure of Janus membrane was examined by ATR-FTIR, XPS, and contact angle test results. A novel double emulsion generator using Janus membranes was developed. The Janus membrane emulsification system features high throughput of double emulsions in an energy-effective way, thereby reducing operation costs. Compared with traditional and advanced techniques, our approach showed better performance, increasing production rates, demonstrating the potential of Janus membrane emulsification for fabricating hollow polymeric microspheres.

6.2 Contributions to the Original Knowledge

Surface modification inspired from nature is a growing field that aims at incorporating biological strategies to fabricate functionalized surfaces for on-demand applications. Plant-inspired chemistry has shown great potential in engineering surface properties, while the conventional CA coating method suffers from the limits of inefficient deposition rate as well as limited hydrophilicity. Specific contributions of this dissertation work to the original knowledge are described below:

1. This research has demonstrated for the first time that SP was used to trigger CA deposition and CA coatings with drastically enhanced hydrophilicity were achieved in a relatively short time in acidic aqueous solution. Although the precise mechanism behind the oxidant-assisted deposition is not fully unraveled, the obtained knowledge broadens the application prospects of plant-inspired chemistry.
2. Oxidant-assisted CA deposition on PVDF membranes provided direct evidence that this approach can impart long-lasting superhydrophilic properties to the PVDF membranes. The as-modified PVDF membranes exhibited much higher pure water flux than those reported

in other studies. Therefore, this work provides a novel and facile technique to modify the membrane surface with the enhanced superhydrophilicity and water permeation for water treatment.

3. Previous studies on using membrane emulsification in the manufacture of double emulsions were limited to O/W/O and W/O/W emulsions. This work successfully fabricated G/O/W emulsions and subsequently synthesized hollow polymeric microcapsules using only one single membrane emulsification. This allows the membrane emulsification technique to answer the requests of fabricating products with specific size, narrow size distribution, complex core–shell or hollow structure, and diverse functions.

Chapter 7 Future Work

Despite the progress, there are also challenges in each project, which need to be resolved in the future. Plant phenols represent a large group of molecules, which are abundant in nature. While this study has concentrated on one simple model compound – catechol, future studies are required to explore the deposition behaviors of a more complex model compound and eventually natural mixtures of phenolic compounds in plant extracts. Moreover, the mechanism of chemical oxidation should be better understood, and more applications should be tested. The surface modification strategy developed in this thesis can be potentially applied in any number of surfaces for an equal number of different purposes. For example, the surface modifications with plant phenols and other zwitterionic polymers may show effectiveness to mitigate membrane fouling problems in the long-term water filtration. The highly hydrophilic polyphenol film will be effective in retarding the favorable deposition of the proteins on the filtration membrane.

Further investigation of the Janus membrane emulsification will improve our fundamental understanding of the dynamic mechanisms contributing to droplet growth and detachment and hence optimization of different parameters. In this study, the feed conditions of oil were the same in all emulsification tests. Therefore, it would be worthwhile to investigate the influence of oil flow rate on the oily bubble formation kinetics. Moreover, the studies conducted in the present thesis are based on just one kind of monomer oil – HDDA, and new products with improved quality and functional properties can be expected when other oils are incorporated into the system. Design optimizations of emulsification setups could also serve as the next step of experimentation, which will eventually help in addressing scale-up issues.

Bibliography

[1] A.G.F. Norman N Li, W. S. Winston Ho, Takeshi Matsuura, Advanced membrane technology and applications, John Wiley & Sons, 2011.

[2] M.G. Buonomenna, Membrane processes for a sustainable industrial growth, Rsc Adv, 3 (2013) 5694-5740.

[3] M. Ulbricht, Advanced functional polymer membranes, Polymer, 47 (2006) 2217-2262.

[4] G. Amy, N. Ghaffour, Z.Y. Li, L. Francis, R.V. Linares, T. Missimer, S. Lattemann, Membrane-based seawater desalination: Present and future prospects, Desalination, 401 (2017) 16-21.

[5] M. Peter-Varbanets, F. Hammes, M. Vital, W. Pronk, Stabilization of flux during dead-end ultra-low pressure ultrafiltration, Water Res, 44 (2010) 3607-3616.

[6] N.L. Le, S.P. Nunes, Materials and membrane technologies for water and energy sustainability, Sustain Mater Techno, 7 (2016) 1-28.

[7] Y.Z. Zhu, D. Wang, L. Jiang, J. Jin, Recent progress in developing advanced membranes for emulsified oil/water separation, Npg Asia Mater, 6 (2014).

[8] Z.L. Chu, Y.J. Feng, S. Seeger, Oil/Water Separation with Selective Superantiwetting/Superwetting Surface Materials, Angew Chem Int Edit, 54 (2015) 2328-2338.

[9] W.B. Zhang, Y.Z. Zhu, X. Liu, D. Wang, J.Y. Li, L. Jiang, J. Jin, Salt-Induced Fabrication of Superhydrophilic and Underwater Superoleophobic PAA-g-PVDF Membranes for Effective Separation of Oil-in-Water Emulsions, Angew Chem Int Edit, 53 (2014) 856-860.

[10] Y.Z. Zhu, F. Zhang, D. Wang, X.F. Pei, W.B. Zhang, J. Jin, A novel zwitterionic polyelectrolyte grafted PVDF membrane for thoroughly separating oil from water with ultrahigh efficiency, J Mater Chem A, 1 (2013) 5758-5765.

[11] Z.X. Xue, S.T. Wang, L. Lin, L. Chen, M.J. Liu, L. Feng, L. Jiang, A Novel Superhydrophilic and Underwater Superoleophobic Hydrogel-Coated Mesh for Oil/Water Separation, Adv Mater, 23 (2011) 4270-4273.

[12] X. Yao, Y.L. Song, L. Jiang, Applications of Bio-Inspired Special Wettable Surfaces, Adv Mater, 23 (2011) 719-734.

[13] S.M. Joscelyne, G. Tragardh, Membrane emulsification - a literature review, Journal of Membrane Science, 169 (2000) 107-117.

[14] C. Charcosset, Preparation of emulsions and particles by membrane emulsification for the food processing industry, J Food Eng, 92 (2009) 241-249.

[15] J.P. Ju, T.M. Wang, Q.H. Wang, A facile approach in fabricating superhydrophobic and superoleophilic poly (vinylidene fluoride) membranes for efficient water-oil separation, J Appl Polym Sci, 132 (2015).

[16] K. Sikhwivhilu, R.M. Moutloali, Functionalized PVDF membrane-immobilized Fe/Ni bimetallic nanoparticles for catalytic degradation of methyl orange dye: a comparative study, Mater Today-Proc, 2 (2015) 4070-4080.

[17] K.P. Prathish, V. Vishnuvardhan, T.P. Rao, Rational Design of In Situ Monolithic Imprinted Polymer Membranes for the Potentiometric Sensing of Diethyl Chlorophosphate - a Chemical Warfare Agent Simulant, Electroanal, 21 (2009) 1048-1056.

[18] J.H. Fu, J. Ji, W.Y. Yuan, J.C. Shen, Construction of anti-adhesive and antibacterial multilayer films via layer-by-layer assembly of heparin and chitosan, Biomaterials, 26 (2005) 6684-6692.

[19] C.X. Liu, D.R. Zhang, Y. He, X.S. Zhao, R.B. Bai, Modification of membrane surface for anti-biofouling performance: Effect of anti-adhesion and anti-bacteria approaches, J Membrane Sci, 346 (2010) 121-130.

[20] Y. Xu, Z.H. Li, K.M. Su, T.T. Fan, L. Cao, Mussel-inspired modification of PPS membrane to separate and remove the dyes from the wastewater, Chem Eng J, 341 (2018) 371-382.

[21] R.A. Barb, C. Hrelescu, L. Dong, J. Heitz, J. Siegel, P. Slepicka, V. Vosmanska, V. Svorcik, B. Magnus, R. Marksteiner, M. Schernthaner, K. Groschner, Laser-induced periodic surface structures on polymers for formation of gold nanowires and activation of human cells, Appl Phys a-Mater, 117 (2014) 295-300.

[22] K. Pan, R.M. Ren, H.Z. Li, B. Cao, Preparation of dual stimuli-responsive PET track-etched membrane by grafting copolymer using ATRP, Polym Advan Technol, 24 (2013) 22-27.

[23] H. Shi, Y. He, Y. Pan, H.H. Di, G.Y. Zeng, L. Zhang, C.L. Zhang, A modified mussel-inspired method to fabricate TiO2 decorated superhydrophilic PVDF membrane for oil/water separation, J Membrane Sci, 506 (2016) 60-70.

[24] T. Yuan, J.Q. Meng, T.Y. Hao, Z.H. Wang, Y.F. Zhang, A Scalable Method toward Superhydrophilic and Underwater Superoleophobic PVDF Membranes for Effective Oil/Water Emulsion Separation, Acs Appl Mater Inter, 7 (2015) 14896-14904.

[25] O. Burtovyy, V. Klep, T. Turel, Y. Gowayed, I. Luzinov, POLY 65-Modification of PET membrane surface with nanothin polymer layers via "grafting to" approach, Abstr Pap Am Chem S, 235 (2008).

[26] J.H. Choi, S.J. Gwon, J.Y. Shon, C.H. Jung, Y.E. Ihm, Y.M. Lim, Y.C. Nho, Preparation of polystyrene-grafted poly(vinylidene fluoride) membranes for lithium secondary batteries, J Ind Eng Chem, 14 (2008) 116-119.

[27] W.Z. Lang, Z.L. Xu, H. Yang, W. Tong, Preparation and characterization of PVDF-PFSA blend hollow fiber UF membrane, J Membrane Sci, 288 (2007) 123-131.

[28] F. Liu, Y.Y. Xu, B.K. Zhu, F. Zhang, L.P. Zhu, Preparation of hydrophilic and fouling resistant poly(vinylidene fluoride) hollow fiber membranes, J Membrane Sci, 345 (2009) 331-339.

[29] M.L. Steen, A.C. Jordan, E.R. Fisher, Hydrophilic modification of polymeric membranes by low temperature H2O plasma treatment, J Membrane Sci, 204 (2002) 341-357.

[30] H.Y. Yu, Y. Xie, M.X. Hu, J.L. Wang, S.Y. Wang, Z.K. Xu, Surface modification of polypropylene microporous membrane to improve its antifouling property in MBR: CO2 plasma treatment, J Membrane Sci, 254 (2005) 219-227.

[31] A.G. Fane, R. Wang, M.X. Hu, Synthetic Membranes for Water Purification: Status and Future, Angew Chem Int Edit, 54 (2015) 3368-3386.

[32] L. Ni, J.Q. Meng, X.G. Li, Y.F. Zhang, Surface coating on the polyamide TFC RO membrane for chlorine resistance and antifouling performance improvement, J Membrane Sci, 451 (2014) 205-215.

[33] H. Lee, S.M. Dellatore, W.M. Miller, P.B. Messersmith, Mussel-inspired surface chemistry for multifunctional coatings, Science, 318 (2007) 426-430.

[34] Y.L. Liu, K.L. Ai, L.H. Lu, Polydopamine and Its Derivative Materials: Synthesis and Promising Applications in Energy, Environmental, and Biomedical Fields, Chem Rev, 114 (2014) 5057-5115.

[35] M.E. Yu, J.Y. Hwang, T.J. Deming, Role of L-3,4-dihydroxyphenylalanine in mussel adhesive proteins, J Am Chem Soc, 121 (1999) 5825-5826.

[36] Y. Lv, H.C. Yang, H.Q. Liang, L.S. Wan, Z.K. Xu, Nanofiltration membranes via co-deposition of polydopamine/polyethylenimine followed by cross-linking, J Membrane Sci, 476 (2015) 50-58.

[37] Y. Lv, Y. Du, W.Z. Qiu, Z.K. Xu, Nanocomposite Membranes via the Codeposition of Polydopamine/Polyethylenimine with Silica Nanoparticles for Enhanced Mechanical Strength and High Water Permeability, Acs Appl Mater Inter, 9 (2017) 2966-2972.

[38] M.B. Wu, H.C. Yang, J.J. Wang, G.P. Wu, Z.K. Xu, Janus Membranes with Opposing Surface Wettability Enabling Oil-to-Water and Water-to-Oil Emulsification, Acs Appl Mater Inter, 9 (2017) 5062-5066.

[39] T.S. Sileika, D.G. Barrett, R. Zhang, K.H.A. Lau, P.B. Messersmith, Colorless Multifunctional Coatings Inspired by Polyphenols Found in Tea, Chocolate, and Wine, Angew Chem Int Edit, 52 (2013) 10766-10770.

[40] S. Quideau, D. Deffieux, C. Douat-Casassus, L. Pouysegu, Plant Polyphenols: Chemical Properties, Biological Activities, and Synthesis, Angew Chem Int Edit, 50 (2011) 586-621.

[41] H. Wagreich, J.M. Nelson, On the oxidation product of catechol when oxidized by means of tyrosinase, J Biol Chem, 115 (1936) 459-465.

[42] J. Yang, M.A.C. Stuart, M. Kamperman, Jack of all trades: versatile catechol crosslinking mechanisms, Chem Soc Rev, 43 (2014) 8271-8298.

[43] S. Dubey, D. Singh, R.A. Misra, Enzymatic synthesis and various properties of poly(catechol), Enzyme Microb Tech, 23 (1998) 432-437.

[44] N. Aktas, N. Sahiner, O. Kantoglu, B. Salih, A. Tanyolac, Biosynthesis and characterization of laccase catalyzed poly(catechol), J Polym Environ, 11 (2003) 123-128.

[45] A.A. Kutyrev, Nucleophilic Reactions of Quinones, Tetrahedron, 47 (1991) 8043-8065.

[46] N. Bandara, H.B. Zeng, J.P. Wu, Marine mussel adhesion: biochemistry, mechanisms, and biomimetics, J Adhes Sci Technol, 27 (2013) 2139-2162.

[47] A.M. Baty, P.K. Leavitt, C.A. Siedlecki, B.J. Tyler, P.A. Suci, R.E. Marchant, G.G. Geesey, Adsorption of adhesive proteins from the marine mussel, Mytilus edulis, on polymer films in the hydrated state using angle dependent X-ray photoelectron spectroscopy and atomic force microscopy, Langmuir, 13 (1997) 5702-5710.

[48] R. Kummert, W. Stumm, The Surface Complexation of Organic-Acids on Hydrous Gamma-Al2o3, J Colloid Interf Sci, 75 (1980) 373-385.

[49] M.P. Deacon, S.S. Davis, J.H. Waite, S.E. Harding, Structure and mucoadhesion of mussel glue protein in dilute solution, Biochemistry-Us, 37 (1998) 14108-14112.

[50] K. Huang, B.P. Lee, D.R. Ingram, P.B. Messersmith, Synthesis and characterization of self-assembling block copolymers containing bioadhesive end groups, Biomacromolecules, 3 (2002) 397-406.

[51] L. Pourcel, J.M. Routaboul, V. Cheynier, L. Lepiniec, I. Debeaujon, Flavonoid oxidation in plants: from biochemical properties to physiological functions, Trends Plant Sci, 12 (2007) 29-36.

[52] G. Ward, R.E. Parales, C.G. Dosoretz, Biocatalytic synthesis of polycatechols from toxic aromatic compounds, Environ Sci Technol, 38 (2004) 4753-4757.

[53] J.R. Jeon, J.H. Kim, Y.S. Chang, Enzymatic polymerization of plant-derived phenols for material-independent and multifunctional coating, J Mater Chem B, 1 (2013) 6501-6509.

[54] H. Bayir, Reactive oxygen species, Crit Care Med, 33 (2005) S498-S501.

[55] F. Behboodi-Sadabad, H.J. Zhang, V. Trouillet, A. Welle, N. Plumere, P.A. Levkin, UV-Triggered Polymerization, Deposition, and Patterning of Plant Phenolic Compounds, Adv Funct Mater, 27 (2017).

[56] Q. Wei, F.L. Zhang, J. Li, B.J. Li, C.S. Zhao, Oxidant-induced dopamine polymerization for multifunctional coatings, Polym Chem-Uk, 1 (2010) 1430-1433.

[57] F. Ponzio, J. Barthes, J. Bour, M. Michel, P. Bertani, J. Hemmerle, M. d'Ischia, V. Ball, Oxidant Control of Polydopamine Surface Chemistry in Acids: A Mechanism-Based Entry to Superhydrophilic-Superoleophobic Coatings, Chem Mater, 28 (2016) 4697-4705.

[58] C. Zhang, Y. Ou, W.X. Lei, L.S. Wan, J. Ji, Z.K. Xu, CuSO4/H2O2-Induced Rapid Deposition of Polydopamine Coatings with High Uniformity and Enhanced Stability, Angew Chem Int Edit, 55 (2016) 3054-3057.

[59] M. Lee, S.H. Lee, I.K. Oh, H. Lee, Microwave-Accelerated Rapid, Chemical Oxidant-Free, Material-Independent Surface Chemistry of Poly(dopamine), Small, 13 (2017).

[60] Z. Wang, C. Xu, Y.X. Lu, G.Y. Wei, G. Ye, T.X. Sun, J. Chen, Microplasma-assisted rapid, chemical oxidant-free and controllable polymerization of dopamine for surface modification, Polym Chem-Uk, 8 (2017) 4388-4392.

[61] Z.X. Xue, Y.Z. Cao, N. Liu, L. Feng, L. Jiang, Special wettable materials for oil/water separation, J Mater Chem A, 2 (2014) 2445-2460.

[62] X.J. Feng, L. Jiang, Design and creation of superwetting/antiwetting surfaces, Adv Mater, 18 (2006) 3063-3078.

[63] W.B. Zhang, Z. Shi, F. Zhang, X. Liu, J. Jin, L. Jiang, Superhydrophobic and Superoleophilic PVDF Membranes for Effective Separation of Water-in-Oil Emulsions with High Flux, Adv Mater, 25 (2013) 2071-2076.

[64] Z.P. Zhou, X.F. Wu, Electrospinning superhydrophobic-superoleophilic fibrous PVDF membranes for high-efficiency water-oil separation, Mater Lett, 160 (2015) 423-427.

[65] M.J. Liu, S.T. Wang, Z.X. Wei, Y.L. Song, L. Jiang, Bioinspired Design of a Superoleophobic and Low Adhesive Water/Solid Interface, Adv Mater, 21 (2009) 665-+.

[66] T. Jiang, Z.G. Guo, W.M. Liu, Biomimetic superoleophobic surfaces: focusing on their fabrication and applications, J Mater Chem A, 3 (2015) 1811-1827.

[67] E. Piacentini, E. Drioli, L. Giorno, Membrane emulsification technology: Twenty-five years of inventions and research through patent survey, J Membrane Sci, 468 (2014) 410-422.

[68] R.A. Williams, S.J. Peng, D.A. Wheeler, N.C. Morley, D. Taylor, M. Whalley, D.W. Houldsworth, Controlled production of emulsions using a crossflow membrane part II: Industrial scale manufacture, Chem Eng Res Des, 76 (1998) 902-910.

[69] A.J. Abrahamse, A. van der Padt, R.M. Boom, W.B.C. de Heij, Process fundamentals of membrane emulsification: Simulation with CFD, Aiche J, 47 (2001) 1285-1291.

[70] C. Charcosset, I. Limayem, H. Fessi, The membrane emulsification process - a review, J Chem Technol Biot, 79 (2004) 209-218.

[71] T. Nakashima, M. Shimizu, M. Kukizaki, Membrane Emulsification by Microporous Glass, Inorganic Membranes : Icim2-91, (1991) 513-516.

[72] V. Schroder, H. Schubert, Production of emulsions using microporous, ceramic membranes, Colloid Surface A, 152 (1999) 103-109.

[73] W. Liu, X.L. Yang, W.S.W. Ho, Preparation of Uniform-Sized Multiple Emulsions and Micro/Nano Particulates for Drug Delivery by Membrane Emulsification, J Pharm Sci-Us, 100 (2011) 75-93.

[74] A.J. Gijsbertsen-Abrahamse, A. van der Padt, R.M. Boom, Status of cross-flow membrane emulsification and outlook for industrial application, J Membrane Sci, 230 (2004) 149-159.

[75] K. Suzuki, I. Fujiki, Y. Hagura, Preparation of Corn Oil/Water and Water/Corn Oil Emulsions Using PTFE Membranes, Food Sci. Technol. Int. Tokyo, 4 (1998) 164-167.

[76] G.T. Vladisavljevic, M. Shimizu, T. Nakashima, Production of multiple emulsions for drug delivery systems by repeated SPG membrane homogenization: Influence of mean pore size, interfacial tension and continuous phase viscosity, J Membrane Sci, 284 (2006) 373-383.

[77] Y. Mine, M. Shimizu, T. Nakashima, Preparation and stabilization of simple and multiple emulsions using a microporous glass membrane, Colloid Surface B, 6 (1996) 261-268.

[78] R. Liu, S.S. Huang, Y.H. Wan, G.H. Ma, Z.G. Su, Preparation of insulin-loaded PLA/PLGA microcapsules by a novel membrane emulsification method and its release in vitro, Colloid Surface B, 51 (2006) 30-38.

[79] R. Berendsen, C. Guell, M. Ferrando, Spray dried double emulsions containing procyanidin-rich extracts produced by premix membrane emulsification: Effect of interfacial composition, Food Chem, 178 (2015) 251-258.

[80] R. Liu, G.H. Ma, F.T. Meng, Z.G. Su, Preparation of uniform-sized PLA microcapsules by combining Shirasu Porous Glass membrane emulsification technique and multiple emulsion-solvent evaporation method, J Control Release, 103 (2005) 31-43.

[81] G.H. Ma, H. Sone, S. Omi, Preparation of uniform-sized polystyrene-polyacrylamide composite microspheres from a W/O/W emulsion by membrane emulsification technique and subsequent suspension polymerization, Macromolecules, 37 (2004) 2954-2964.

[82] J. Lee, D.R. Hwang, S.E. Shim, Y.M. Rhym, Controlling Morphology of Polymer Microspheres by Shirasu Porous Glass (SPG) Membrane Emulsification and Subsequent Polymerization: from Solid to Hollow, Macromol Res, 18 (2010) 1142-1147.

[83] M. Hunger, J. Weitkamp, In situ IR, NMR, EPR, and UV/Vis spectroscopy: Tools for new insight into the mechanisms of heterogeneous catalysis, Angew Chem Int Edit, 40 (2001) 2954-2971.

[84] W. Ogieglo, H. Wormeester, K.J. Eichhorn, M. Wessling, N.E. Benes, In situ ellipsometry studies on swelling of thin polymer films: A review, Prog Polym Sci, 42 (2015) 42-78.

[85] W. Ogieglo, H. Wormeester, M. Wessling, N.E. Benes, Spectroscopic Ellipsometry Analysis of a Thin Film Composite Membrane Consisting of Polysulfone on a Porous alpha-Alumina Support, Acs Appl Mater Inter, 4 (2012) 935-943.

[86] M.T. Postek, A.E. Vladar, Helium Ion Microscopy and Its Application to Nanotechnology and Nanometrology, Scanning, 30 (2008) 457-462.

[87] S.A. Boden, A. Asadollahbaik, H.N. Rutt, D.M. Bagnall, Helium ion microscopy of Lepidoptera scales, Scanning, 34 (2012) 107-120.

[88] C.S. Fadley, X-ray photoelectron spectroscopy: Progress and perspectives, J Electron Spectrosc, 178 (2010) 2-32.

[89] B. Feuerbacher, B. Fitton, R.F. Willis, Photoemission and the electronic properties of surfaces, Wiley, London ; New York, 1978.

[90] M.M. Blum, H. John, Historical perspective and modern applications of Attenuated Total Reflectance - Fourier Transform Infrared Spectroscopy (ATR-FTIR), Drug Test Anal, 4 (2012) 298-302.

[91] J. Genzer, K. Efimenko, Recent developments in superhydrophobic surfaces and their relevance to marine fouling: a review, Biofouling, 22 (2006) 339-360.

[92] S. Ferraris, M. Cazzola, V. Peretti, B. Stella, S. Spriano, Zeta Potential Measurements on Solid Surfaces for in Vitro Biomaterials Testing: Surface Charge, Reactivity Upon Contact With Fluids and Protein Absorption, Front Bioeng Biotech, 6 (2018).

[93] S. Nishimura, K. Yao, M. Kodama, Y. Imai, K. Ogino, K. Mishima, Electrokinetc study of synthetic smectites by flat plate streaming potential technique, Langmuir, 18 (2002) 188-193.

[94] X.D. Chen, B. Zheng, H. Liu, Optical and digital microscopic imaging techniques and applications in pathology, Anal Cell Pathol, 34 (2011) 5-18.

[95] E.T. Urbansky, Total organic carbon analyzers as tools for measuring carbonaceous matter in natural waters, J Environ Monitor, 3 (2001) 102-112.

[96] L. Marton, L.I. Schiff, Determination of object thickness in electron microscopy, J Appl Phys, 12 (1941) 759-765.

[97] S.H. Ku, J. Ryu, S.K. Hong, H. Lee, C.B. Park, General functionalization route for cell adhesion on non-wetting surfaces, Biomaterials, 31 (2010) 2535-2541.

[98] V.K. Thakur, M.-F. Lin, E.J. Tan, P.S. Lee, Green aqueous modification of fluoropolymers for energy storage applications, Journal of Materials Chemistry, 22 (2012) 5951.

[99] Z.-X. Wang, C.-H. Lau, N.-Q. Zhang, Y.-P. Bai, L. Shao, Mussel-inspired tailoring of membrane wettability for harsh water treatment, J. Mater. Chem. A, 3 (2015) 2650-2657.

[100] N.G.P. Chew, S. Zhao, C. Malde, R. Wang, Superoleophobic surface modification for robust membrane distillation performance, J. Membr. Sci., 541 (2017) 162-173.

[101] G. Wang, X. Huang, P. Jiang, Bio-Inspired Fluoro-polydopamine Meets Barium Titanate Nanowires: A Perfect Combination to Enhance Energy Storage Capability of Polymer Nanocomposites, ACS Appl. Mater. Interfaces, 9 (2017) 7547-7555.

[102] M. Liao, P. Wan, J. Wen, M. Gong, X. Wu, Y. Wang, R. Shi, L. Zhang, Wearable, Healable, and Adhesive Epidermal Sensors Assembled from Mussel-Inspired Conductive Hybrid Hydrogel Framework, Adv. Funct. Mater., 27 (2017) 1703852.

[103] Y. Liu, K. Ai, L. Lu, Polydopamine and its derivative materials: synthesis and promising applications in energy, environmental, and biomedical fields, Chem Rev, 114 (2014) 5057-5115.

[104] Y. Bozzi, E. Borrelli, The role of dopamine signaling in epileptogenesis, Front Cell Neurosci, 7 (2013) 157.

[105] D.G. Barrett, T.S. Sileika, P.B. Messersmith, Molecular diversity in phenolic and polyphenolic precursors of tannin-inspired nanocoatings, Chem. Commun. (Cambridge, U. K.), 50 (2014) 7265-7268.

[106] W.-Z. Qiu, Q.-Z. Zhong, Y. Du, Y. Lv, Z.-K. Xu, Enzyme-triggered coatings of tea catechins/chitosan for nanofiltration membranes with high performance, Green Chem., 18 (2016) 6205-6208.

[107] T.S. Sileika, D.G. Barrett, R. Zhang, K.H. Lau, P.B. Messersmith, Colorless multifunctional coatings inspired by polyphenols found in tea, chocolate, and wine, Angew. Chem., Int. Ed. Engl., 52 (2013) 10766-10770.

[108] J. Yang, M.A. Cohen Stuart, M. Kamperman, Jack of all trades: versatile catechol crosslinking mechanisms, Chem Soc Rev, 43 (2014) 8271-8298.

[109] Q. Wei, R. Haag, Universal polymer coatings and their representative biomedical applications, Materials Horizons, 2 (2015) 567-577.

[110] S. Geissler, A. Barrantes, P. Tengvall, P.B. Messersmith, H. Tiainen, Deposition Kinetics of Bioinspired Phenolic Coatings on Titanium Surfaces, Langmuir, 32 (2016) 8050-8060.

[111] X. Zhang, P.-F. Ren, H.-C. Yang, L.-S. Wan, Z.-K. Xu, Co-deposition of tannic acid and diethlyenetriamine for surface hydrophilization of hydrophobic polymer membranes, Appl. Surf. Sci., 360 (2016) 291-297.

[112] Z. Wang, S. Ji, F. He, M. Cao, S. Peng, Y. Li, One-step transformation of highly hydrophobic membranes into superhydrophilic and underwater superoleophobic ones for high-efficiency separation of oil-in-water emulsions, J. Mater. Chem. A, 6 (2018) 3391-3396.

[113] H. Wang, J. Wu, C. Cai, J. Guo, H. Fan, C. Zhu, H. Dong, N. Zhao, J. Xu, Mussel inspired modification of polypropylene separators by catechol/polyamine for Li-ion batteries, ACS Appl. Mater. Interfaces, 6 (2014) 5602-5608.

[114] W.-Z. Qiu, H.-C. Yang, L.-S. Wan, Z.-K. Xu, Co-deposition of catechol/polyethyleneimine on porous membranes for efficient decolorization of dye water, J. Mater. Chem. A, 3 (2015) 14438-14444.

[115] Y.C. Xu, Y.P. Tang, L.F. Liu, Z.H. Guo, L. Shao, Nanocomposite organic solvent nanofiltration membranes by a highly-efficient mussel-inspired co-deposition strategy, J. Membr. Sci., 526 (2017) 32-42.

[116] J.-R. Jeon, J.-H. Kim, Y.-S. Chang, Enzymatic polymerization of plant-derived phenols for material-independent and multifunctional coating, J. Mater. Chem. B, 1 (2013).

[117] F. Behboodi-Sadabad, H. Zhang, V. Trouillet, A. Welle, N. Plumeré, P.A. Levkin, UV-Triggered Polymerization, Deposition, and Patterning of Plant Phenolic Compounds, Adv. Funct. Mater., 27 (2017).

[118] Q. Wei, F. Zhang, J. Li, B. Li, C. Zhao, Oxidant-induced dopamine polymerization for multifunctional coatings, Polymer Chemistry, 1 (2010) 1430.

[119] S.H. Hong, S. Hong, M.-H. Ryou, J.W. Choi, S.M. Kang, H. Lee, Sprayable Ultrafast Polydopamine Surface Modifications, Adv. Mater. Interfaces, 3 (2016) 1500857.

[120] C. Zhang, Y. Ou, W.X. Lei, L.S. Wan, J. Ji, Z.K. Xu, CuSO4/H2O2-Induced Rapid Deposition of Polydopamine Coatings with High Uniformity and Enhanced Stability, Angew. Chem., Int. Ed. Engl., 55 (2016) 3054-3057.

[121] C. Luo, Q. Liu, Oxidant-Induced High-Efficient Mussel-Inspired Modification on PVDF Membrane with Superhydrophilicity and Underwater Superoleophobicity Characteristics for Oil/Water Separation, ACS Appl. Mater. Interfaces, 9 (2017) 8297-8307.

[122] F. Ponzio, J. Barthès, J. Bour, M. Michel, P. Bertani, J. Hemmerlé, M. d'Ischia, V. Ball, Oxidant Control of Polydopamine Surface Chemistry in Acids: A Mechanism-Based Entry to Superhydrophilic-Superoleophobic Coatings, Chemistry of Materials, 28 (2016) 4697-4705.

[123] N.G.P. Chew, S. Zhao, C. Malde, R. Wang, Polyvinylidene fluoride membrane modification via oxidant-induced dopamine polymerization for sustainable direct-contact membrane distillation, J. Membr. Sci., 563 (2018) 31-42.

[124] F.-N. Meng, M.-Q. Zhang, K. Ding, T. Zhang, Y.-K. Gong, Cell membrane mimetic PVDF microfiltration membrane with enhanced antifouling and separation performance for oil/water mixtures, J. Mater. Chem. A, 6 (2018) 3231-3241.

[125] S. Hong, Y.S. Na, S. Choi, I.T. Song, W.Y. Kim, H. Lee, Non-Covalent Self-Assembly and Covalent Polymerization Co-Contribute to Polydopamine Formation, Adv. Funct. Mater., 22 (2012) 4711-4717.

[126] G.F.P.a.M.V. Chaubal, Enzyme-catalysed polymer modification: reaction of phenolic compounds with chitosan films, Polymer, 37 4643−4648.

[127] H. Shi, Y. He, Y. Pan, H. Di, G. Zeng, L. Zhang, C. Zhang, A modified mussel-inspired method to fabricate TiO2 decorated superhydrophilic PVDF membrane for oil/water separation, J. Membr. Sci., 506 (2016) 60-70.

[128] S.W.W.a.E.T. Kaiser, The Mechanism of the Periodate Oxidation of Aromatic Systems. III. A Kinetic Study of the Periodate Oxidation of Catechol, Journal of the American Chemical Society, 88 (1966) 5820-5827.

[129] Z. Shami, S.M. Amininasab, P. Shakeri, Structure-Property Relationships of Nanosheeted 3D Hierarchical Roughness MgAl-Layered Double Hydroxide Branched to an Electrospun Porous Nanomembrane: A Superior Oil-Removing Nanofabric, ACS Appl. Mater. Interfaces, 8 (2016) 28964-28973.

[130] M. Liu, S. Wang, Z. Wei, Y. Song, L. Jiang, Bioinspired Design of a Superoleophobic and Low Adhesive Water/Solid Interface, Adv. Mater., 21 (2009) 665-669.

[131] G.-E. Chen, W.-G. Sun, Y.-F. Kong, Q. Wu, L. Sun, J. Yu, Z.-L. Xu, Hydrophilic Modification of PVDF Microfiltration Membrane with Poly (Ethylene Glycol) Dimethacrylate through Surface Polymerization, Polym.-Plast. Technol. Eng., 57 (2017) 108-117.

[132] Y. Chen, Q. Deng, J. Xiao, H. Nie, L. Wu, W. Zhou, B. Huang, Controlled grafting from poly(vinylidene fluoride) microfiltration membranes via reverse atom transfer radical polymerization and antifouling properties, Polymer, 48 (2007) 7604-7613.

[133] H. Fan, Y. Peng, Application of PVDF membranes in desalination and comparison of the VMD and DCMD processes, Chem. Eng. Sci., 79 (2012) 94-102.

[134] J. Gu, P. Xiao, L. Zhang, W. Lu, G. Zhang, Y. Huang, J. Zhang, T. Chen, Construction of superhydrophilic and under-water superoleophobic carbon-based membranes for water purification, RSC Adv., 6 (2016) 73399-73403.

[135] Z. Zhou, W. Lin, X.-F. Wu, Electrospinning ultrathin continuous cellulose acetate fibers for high-flux water filtration, Colloids Surf., A, 494 (2016) 21-29.

[136] J.P. Bothma, J. de Boor, U. Divakar, P.E. Schwenn, P. Meredith, Device-Quality Electrically Conducting Melanin Thin Films, Adv. Mater., 20 (2008) 3539-3542.

[137] F.-f. Ma, N. Zhang, X. Wei, J.-h. Yang, Y. Wang, Z.-w. Zhou, Blend-electrospun poly(vinylidene fluoride)/polydopamine membranes: self-polymerization of dopamine and the excellent adsorption/separation abilities, J. Mater. Chem. A, 5 (2017) 14430-14443.

[138] Y. Cao, N. Liu, W. Zhang, L. Feng, Y. Wei, One-Step Coating toward Multifunctional Applications: Oil/Water Mixtures and Emulsions Separation and Contaminants Adsorption, ACS Appl. Mater. Interfaces, 8 (2016) 3333-3339.

[139] J. Sun, H. Bi, S. Su, H. Jia, X. Xie, L. Sun, One-step preparation of GO/SiO 2 membrane for highly efficient separation of oil-in-water emulsion, J. Membr. Sci., 553 (2018) 131-138.

[140] Y. Huang, H. Li, L. Wang, Y. Qiao, C. Tang, C. Jung, Y. Yoon, S. Li, M. Yu, Ultrafiltration Membranes with Structure-Optimized Graphene-Oxide Coatings for Antifouling Oil/Water Separation, Adv. Mater. Interfaces, 2 (2015).

[141] Z. Wang, S. Ji, J. Zhang, Q. Liu, F. He, S. Peng, Y. Li, Tannic acid encountering ovalbumin: a green and mild strategy for superhydrophilic and underwater superoleophobic modification of various hydrophobic membranes for oil/water separation, J. Mater. Chem. A, 6 (2018) 13959-13967.

[142] W.-Z. Qiu, H.-C. Yang, L.-S. Wan, Z.-K. Xu, Co-deposition of catechol/polyethyleneimine on porous membranes for efficient decolorization of dye water, J. Mater. Chem. A, 3 (2015) 14438-14444.

[143] Y.C. Xu, Y.P. Tang, L.F. Liu, Z.H. Guo, L. Shao, Nanocomposite organic solvent nanofiltration membranes by a highly-efficient mussel-inspired co-deposition strategy, J. Membr. Sci., 526 (2017) 32-42.

[144] J. Liu, T. Mak, Z. Zhou, Z. Xu, Fundamental study of reactive oily-bubble flotation, Miner Eng, 15 (2002) 667-676.

[145] G. Muschiolik, Multiple emulsions for food use, Curr Opin Colloid In, 12 (2007) 213-220.

[146] E. Lorenceau, A.S. Utada, D.R. Link, G. Cristobal, M. Joanicot, D.A. Weitz, Generation of polymerosomes from double-emulsions, Langmuir, 21 (2005) 9183-9186.

[147] S. Okushima, T. Nisisako, T. Torii, T. Higuchi, Controlled production of monodisperse double emulsions by two-step droplet breakup in microfluidic devices, Langmuir, 20 (2004) 9905-9908.

[148] F. Zhou, L.X. Wang, Z.H. Xu, Q.X. Liu, M.J. Deng, R. Chi, Application of reactive oily bubbles to bastnaesite flotation, Miner Eng, 64 (2014) 139-145.

[149] B. Xu, H.J. Dou, K. Tao, K. Sun, J. Ding, W.B. Shi, X.S. Guo, J.Y. Li, D. Zhang, K. Sun, "Two-in-One" Fabrication of Fe3O4/MePEG-PLA Composite Nanocapsules as a Potential Ultrasonic/MRI Dual Contrast Agent, Langmuir, 27 (2011) 12134-12142.

[150] K.P. Pancholi, U. Farook, R. Moaleji, E. Stride, M.J. Edirisinghe, Novel methods for preparing phospholipid coated microbubbles, Eur Biophys J Biophy, 37 (2008) 515-520.

[151] Q. Xu, M. Nakajima, S. Ichikawa, N. Nakamura, P. Roy, H. Okadome, T. Shiina, Effects of surfactant and electrolyte concentrations on bubble formation and stabilization, J Colloid Interf Sci, 332 (2009) 208-214.

[152] M.B. Romanowsky, A.R. Abate, A. Rotem, C. Holtze, D.A. Weitz, High throughput production of single core double emulsions in a parallelized microfluidic device, Lab Chip, 12 (2012) 802-807.

[153] A. Abbaspourrad, W.J. Duncanson, N. Lebedeva, S.H. Kim, A.P. Zhushma, S.S. Datta, P.A. Dayton, S.S. Sheiko, M. Rubinstein, D.A. Weitz, Microfluidic Fabrication of Stable Gas-Filled Microcapsules for Acoustic Contrast Enhancement, Langmuir, 29 (2013) 12352-12357.

[154] M.S. Manga, D.W. York, Production of Concentrated Pickering Emulsions with Narrow Size Distributions Using Stirred Cell Membrane Emulsification, Langmuir, 33 (2017) 9050-9056.

[155] S. van der Graaf, C.G.P.H. Schroen, R.M. Boom, Preparation of double emulsions by membrane emulsification - a review, Journal of Membrane Science, 251 (2005) 7-15.

[156] V. Eisinaite, D. Juraite, K. Schroen, D. Leskauskaite, Preparation of stable food-grade double emulsions with a hybrid premix membrane emulsification system, Food Chem, 206 (2016) 59-66.

[157] X. Na, W. Zhou, T. Li, D. Hong, J. Li, G. Ma, Preparation of double-emulsion-templated microspheres with controllable porous structures by premix membrane emulsification, Particuology, (2019).

[158] T. Nakashima, M. Shimizu, M. Kukizaki, Particle control of emulsion by membrane emulsification and its applications, Adv Drug Deliver Rev, 45 (2000) 47-56.

[159] N. Yamazaki, H. Yuyama, M. Nagai, G.-H. Ma, S. Omi, A Comparison of Membrane Emulsification Obtained Using SPG (Shirasu Porous Glass) and PTFE [Poly(Tetrafluoroethylene)] Membranes, Journal of Dispersion Science and Technology, 23 (2002) 279-292.

[160] M.B. Wu, H.C. Yang, J.J. Wang, G.P. Wu, Z.K. Xu, Janus Membranes with Opposing Surface Wettability Enabling Oil-to-Water and Water-to-Oil Emulsification, ACS Appl Mater Interfaces, 9 (2017) 5062-5066.

[161] Y. Chen, Q. Liu, Oxidant-induced plant phenol surface chemistry for multifunctional coatings: Mechanism and potential applications, Journal of Membrane Science, 570-571 (2019) 176-183.

[162] N.E. Hotrum, T. van Vliet, M.A.C. Stuart, G.A. van Aken, Monitoring entering and spreading of emulsion droplets at an expanding air/water interface: A novel technique, J Colloid Interf Sci, 247 (2002) 125-131.

[163] J.J. Janke, W.F.D. Bennett, D.P. Tieleman, Oleic Acid Phase Behavior from Molecular Dynamics Simulations, Langmuir, 30 (2014) 10661-10667.

[164] R. Chen, P.F. Dong, J.H. Xu, Y.D. Wang, G.S. Luo, Controllable microfluidic production of gas-in-oil-in-water emulsions for hollow microspheres with thin polymer shells, Lab Chip, 12 (2012) 3858-3860.